# Screen-Printable Polymer Fabrication with Applications to Wearable Nanocomposite Electronics and Microfluidic Systems

**by**

**Daehan Chung**

B.Sc., Korea University, 2008

M.A.Sc, Simon Fraser University, 2012

Thesis Submitted in Partial Fulfillment of the
Requirements for the Degree of
Doctor of Philosophy

in the
School of Engineering Science
Faculty of Applied Science



SIMON FRASER UNIVERSITY

Fall 2018

# Approval

| | |
|---|---|
| **Name:** | **Daehan Chung** |
| **Degree:** | **Doctor of Philosophy** |
| **Title:** | **Screen-Printable Polymer Fabrication with Applications to Wearable Nanocomposite Electronics and Microfluidic Systems** |
| **Examining Committee:** | **Chair:** **Michael Adachi**<br>Assistant Professor |
| | **Bonnie L. Gray**<br>Senior Supervisor<br>Professor |
| | **Ash M. Parameswaran**<br>Supervisor<br>Professor |
| | **Edward Jung Wook Park**<br>Internal Examiner<br>Professor<br>School of Mechatronic Systems Engineering |
| | **Jessica E. Koehne**<br>External Examiner<br>Scientist<br>NASA Ames Research Center<br>The National Aeronautics and Space Administration (NASA) |
| **Date Defended/Approved:** | September 19, 2018 |

## Abstract

Wearable devices and systems are already important to our lives and have the potential for even greater impact. Many researchers are developing wearable devices and systems, and many different technologies are investigated. However, most of these technologies have limitations in flexibility, long fabrication times, lack of reusability, or complicated attachment mechanisms. Furthermore, many systems are limited in the functions that they can perform. Most systems are also confined to electronic functionality; there is not a fully successful wearable microfluidic technology developed with wearable fluidic channels for microfluidic devices, e.g., foldable microfluidic mixers or flexible bio-fluid sensors for wearable analysis systems. As an alternative approach, we develop new methods to screen-print electronic and fluidic devices on clothing that employ materials designed specifically for printing on textile. We present a new screen-printable silver conductive nanoparticle composite polymer (C-NCP) that can be applied to wearable systems for electronic functionality. We also develop a new technique to realize fully wearable microfluidic devices. Screen printable C-NCPs benefit the development of wearable devices due to their high degree of flexibility, good conductivity, and ability to be easily patterned into electrical and microfluidic devices. The new microfluidic device fabrication method enables easy, simple, and fast development of wearable microfluidic devices using inexpensive materials and equipment. In this thesis, a screen-printable C-NCP is developed and characterized, and its potential for wearable devices and systems is explored through a variety of demonstrator systems. The new microfluidic device fabrication method is explained in detail with optimization and characterization. Passive wearable microfluidic devices are fabricated on fabric, and active wearable microfluidic devices with electrical structures are also fabricated by combining wearable microfluidic structures with silver C-NCP as electronic routing and electrodes. The following demonstration devices and systems are developed to showcase different aspects of the new materials and fabrication techniques: 1) flexible dry electrocardiogram (ECG) electrodes screen printed on textile to measure heart bioelectrical signals; 2) flexible electrical routing printed on a safety vests for LED attachment and lighting system demonstration; 3) wearable microfluidic mixer fabricated on textiles; 4) and a wearable fluid conductivity sensor that combines C-NCP with flexible microfluidics.

**Keywords**: Wearable electronics; flexible electronics; wearable microfluidics; flexible microfluidics; conductive nanoparticle composite polymers; screen printing; plastisol

## Dedication

*To God and my family, my strength and love*

## Acknowledgements

I would like to thank to my senior supervisor Dr. Bonnie L. Gray first for her patience, support, and guidance through my studies. Without her encouragement and support, the projects in this thesis would never succeed. I could have not asked for more. I also would like to thank my defense committee members, Professor Michael Adachi, professor Ash M. Parameswaran, Professor Edward Jung Wook Park, and Dr. Jessica Koehne for taking time to review my work.

I would like to thank all the members within the Microinstrumentation Laboratory. Thanks for all your suggestions and helpful discussions. I also would like thank the Canadian National Engineering and Science Research Council (NSERC) for their financial support.

Finally, my deepest gratitude goes to God and my family. Without strength from God, and without the support and pray of my family, I would not be where I am today.

# Table of Contents

Approval ..... ii
Abstract ..... iii
Dedication ..... v
Acknowledgements ..... vi
Table of Contents ..... vii
List of Tables ..... x
List of Figures ..... xi

**Chapter 1. Introduction and Contributions ..... 1**

**Chapter 2. Background, Challenges, and Overall Solution ..... 6**
2.1. Fabrication Methods and Materials for Wearable Devices and Systems ..... 7
2.1.1. Metal Deposition on Flexible Substrates ..... 7
2.1.2. Flexible Conductive Composites ..... 8
2.1.3. Conductive Fibers ..... 10
2.2. Wearable and Flexible Microfluidic Devices ..... 11
2.2.1. Paper Microfluidics ..... 11
2.2.2. Microfluidics on Textile with Wax Printing ..... 12
2.2.3. Wearable Microfluidic Patches ..... 12
2.3. Methods and Materials Used in This Thesis ..... 13
2.3.1. Screen Printable Polymer ..... 13
2.3.2. Conductive Nanoparticles ..... 15
2.3.3. Screen Printing Techniques ..... 16
2.3.4. Patterning of Films by Laser Cutter ..... 17
2.4. Addressing Limitations of Prior Art: New Approach Presented in the Thesis ..... 18
2.5. Summary of Prior Art and Solutions ..... 19

**Chapter 3. Screen-Printable Polymers for Wearable Microfluidics and Electronics 22**
3.1. Plastisol for Wearable Devices and Systems ..... 22
3.2. Screen-Printable Silver Conductive Nanoparticle Composite Polymers (C-NCP). 25
3.2.1. Desired Properties ..... 25
3.2.2. Development of Screen-Printable C-NCP ..... 26
3.3. Characteristics of Screen-Printable Silver C-NCP ..... 28
3.3.1. Effect of Nanoparticle/Polymer Ratio on Resistivity ..... 28
3.3.2. Effect of Flexing on Resistivity ..... 30
3.3.3. Effect of Nanoparticle Density on Stretchability ..... 31
3.3.4. Suitability for Long Term Use and Washability ..... 34
3.4. Screen Printed Silver C-NCP ..... 35

**Chapter 4. Applications of Screen-Printable C-NCP to Wearable Electronics for Health and Safety ..... 38**

4.1. Application 1: Screen Printed Wearable Electrocardiogram (ECG) Electrodes ....39
4.1.1. Development of Wearable Dry ECG Electrodes....39
4.1.2. Experiments and Test Results....41
4.2. Application 2: Screen Printed Safety Vest with LEDs....43
4.2.1. Flexible Electrical Routing on Textile....44
4.2.2. Fabrication of Safety Vest with LEDs....45

**Chapter 5. Wearable and Flexible Microfluidic Systems....48**
5.1. Fabrication of Wearable Microfluidic Devices....48
5.2. Key Processes for Optimization of the Fabrication....51
5.2.1. Plastisol Coating and Control of the Thickness of the Plastisol Film....51
5.2.2. Planarization of the Plastisol Films....54
5.2.3. Thermal Fusion Bonding....56
5.2.4. Pattern Resolution....57
5.2.5. Sample Microfluidic Channels....62
5.3. Characterization of the Flexible Microfluidic Devices....64
5.3.1. Stretchability of Plastisol-based Microfluidic Channels....64
5.3.2. Flexibility of Microfluidic Channels....67
5.4. Wearable Microfluidic Mixer....69

**Chapter 6. Active Wearable Microfluidic Device Combined with Screen-Printable Silver C-NCP....71**
6.1. Design and Fabrication Method....71
6.2. Experimental Methods and Results....75

**Chapter 7. Future Work and Conclusions....80**
7.1. Future Work....80
7.1.1. Additional Characterization....80
7.1.2. Development of New Materials and Devices....81
7.2. Conclusions....82

**References....87**

**Appendix A. List of Publications....95**

**Appendix B. Data of Plastisol Film Stretchability Test....96**

**Appendix C. Data of silver C-NCP resistivity....97**

**Appendix D. Data of Resistivity Change with Different Bending....98**

**Appendix E. Data of Stretchability of the silver C-NCP....100**

**Appendix F. Data of Plastisol Film Thickness Measurements....101**

**Appendix G. Data of Saline Solution Tests with Conductivity Sensor....102**

**Appendix H. Wearable Microfluidic Mixer Design....104**

**Appendix I. Wearable Microfluidic Conductivity Sensor Design.....105**

# List of Tables

Table 5.1. Achievable widths as measured at different laser speeds with design of 76 µm (the finest) channel width. These results are for a single experiment at each width. [85].....58

Table 5.2. Achievable widths as measured at different laser power with design of 76 µm (the finest) channel width. These results are for a single experiment at each width. [85].....59

Table 5.3. Width change measurements at different numbers of bonding repetitions (repeat cycle). Data is only provided for three lamination process steps and greater since at least three repetitions of the lamination process must be performed in order to ensure good bonding of plastisol films. [85].....61

# List of Figures


Figure 1. Screen printing process using C-NCP as an example: (a) The screen is place on the fabric (substrate). (b) The polymer ink is applied on the screen and distributed usinga squeegee. (c) The screen is removed so that only the patterned polymer remains on the fabric. [77] .....17

Figure 2. Design of the micro-ruler, and test scheme: (a) Design of the ruler for sample stretching. Each line is separated by 200 μm to measure the stretch (elongation) of the plastisol film in increments of 200 μm. (b) Test scheme. The bottom of the sample is fixed and the top is aligned to the lines on the ruler via stretching. Samples are stretched by 200 μm increments until failure. [79] .....24

Figure 3. Stretchability test results. Maximum stretchable distance increases as the thickness of plastisol film increases until certain point (around 400 μm) for films 30 mm width × 40 mm length in size. After that point, the breaking point levels off. The vertical error bars show the range of the breaking points and the horizontal bars show the range of thicknesses of each sample group. [79] .....25

Figure 4. Preparation of screen-printable silver C-NCP, and SEM image of silver particles embedded in plastisol meatrix: (a) Mixing processes for the silver C-NCP. (b) Silver particles are connected to each other to form electrical paths. .....28

Figure 5. Resistivity measurements of the screen printable silver C-NCP at different wt% of silver: (a) Test procedure. (b) Graph of resistivity of screen printable silver C-NCP vs. silver wt-%. The point at 58 wt-% is not shown because it has very low conductivity that is very unstable and can not be measured using current equipment. [77] .....29

Figure 6. Resistivity measurements of the screen printable silver C-NCP at different bending angles: (a) Top view and cross view of test procedure. (b) Results showing resistivity versus bending angle for four different wt-% of silver particles (61, 64, 67, and 70 wt-%). The smallest deviation and average resistivity change at all angles are observed at 70 wt-% of silver particles. [77].....31

Figure 7. Stretchability test of silver C-NCP: (a) Photographs of the silver C-NCP structures (70 wt-%) and close-up of damaged structure after breaking point is reached. Physical damage occurs when the C-NCP is stretched beyond a certain distance. (b) Results from C-NCPs with different wt-% of silver. Strechable distance decreases as the amount of silver particle increases.....33

Figure 8. Resistivity change of silver composite polymer: (a) Resistivity change over 10 day period of typical wear and tear on electrodes. (b) Resistivity change with hand-washing. [77] .....35

Figure 9. Screen printed C-NCP on fabric: (a) 2mm diameter circle electrode array pattern. (b) example printed circuit board (PCB) pattern. [77].....36

Figure 10. Printing resolution: (a) A straight line with a 100 μm width is printed on fabric. (b) An array of circle electrodes each with 100 μm diameter is printed on fabric. (c) Close-up of a circle electrode. ..... 37
Figure 11. Fabrication process for flexible, wearable ECG electrodes: (a) Punch the fabric for electrical connection between the sensing electrode and electrical routing. (b) Print silver C-NCP on the front side first and cure it. (c) Print the back side and cure it. (d) Encapsulate partial area on the back side and chloridize the front side to make Ag/AgCl electrodes. [77] ..... 41
Figure 12. Photos of wearable dry ECG electrode: (a) Front side, showing sensing electrode. (b) Back side, showing electrical routing. [77] ..... 41
Figure 13. ECG instrumentation right leg driven signal amplifier. [77] ..... 42
Figure 14. ECG signal acquired using simple driven right leg circuit with input from: (a) ECG simulator. (b) Commercial macro-scale ECG electrodes. (c) Fabricated flexible dry ECG C-NCP electrodes. [77] ..... 43
Figure 15. A Single LED on fabric connected to power supply equipment to show proof-of-concept of the C-NCP for electronic routing between components. ..... 44
Figure 16. Five surface mount LEDs on fabric with battery: (a) Front side with switch and LEDs. (b) Back side with silver C-NCP routing. The battery is connected to the C-NCP routing through the wires. (c) powered LEDS. . 45
Figure 17. Fabrication process of the safety vest with lighting system: (a) Punch the fabric for electrical connection between front side and back side of the fabric. (b) Screen print silver C-NCP on the front side first and cure it. (c) Screen print the back side and cure it. (d) Encapsulate the back for physical protection of the electrical routing. (e) Attach LEDs by soldering. (f) Attach the Battery holder. (g) Encapsulate the front side for physical protection. ..... 46
Figure 18. Photographs of the safety vest with LEDs: (a) Front side with LEDs. (b) Back side with electrical routing, a coin battery, and a resistor. ..... 47
Figure 19. Lighted LEDs on the safety vest: (a) in daylight. (b) in the dark. ..... 47
Figure 20. Fabrication procedure for wearable microfluidic devices: (a) Coat the screen printable plastisol ink on a sheet of paper. (b) Pattern channels on the ink-coated paper with laser cutter. (c) Print the bottom layer on fabric, and bond channel layer. (d) Detach the paper. (e) Prepare the top layer and bond it. (f) Detach the paper. [85] ..... 50
Figure 21. Plastisol ink coating process on paper. Tape is used as an example mask to control the thickness of the plastisol film, and conventional screen-printing squeegee is used to spread the ink. [85] ..... 52
Figure 22. Details for thickness measurement and results: (a) Showing approximately where the nine points for thickness measurements are performed on each film. (b) Comparison between target thickness and measured average thickness with maximum deviation (vertical bars shows the range of values). [85] ..... 53
Figure 23. Photographs showing the effect of squeegee edge roughness: (a) Uneven edge of a squeegee. (b) Photo of uneven surface of coated

plastisol film before planarization, and its surface profile as measured by profilometer. (c) Photo of flattened surface of coated plastisol film after planarization, and its improved surface profile. [85] ..... 55

Figure 24. Measured average thickness of the plastisol film after planarization. The average thickness is decreased due to the applied pressurization of the squeegee during planarization. Vertical bars show the measured ranges of the film thicknesses. [85] ..... 56

Figure 25. Dimension difference as a result of different laser speeds: (a) Expected design showing as-designed dimension for each line width of 76 μm. (b) Patterned lines. The width for each line is different since a different laser setting is used for each line: higher speeds of the laser result in narrower widths. [85] ..... 58

Figure 26. Dimension difference with different laser powers: (a) showing as-designed dimension for each line of 76 μm. (b) Patterned lines. The width for each line is different since a different laser setting is used for each line. Higher power of the laser results in thicker line width. The resulting widths as-fabricated are shown in Table 2. [85] ..... 59

Figure 27. Cross-sectional view of example laser-patterned materials: (a) V-shaped profile on solid polymethyl methacrylate (PMMA) substrate. (b) V-shaped profile on plastisol-coated paper film. [85] ..... 60

Figure 28. Cross-sectional view of the sample microfluidic channel showing the different plastisol polymer layers used to make the channel. [85] ..... 62

Figure 29. Designs and photographs of multi-layer microfluidic channels: (a) Design of parallel channels. Two channels are in parallel on different levels. (b) Photo of a cross-section of the parallel channels. (c) Design of two channels on different levels that intersect. (d) Photograph of cross-section of the device at the microfluidic channels' intersection point. [79] ..... 63

Figure 30. Design of sample channels for stretchability test: (a) Vertical channel. (b) Horizontal channel. Both channels have the same dimensions including thickness. [79] ..... 65

Figure 31. Design of micro-rulers for stretchability test of microfluidic channels: (a) Ruler for microfluidic channel stretching. The microfluidic channel device is attached and aligned to the ruler, and stretched in increments of 500 μm. (b) Ruler for measurement of length increase for the vertical channel. The channel is aligned to the ruler and change in length is observed. (c) Ruler for measurements of width decrease for the vertical channel. (d) Ruler for measurements of length decrease for the horizontal channel. (e) Rulers for measurement of width increase for the horizontal channel. The channel is aligned to the ruler and change in width is observed. [79] ..... 65

Figure 32. Photographs of the sample and channel width measurement: (a) Horizontal channel before stretch. (b) Stretched channel. (c) Broken sample at breaking point. (d) Measurement of the increase in width of the horizontal channel. The initial channel width is 500 μm, and the width is increased upon stretching. It is shown that the width is increased by 150 μm. [79] ..... 67

Figure 33. Photographs of the paper pillars and the testing of microfluidic channel flexibility: (a) Paper pillars with different diameters (5 cm, 4 cm, 3 cm, 2

cm, 1 cm). (b) Test set-up. The flexible channel is attached on the paper pillar, and red ink is injected through the channel using a syringe pump at volumetric flow rate of 5 ml/min. [79] ..... 68

Figure 34. Working flexible microfluidic channel (plastisol only, no textile substrate): (a) Working channel wrapped twice around a paper pillar 1 cm in diameter. (b) Using ball-point pens to demonstrate flexibility that can be achieved yet still result in a working device. [79] ..... 68

Figure 35. Microfluidic mixer: (a) Design of the mixer from top view. (b) Photograph of fabricated mixer with close-ups. [85] ..... 69

Figure 36. Testing of the flexible fluidic mixer: (a) Test on a flat surface showing mixing. (b) Test on a curved cylinder showing unaltered mixing operation. No leakage is observed in either case. [85] ..... 70

Figure 37. Flexible and wearable fluid conductivity sensor design: (a) Cross-sectional view of the device showing one electrode, its electrical routing, and contact pad. The electrode is inside the channel, and the electrical routing is embedded in the device. (b) Top-down view of the device. A pair of silver C-NCP electrodes and a pair of conductive epoxy electrodes are aligned with a microfluidic channel. (c) Detail of the electrodes' design. Each electrode is connected to the contact pad through the electrical routing. [79] ..... 72

Figure 38. Integrated fabrication process for flexible and wearable conductivity sensor: (a) Print the bottom layer on fabric, and print C-NCP electrodes, electrical routing, and contact pads on the bottom layer. (b) Print conductive epoxy electrodes, electrical routings, and contact pads using silver epoxy ink. (c) Prepare the first channel layer, align the channel to the electrodes, and bond to the bottom layer on the same level with electrodes. (d) Print contact pads for both types of electrodes, and prepare and bond the second channel layer. Contact pads are on the same level with the second channel layer. (e) Print the contact pads again, and prepare and bond the top layer. Only the contact pads and inlet/outlet holes are exposed on the device, with all other structures (electrodes, channel, etc.) embedded in the device. [79] ..... 74

Figure 39. Photographs of the device with close-ups and microscope images: (a) Top view of the device and close-up of the conductive active component. The close-up shows a C-NCP electrode in the microfluidic channel so that fluids can flow on the electrode. (b) Cross-sectional view of the silver C-NCP contact pad. (c) Cross-sectional view of the channel on the silver C-NCP electrode. [79] ..... 75

Figure 40. Device test set-up. AC voltage is applied between same type of electrodes, and multimeter is connected in serial to measure the current. The current measurements are performed for all saline concentrations at each applied voltage. [79] ..... 76

Figure 41. Current measurement results: (a) Results from silver C-NCP electrodes. As expected, the current appears to increase linearly as the applied voltage increases. In addition, also as expected, the current increases as the concentration of salt increases. (b) Results from silver epoxy electrodes. The current increases linearly as the concentration of salt increases and applied voltage increases. [79] ..... 77

Figure 42. Comparison between silver C-NCP electrodes and silver epoxy electrodes: (a) Results at 2.0 wt-% of salt concentration with change of applied voltage. (b) Results at 3V of voltage with change of salt concentration. Though the conductivity and sensitivity of silver C-NCP are lower than those of silver epoxy, silver C-NCP electrodes still work in a similar manner with silver epoxy electrodes. [79].....79

# Chapter 1.

# Introduction and Contributions

Wearable and flexible technologies open great possibilities of improving human lives, and have generated a lot of academic and commercial research [1]. For example, wearable technologies enable development of wearable bio-sensors for monitoring of individuals' bio-signals such as long-term in-home monitoring of electrocardiogram (ECG) signals for patients with potential cardiac problems [1]. Wearable motion sensors can be used for rehabilitation of people with physical disabilities [2], and wearable compression textiles with active elements are applied to the field of athletics [3]. In addition, wearable chemical sensors may also be used for monitoring of biological fluids such as perspiration, interstitial fluids, breath, and saliva [4]. In particular, technologies for wearable and flexible microfluidics have enormous potential for healthcare applications [5]. Wearable technologies for collecting and analyzing body fluids enable development of portable and lightweight health monitoring devices that enable early diagnosis [1]. For example, microfluidic devices such as perspiration pH, salt content, or lactate sensors may be combined with flexible technologies, and form a wearable medical platform [6].

Although many different technologies exist for the development of wearable devices and systems, technologies for textile-based wearable electronics and microfluidic systems are not yet fully realized. In this thesis, technologies that can be applied to fabricate devices on textile substrates are developed and demonstrated. The use of clothing for wearable devices and systems has many advantages over other types of wearable technologies. For example, most current wearable technologies involve traditional plastic-encased devices (e.g, watch, glasses, etc.) that must be attached to the user, whereas textile-based technologies involve flexible devices that have a more natural fit to the curves of the human body. Hard plastic-encased devices are accessories that may not encourage usability, whereas clothing is something that is commonly worn on a daily basis. Textile-based devices may be combined with a garment, and can eliminate the need to use external devices that may have complicated attachment procedures. In addition, textile-based devices may enable real-time monitoring without hindering human motion or activity. Although some flexible

technologies, such as wearable tattoo sensors, or paper-based devices, can be applied to wearable systems [7, 8], they have limitations such as difficulty in long term use, and vulnerability to physical damage.

For conventional flexible devices and microfluidic devices, the silicone-based elastomer polydimethylsiloxane (PDMS) is widely used due to its low toxicity, thermal stability, low electrical conductivity, and low cost for prototyping [9]. It is also highly flexible, making it a candidate for wearable systems. However, PDMS is primarily satisfactory for passive microfluidic structures; PDMS-based devices that are active, e.g., sensors or fluid manipulation components such as valves, must include other materials such as metals in order to function. This is not a problem for devices that are not meant to be flexible and wearable. However, for flexible and wearable microfluidic devices and systems, PDMS must be integrated with other materials for electrical function, which can prove difficult because of weak adhesion between PDMS and these other materials [10]. In addition, PDMS and other flexible polymers such as polyimide are employed for a few existing wearable and flexible microfluidic devices and systems [11, 12]. However, PDMS and many other polymers are not designed specifically for patterning on textiles for textile-based wearable microfluidic systems. In particular, PDMS is a difficult material to work with in terms of curing times and low viscosity which can deform patterns on textile substrates.

In order to overcome these limitations, new materials and fabrication methods must be developed and investigated for electronic and microfluidic systems on textile substrates. One potential solution is to employ materials designed specifically for printing on textiles for engineering rather than artistic designs. Many methods such as soft lithography, polymer micromolding, and wax printing are used for wearable and flexible microfluidic systems [13, 14, 15], but most of these techniques cannot be used for the fabrication of microfluidic devices directly on textiles. Although wax printing processes are performed on textiles, resulting devices are disposable and cannot be used repeatedly. Wearable devices must be essentially adhered to the textile substrates afterwards without hindering the flexibility of the textile.

In addition to passive microfluidic structures (e.g., fluidic channels and chambers), active devices must also be developed. To overcome the aforementioned problems of integration between flexible polymers and metals, functional polymers embedded with

nanoparticles for applications in smart textiles, wearable electronics, health monitoring systems, sensors, microfluidics, and microelectromechanical systems (MEMS) are developed. To develop nanoparticle composite polymers, silicone elastomers such as PDMS and the silicone based elastomer sealant (Dow Corning 734) are previously demonstrated by the Simon Fraser University (SFU) Microinstrumentation Lab for development of conductive nanoparticle composite polymers (C-NCPs) and magnetic nanoparticle composite polymers which are micro patterned on PDMS substrates for electronic routing, sensors, mixers and valves [16, 17]. However, as mentioned, PDMS is not an optimal material for patterning on textile substrates.

In this thesis, we present the development and investigation of the PVC-based screen-printable polymer plastisol for development of wearable electronics and wearable microfluidic devices on textiles. A new C-NCP material is designed using plastisol as the polymer base and silver nanoparticles for conductivity (resulting in silver C-NCP), and a new fabrication method for plastisol-based wearable microfluidics is developed. Thus, one of the two main goals of this thesis is to develop a new type of screen-printable C-NCP by using the new base polymer plastisol for wearable devices and systems. The new plastisol-based C-NCP provides good adhesion to textiles, and the fabrication process enables fabrication of electronic structures via screen-printing directly on textiles. The C-NCP is patterned on textiles using a simple screen printing technique which is easy, inexpensive, and has a long history of being applied to making multi-level patterns on clothing. The C-NCP is then demonstrated in applications that include a wearable health monitoring application (ECG), and a safety application (safety vest with lighting systems), that both showcase different aspects of the screen printable C-NCP's potential.

The second main goal of the thesis is to develop fully wearable and flexible microfluidic devices and systems that are cheap, simple, and easy to fabricate. In this thesis, a new fabrication method for wearable microfluidic devices and systems is presented. The new fabrication method is easy, simple, and fast, and the microfluidic devices can be directly fabricated on textiles using plastisol polymer. In addition, by combining the screen printable C-NCP and new microfluidic fabrication methods, wearable active microfluidic devices that have electrically-active components (e.g., electrodes, or electrical routing) are fabricated. The fabrication process is then

demonstrated in applications that include a simple wearable passive microfluidic mixer, and a combined C-NCP combined wearable microfluidic fluid conductivity sensor.

In summary, the contributions of this thesis are as follows:

1. Development of fabrication processes for flexible wearable devices and systems on textile substrates featuring a plastisol polymer that is intended for screen-printing based patterning on textiles:

    1a. Development of a screen printable C-NCP, together with a screen-printing based fabrication method, for patterning on textiles.

    1b. Development of a multi-level wearable microfluidic technology using paper as a sacrificial substrate.

    1c. Combined wearable microfluidic and C-NCP electronic fabrication process on textiles for active microfluidic devices.

2. Demonstration of various devices that showcase the new material and fabrication processes. Each of these new devices not only showcases the new materials and fabrication technologies, but makes significant contributions to the fields of wearable health and safety devices:

    2a. Wearable dry ECG electrodes for measuring heart signals, showing comparable performance to commercially available electrodes.

    2b. Wearable safety vest lighting system that operates in flexed and non-flexed conditions with user-defined pattern.

    2c. Wearable passive microfluidic device (microfluidic mixer) that operates in flexed and non-flexed conditions.

    2d. Wearable active microfluidic devices (fluid conductivity sensors) with integrated microfluidic and C-NCP electronic structures.

This thesis consists of seven chapters. In chapter 2, a summary of prior research by other researchers and their limitations are given in order to motivate the proposed work. Also, materials and methods used to solve the limitations are introduced. In chapter 3, flexibility tests for plastisol films are performed, and a general explanation of

the screen printable C-NCP is presented. The required properties of a good C-NCP, the procedure of preparation, and the electrical characterization of the newly developed screen-printable C-NCP are presented. In chapter 4, demonstrator devices are presented that use the technologies developed for C-NCPs for this thesis. Dry wearable ECG electrodes are demonstrated as a biomedical application with fabrication process and test results. In addition, a safety vest with lighting system is also demonstrated whereby C-NCP is patterned on a commercially available safety vest and used as electrical routing for surface mount LEDs. Chapter 5 introduces the new fabrication process for wearable and flexible microfluidic devices in detail. In addition, optimization and characterization for the fabrication method are presented. In chapter 6, the screen-printable C-NCP is combined with the new microfluidic fabrication method for wearable microfluidics to demonstrate fully flexible active microfluidic devices. A fluid conductivity sensor is developed, characterized, and tested. Lastly, the overall conclusions and summary are presented in chapter 7.

# Chapter 2.

# Background, Challenges, and Overall Solution

Wearable devices are typically electronic devices with micro-controllers that can be worn on the human body as accessories or implants [18]. Extensive efforts are made in research and development of wearable devices and systems, and the field of wearable systems continues to grow. In addition, as the world population ages, development of wearable devices such as microfluidic sensors for health monitoring is accelerating [19].

Many technologies are developed and applied to the development of wearable devices, including the development of flexible electronics and other microsystems that enable lower profile wearable systems that may conform to the body or tissues. In order to achieve high flexibility, many kinds of materials and methods are used to fabricate flexible wearable devices [19]. For example, carbon-based nanomaterials, metallic nanoparticles, conductive textiles, and conductive polymers can be used as conductive materials for wearable devices [20, 21, 22]. Fabrication methods such as photolithography, soft-lithography, thin film deposition, different kinds of printing techniques, and different kinds of coating techniques are used to fabricate wearable devices [23, 24, 25]. Although these materials and methods can be used for flexible electronics and applied to wearable applications, many of them cannot be used for textile-based wearable devices and systems. Textile-based wearable systems are a type of wearable system that is typically defined as electronic devices that can be embedded unobtrusively in a user's clothing [26], and some methods such as conductive fibers and textile-based microfluidic devices are used for textile-based devices. However, there are many limitations and disadvantages to current technologies for wearable systems on textiles.

In this chapter, prior works by other researchers are reviewed briefly and limitations of the works are summarized. In addition, the new materials and methods developed for the thesis that are used to address limitations of prior works are introduced, and the needed background for these techniques discussed. The basic

properties and benefits of the materials and methods are also explained. Lastly, limitations that are addressed by the thesis work are and identified and summarized.

## 2.1. Fabrication Methods and Materials for Wearable Devices and Systems

Different methods can be used to develop flexible and wearable devices. Some of them are not textile-based, but can be applied to wearable applications and also have a high level of flexibility. Some other methods are textile-based such that the wearable devices are fabricated in or on textiles. In this section, general methods that are applied to flexible wearable devices and systems are reviewed, along with a discussion of their benefits and limitations.

### 2.1.1. Metal Deposition on Flexible Substrates

One approach to develop wearable electronic devices is to coat or pattern thin metal films on flexible substrates. For example, H. Kudo et al. develop a wearable glucose sensor using flexible electrodes [23]. Thin metal films are patterned on flexible PDMS substrates using microfabrication techniques. Metal films are coated on PDMS substrates directly using methods such as metal sputtering, and UV lithography is used for patterning. However, these methods require a relatively complicated fabrication process, expensive equipment in cleanroom facilities, and long fabrication times. Furthermore, metal films on PDMS easily crack when they experience stress, and they may be easily peeled off due to weak adhesion between metal and PDMS [27].

To address the problems of weak adhesion between metal films and polymer substrates and metal cracking, some researchers use different techniques. C. Chen et al. develop a PDMS electrode for a wearable and wireless bio-potential acquisition device [28]. They deposit a gold layer on PDMS using an E-beam, and perform a surface treatment with a $CO_2$ laser to increase the adhesion between the gold layer and PDMS. Although the adhesion between the gold layer and PDMS is increased, a surface treatment process must be added to increase the adhesion, and a clean room facility and E-beam must be used. Thus, the fabrication method requires some expensive equipment, cleanroom facilities, and relatively long fabrication times. R. Matsuzaki et al. also develop stretchable strain sensing electrodes for wearable electronics [29]. They

use liquid metals instead of solid metals to acquire more stretchability (capacity for extension to the full length). GaInSn liquid metal is embedded between two PDMS layers. The problem of solid metal film cracking is addressed using this method, but complex photolithography techniques are required, and the risk of leakage of the liquid metal exists.

Recently, tattoo-based wearable devices (so-called for their resemblance to temporary tattoos) are also developed by coating conductive materials on flexible substrates. Tattoo-based devices can then be attached directly to skin using adhesives for monitoring of bioelectric signals or bio-fluids. The basic fabrication process includes the printing of active ink materials like carbon and silver/silver chloride (Ag/AgCl) on temporary tattoo papers to form electrodes. Encapsulation of the electrodes is also carried out by printing insulator films to protect the electrodes. A. J. Bandodkar et al. develop tattoo-based device for glucose monitoring [7], and T. Guinovart et al. develop a potentiometric tattoo sensor for ammonium monitoring in sweat [30]. Ag/AgCl ink and carbon ink are used for both devices. The process is simple, but the device is disposable and not suitable for long term use because the lifespan of temporary tattoo devices is not long (typically 3 to 7days) [31].

### 2.1.2. Flexible Conductive Composites

Instead of patterning metal films on flexible substrates, other researchers develop conductive composites by mixing conductive materials into non-conductive polymers. These conductive composites can be prepared using different kinds of conductive particles (e.g., metals, alloys, or carbon nanotubes) and base polymers (e.g., silicones), and can be mixed by techniques like ultrasonification, ball milling, and shear mixing [32, 33, 34]. Conductive composites can be applied to flexible applications that require both electrical function and mechanical flexibility.

To develop conductive composites, many researchers use carbon nanotubes (CNTs) due to their good mechanical, electrical, and thermal properties and relatively inexpensive price if specific nanotubes (e.g., single-walled) are not required. CNTs are widely used for their electrical conductivity and mechanical stiffness, and mixing CNTs with a polymer is a simple and easy way to prepare conductive composites. For example, H. Jung et al. fabricate wearable flexible dry ECG electrodes using a carbon nanotube

(CNT)/PDMS composite [20]. They simply mix CNTs with PDMS, pattern via soft lithography, and use the resulting C-NCP for electrodes. In a different paper, A. Giuliani et al. use a different polymer than PDMS [32]. They use ultrasonication to mix CNTs with a poly(vinylbenzyl chloride) derivative with triethylamine (PVBC_Et3N) to develop wearable skin temperature sensors. PVBC_Et3N is used due to its high glass transition temperature, which is suitable for temperature sensing, and better interaction with CNTs. J. Lee et al. also develop CNT/PDMS composites for ear electrodes that fit in the ear canal for electroencephalogram (EEG) recording [35], and Q. Li et al. develop CNT/PDMS composite for wearable motion sensors [36]. With the conductive composites, problems of metal cracking and weak adhesion can also be addressed. However, the conductivity of CNTs is lower than the conductivity of metal, and its polarizable property is not suitable for many biomedical applications. For biomedical applications, non-polarizable electrodes are often desired because polarizable electrodes change their behavior when charged as they have a high capacitive element, and thus are not stable over a wide frequency range [37]. Furthermore, while the devices that employ CNT composites are flexible and may be applied to wearable applications, they do not appear to be typically fabricated on textiles.

A number of researchers use metallic nanoflakes, or nanowires to make conductive composites. R. Zhang et al. develop a highly conductive composite by thermal sintering of silver nanoparticles with silver flakes dispersed in a polymer matrix [21]. B. You et al. develop a wearable piezo-capacitive pressure sensor using silver nanowire composite [38], and S. Choi et al. also use silver nanowire composite to fabricate stretchable heaters [39]. By using metallic nanomaterials, higher conductivity than CNTS may be achieved. However, metallic nanowires and nanoflakes are more expensive than nanopowders [40]. Furthermore, screen printable conductive composites that can be printed on textiles are not demonstrated in these papers.

There is some existing research in patterning conductive materials on textiles. G. Paul et al. screen print commercial silver inks on textiles, and test the durability of the conductive tracks [41]. However, they find that the commercial silver inks are not entirely flexible, and the conductive tracks must be encapsulated with polyurethane for protection. Z. Stempien et al. print commercial conductive materials such as polyaniline (PANI) and polypyrrole (PPy) on textiles by reactive inkjet printing [42]. However, an

inkjet printer designed to dispense one or more reactants onto a substrate is required to generate a physical or chemical reaction, and hazardous chemicals such as ammonium peroxydisulfate, and aniline hydrochloride are used.

### 2.1.3. Conductive Fibers

Unlike metal film deposition on flexible substrate, or developing conductive composites by mixing conductive particles with polymer, another way to develop wearable devices with electronic functionality is to make conductive fibers (threads), and use them for active electrical components such as sensors, electrodes, or electrical routing. Such fibers can be employed using different kinds of methods. For example, L. Hu et al. develop conductive textiles for energy storage devices [22]. B. Shim et al. also develop conductive textiles, and use them for biomonitoring sensors [24], and J. Han et al. develop an ammonia sensor on cotton textiles using CNT-coated yarns [43]. All of these devices employ CNTs to make the fabric conductive, and use a dip-coating process. Conductive textiles are prepared by dipping threads or small textile pieces into an aqueous single walled carbon nanotube (SWCNT) ink followed by drying. However, even though carbon-based conductive fibers obtained from the dip-coating process appear to have good stability, their conductivity is lower than the conductivity of metals.

Instead of using carbon materials, some researchers use metal to metalize textile fibers and render them conductive. B. K. Little et al. perform metallization of Kevlar yarns using an electrochemical gold plating processes [44], and F. Ochanda et al. develop conductive fibers using an electroless deposition method [45]. X. Liu et al. also use an electroless deposition method to prepare conductive fibers [46]. Both electro- and electroless-plating processes have excellent electrical properties, but the stability is very poor. The conductive fibers show decay of electrochemical stability over time. As a result, deposition and plating methods cannot be used for long term use. G. Gioberto et al. also develop a stretch sensor using silver-coated nylon [47]. They use an industrial overlock machine to develop the sensor, and commercial conductive fibers are used.

## 2.2. Wearable and Flexible Microfluidic Devices

Microfluidic is the technology that manipulates liquids with channels in micro-scale, and has been widely used in biomedical field with the lab-on-a-chip, or in cell biology [48]. Wearable microfluidic technologies are of great interest due to their potential for wearable technologies in healthcare applications. Wearable technologies combined with garments for collecting and analyzing of body fluids enable development of portable and lightweight real-time health monitoring devices. However, fully wearable microfluidic devices and systems that are suitable for long-term use are not realized yet.

As the world population ages, technologies for wearable and flexible microfluidics and biomedical devices offer new methods to diagnose disease and monitor health. For flexible and wearable microfluidics, two types of materials are most commonly used; paper and textiles. In this section, different approaches for wearable and flexible microfluidics based on both types of materials are reviewed and summarized. Paper-based microfluidics, microfluidics on textile, and wearable patches that may involve both types of materials, are reviewed, and their advantages and limitations are discussed.

### 2.2.1. Paper Microfluidics

Many researchers develop paper-based microfluidics for portable and inexpensive diagnostic devices. Paper-based microfluidic devices are fabricated by selectively making the paper hydrophobic. The hydrophilic areas work as a channel by absorbing the liquid and acting as the “channel” for liquid flow, and hydrophobic areas define the boundaries where liquid does not penetrate. Different methods can be used to make hydrophobic barriers. Z. Nie et al. develop paper-based microfluidic devices for electrochemical sensing [49], and A. W. Martinez et al. develop a paper-based platform for bioassays [8] using SU-8 photolithography to fabricate the devices. The S-8 photoresist is used to block the pores in paper, and make the paper hydrophobic. Photolithography enables high resolution of microfluidic channels. However, as mentioned earlier, photolithography requires relatively expensive equipment, and an extra washing step is required to remove un-crosslinked photoresist. Furthermore, patterning paper with photoresist is less flexible compared to patterning with wax [50].

Other methods such as inkjet printing and wax printing can also be used for paper microfluidics. J. L. Delaney et al. and X. Li et al. develop paper microfluidic devices using inkjet printing [25, 51].Chemical modification of fibre surfaces is performed to make the paper hydrophobic using the inkjet printer machine. Inkjet printing is simple and suitable for mass production, but requires a modified inkjet printer machine. Y. Lu et al. and W. Dungchai et al. use wax printing techniques to fabricate paper-based microfluidic devices [52, 53]. They physically print solid wax on the paper to make the paper hydrophobic. Wax printing is a simple and fast method; however, wax printing has fairly low resolution and requires specialized wax printing equipment that is no common [54]. Also, although paper-based microfluidic devices have some advantages, paper-based devices are disposable and typically have low reproducibility and low sensitivity [55]. Moreover, paper-based microfluidic devices require large volumes of samples compared to conventional microfluidic devices due to the slow wicking process [56].

### 2.2.2. Microfluidics on Textile with Wax Printing

Instead of using a paper, some researchers develop textile-based wearable microfluidic devices. By selectively making the textiles hydrophobic, liquid flow can be controlled. The textile absorbs the liquids and works as a channel using capillary flow, or “wicking” to move the fluid. R. S. P. Malon et al. fabricate fabric-based electrochemical devices [57], and M. Liu et al. and A. Nilghaz et al. also develop textile-based microfluidic analytical devices [14, 58]. All of this research uses wax printing techniques to make the textiles hydrophobic. However, textile-based microfluidic devices suffer from many problems, such as difficulty in use for different types of liquids, and difficulty in repetitive use [14, 57, 58]. It is speculated that biological components in the liquid may be attracted to textiles fibers, resulting in loss of biological component or contamination. Thorough washing may need to be performed in order to remove contaminants.

### 2.2.3. Wearable Microfluidic Patches

Making paper or a textile selectively hydrophobic is one way to develop flexible and wearable microfluidics. However, paper and textiles can also be used in other ways for flexible and wearable microfluidic. Some researchers develop flexible microfluidic devices that can be adhered as patched onto the human body using the paper or textile.

X. Xu et al. develop a wearable fluorescence device for chloride analysis in sweat [59]. They use a piece of cotton as the substrate material. The cotton is coated with chloride sensing materials and attached to a band-aid for chloride sensing. S. Anastasova et al. also develop a sweat monitoring patch with a flexible microfluidic platform [60]. The microfluidic patch consists of layers of polymethyl methacrylate (PMMA) polymer, paper microfluidics, and sensors in the paper channel. The channel and sensors are placed between two PMMA substrates. Similarly, J. Heikenfeld et al. develop a microfluidic patch for sweat sensing [61]. Paper is used to wick sweat from the skin and the sensor is combined with circuitry to calculate the ion concentration. The paper channel and circuitry are covered by textile and a sweat-porous adhesive is used as the bottom layer for attachment to skin. All devices are tested on the human body, and the fabrication methods are simple. However, the devices are disposable and not suitable for reuse. The devices are designed for single use.

A. Koh et al. also develop a sweat sensing patch [62]. To develop the device, PDMS is used as a base polymer and an adhesive layer is used for attachment to skin. Instead of using electrodes, they use a colorimetric sensing method. However, the device is not combined with textiles and is disposable. Similarly, J. Choi et al. develop skin-mounted microfluidic systems using PDMS [63], but active electrical components are not used, and the devices cannot be used repeatedly.

## 2.3. Methods and Materials Used in This Thesis

This section serves to provide a general introduction and background information for materials and techniques developed in the remainder of the thesis. The discussed materials and techniques are designed for printing on textiles, and used to develop textile-based devices.

### 2.3.1. Screen Printable Polymer

A polymer for printing of biomedical and microfluidic devices on textiles should be flexible, easily printable on fabric for wearable applications, and easily patternable. PDMS is also well known silicone elastomer with good chemical stability, durability, and mechanical flexibility [9]. However, PDMS requires an additional curing agent, and the

curing time is more than 48 hours at room temperature and 30 minutes at 100 °C. Also, when PDMS is screen-printed, PDMS residue on the screen can easily block the screen because PDMS is curable at room temperature. The blocking causes deformation of the pattern on the screen. Furthermore, due to the curing time and relatively low viscosity of PDMS (about 3500 cPs), deformation of the printed PDMS pattern is observed even with a carefully controlled process.

A plastisol is a non-conductive liquid ink containing polyvinyl chloride (PVC) resin dispersed in a plasticizer. PVC is the world's third-most widely produced thermoplastic polymer, and can be made flexible by mixing with plasticizers [64]. When the PVC plastisols are heated, the plasticizers diffuse into the dispersed polymer particles, and produce plasticization of the PVC plastisols. Unlike PDMS, screen printable plastisol inks can be printed on textiles easily and cured in a short time. Also, the viscosity of the plastisol can easily be tailored from very high to very low by controlling the amount of PVC in the plastisol [65], with high viscosity plastisols resulting in patterns with low deformation. Plastisol inks are commonly used for printing artistic designs on textiles [64], and are washable because they are not water-soluble and hydrophobic. These properties make plastisol inks suitable for wearable applications where devices are screen-printed on textiles. In addition, they are very inexpensive and not curable at room temperature, and do not require a curing agent.

In this thesis, we employ an inexpensive and easy-to-use screen printable plastisol ink (LFP-1060 crystal gel, P-5011 curable reducer, QCM Polymers). Some other plastisol inks that contain phthalates in the plasticizer can be toxic. However, plastisol inks from QCM don't use phthalates, and are suitable for biomedical applications. Some researchers also use non-toxic plastisol inks for biomedical applications. G. M. Spirou et al. use plastisol for tissue phantom fabrication [66], and A. K. Singh et al. develop lead free X-ray shielding polymer composites using plastisol [67]. The plastisol from QCM contains 10-30 weight percentage (wt-%, the ratio of a substance's mass to the total mass of the mixture) of PVC, and is designed to work below 204 °C. The flexibility of the plastisol ink is high, and its mechanical properties are characterized in chapter 3.

### 2.3.2. Conductive Nanoparticles

According to the Publicly Available Specification 71 (PAS71) document developed in the UK, a nanoparticle is a particle of the order of 100 nm or less, i.e., at least one dimension of the particle should be smaller than 100 nm. Many properties of nanoparticles are different from those that have sizes measured in micrometers, or from bulk material [68]. Many types of nanoparticles that consist of metal (gold, aluminum, or silver), elements (graphene, CNT's, or carbon), alloys (Zinc Iron, or Nobium), or oxides (Iron III oxide) have become commercially available [69] which makes researching with these particles easier than in previous years.

Nanoparticles can be classified according to their shape: nanopowders, nanotubes, nanoflakes, nanoplates, nanowires, etc. A nanoparticle's shape is an important factor to be considered when developing a conductive polymer employing the nanoparticle because the shape of the particle significantly affects the electrical properties of the nanocomposites. According to electromagnetic wave percolation theory, if the dimension of the conductive particle is nanometer-sized and has a high-aspect ratio, the particles can more easily form a conductive network at smaller wt-% [70]. In other words, it is easier to get high conductivity with high aspect ratio particles such as nanotubes or nanorods because these particles can make electrical paths more easily. It is also proven that the needed amount of particles is reduced if the particles have high-aspect ratio [71]. The percolation threshold, which is the critical value of density when formation of long-range connectivity in random systems first occurs [72], is inversely proportional to the aspect ratio of the particle.

For this thesis, silver nanopowders (NanoAmor, 99% purity, 90-210nm size) are chosen as the conductive nanoparticles. Other materials such as gold or platinum are also available, but silver particles are chosen for their high conductivity, relatively low price (compared to, e.g., gold or platinum), and their potential to make nonpolarizable Ag/AgCl electrodes, which is proper for biomedical applications, through a subsequent surface chlorination step. The Ag/AgCl electrode is a practical electrode that satisfies the characteristics of a near-perfect nonpolarizable electrode, and can be used as a reference electrode as well. Many researchers also use silver nanoparticle composite polymers for biomedical applications [73, 74, 75] due to long-lasting antimicrobial property.

### 2.3.3. Screen Printing Techniques

In order to develop wearable and flexible devices, screen printing is selected to print both the non-conductive plastisol and the C-NCP on textiles. This technique forces a polymer through a screen or mask by applying pressure from the reverse side using a “squeegee” [76]. The traditional screen is made of mesh stretched over a frame, and a stencil is formed by blocking parts of the screen so that polymers only flow through the open spaces. We have found that this method, using a screen and plastisol-based silver C-NCP, works well (much better than, e.g., silver/PDMS C-NCP); however for most of the work in this thesis, thin flat materials (e.g. a piece of paper, thin PMMS substrate, or adhesive tape) with open areas are used as “screens” instead. To make such screens, a $CO_2$ laser ablation machine (VLS3.60, VersaLASER) is used to cut the thin materials. Different kinds of screens with different patterns are prepared using different materials and pattern designs. Figure 1 shows the general screen printing process being used for C-NCP; however, this process of course also works for the plastisol polymer that does not contain nanoparticles. First, the fabric is placed on the plate of screen printing equipment. Then the screen is placed and aligned on the fabric. After alignment, the prepared C-NCP is applied on the screen and scraped using the squeegee so that the polymer passes through only the open areas. Lastly, the screen is removed so that only the patterned polymer remains on the fabric. Because of the high viscosity and short curing time of the plastisol and plastisol-based nanocomposite polymer, it is possible to produce very homogeneous conductive patterns with uniformly dispersed conductive particles in the polymer base. It is also possible that pressure applied by the squeegee during the scraping process also aids in maintaining homogeneity of the patterns and uniformity of particle distribution, which in turn results in more reliable performance and lower energy consumption.

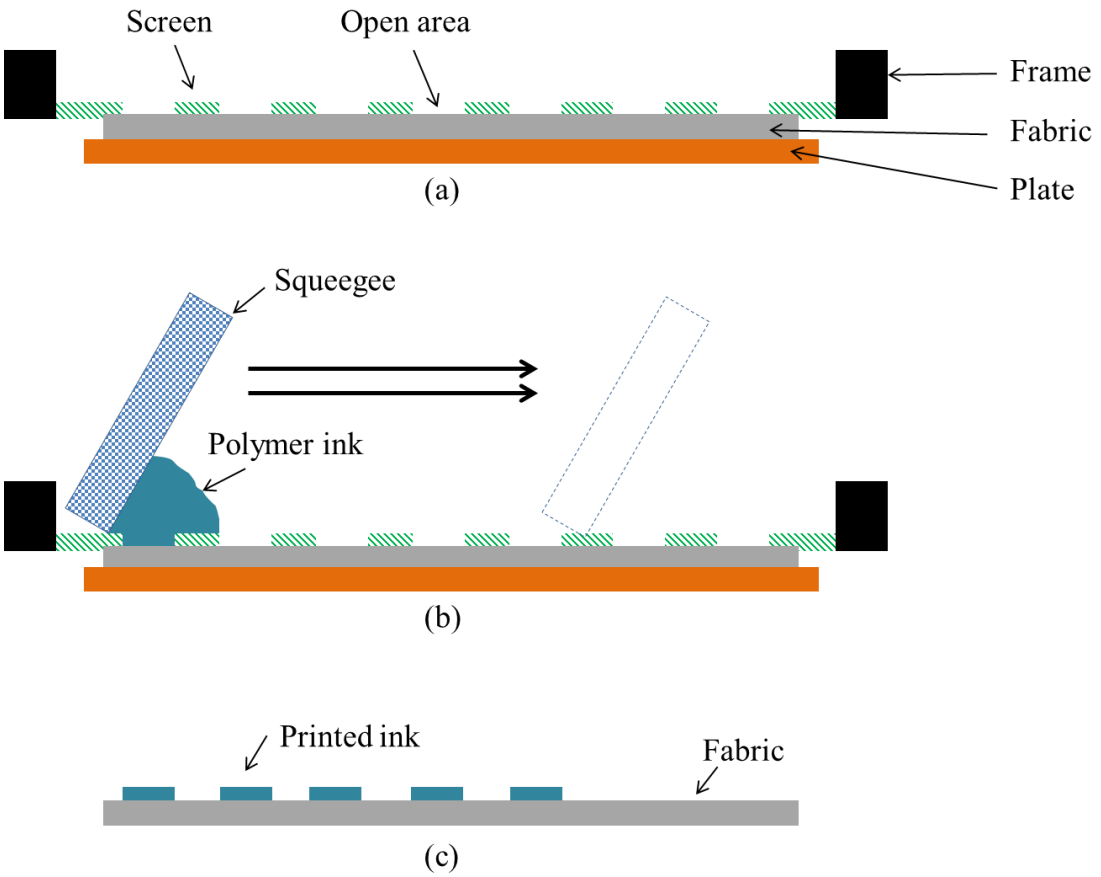


**Figure 1.** **Screen printing process using C-NCP as an example: (a) The screen is place on the fabric (substrate). (b) The polymer ink is applied on the screen and distributed usinga squeegee. (c) The screen is removed so that only the patterned polymer remains on the fabric. [77]**

### 2.3.4. Patterning of Films by Laser Cutter

Laser cutting technique can be used to prepare screens from different kinds of materials. The output of a high-power laser is used to cut the materials, and the laser can be controlled using a motion control system. The focused laser beam is directed at the material to either melt or burn it, and the extent of the melting and burning depends on the power and speed of the laser. Different power and speed setting can be used depends on the type and thickness of the materials (detailed characterization for power and speed change effect is explained in section 5.2). In this thesis, laser cutting is used because it is very simple and easy to use. Almost any kind of pattern can be designed using a computer program called CorelDraw, and the laser machine receives the design

from the computer directly and starts working. In addition, different kinds of materials such as paper, wood substrate, hard plastic substrate, flexible polymer film, and thin metal film can be cut using the laser machine. Different types of screens can be prepared easily. Lastly, micro-scale resolution can be patterned using the laser machine: microstructures that have 100 μm size can be cut using the laser machine [69].

## 2.4. Addressing Limitations of Prior Art: New Approach Presented in the Thesis

To address the limitations of previous biomedical and microfluidic device fabrication techniques, we develop new fabrication methods for wearable microfluidic devices with electronic functionality using new plastisol-based materials and microfabrication techniques. The materials have suitable properties for wearable applications, and the fabrication method provides an easy, simple and fast way for wearable devices on textiles.

Plastisol-based C-NCP is developed by mixing conductive nanoparticles with plastisol polymer, and directly printed on textiles for electrical functionality. The C-NCP is used as electrodes and electronic routing, and can be covered with non-conductive plastisol such that electronic routing is embedded while other surfaces, e.g., electrodes, remain exposed to skin or biofluids. Wearable devices and systems with small size, mechanical flexibility, good conductivity, and long life time are developed. New fabrication techniques for textile-based wearable microfluidics are also developed using the plastisol ink. Each layer of the device is prepared separately and bonded together to form the device. A simple screen printing technique is used to form thin plastisol films, and a laser cutter machine is used to pattern the plastisol films. Using this new method, flexible microfluidic devices are fabricated directly on textiles with enclosed microfluidic channels. Unlike textile-based microfluidics with wax printing, the textile acts as a substrate for the electrical and microfluidic devices, and therefore, the fluid sample can be isolated in the channel, thus minimizing the problem of change in signal with sample evaporation, as can happen with other wearable devices rely on wicking and where channels are not enclosed. Lastly, the screen-printable C-NCP is combined with the new microfluidic fabrication method to develop fully wearable active microfluidic devices.

## 2.5. Summary of Prior Art and Solutions

In summary, the limitations of prior research for flexible and wearable systems, including those based on textiles, are as follows:

1. Materials:

    1a. Weak adhesion between metal film and polymer substrate where metal-on-polymer structures are used

    1b. If employed, low conductivity of conductive polymers (e.g., CNTs)

    1c. Use of polarizable electrodes which are not suitable for many biomedical applications

2. Fabrication process:

    2a. Complicated fabrication methods, expensive equipment, and long fabrication times

    2b. Difficulty in fabrication on textiles

3. Performance:

    3a. Disposable devices which are not suitable for long term use

    3b. Evaporation of fluid sample which may cause the problem of change in signal

    3c. Partially flexible devices which can hinder human motion or activity

In this thesis, the problems mentioned above are addressed and potential methods to help solve these problems are investigated. The proposed solutions are as follows:

1. Materials:

    1a. New screen-printable C-NCP is developed using the same base polymer for good adhesion

1b. Silver nanoparticles are used to achieve relatively high conductivity

1c. Non-polarizable Ag/AgCl electrodes are developed

2. Fabrication process:

2a. Simple and easy fabrication methods are used

2c. New fabrication methods which enable direct fabrication on textiles are developed

3. Performance:

3a. Devices which can be used repeatedly are developed

3b. Wearable microfluidic devices that can isolate sample fluid are developed to prevent sample evaporation

3b. Fully flexible devices are fabricated without hindering the flexibility of the textile

Detailed preparation and characterization of the screen-printable C-NCP are introduced in chapter 3. The C-NCP addresses the problems of low conductivity of conductive polymer by using highly conducive silver nanoparticles, and Ag/AgCl C-NCP is prepared to achieve non-polarizable property. The use of plastisol ink enables direct printing of C-NCP on textiles, and provides good adhesion to non-conductive plastisol substrates. Also, the flexibility and high conductivity of the screen-printable C-NCP enables development of fully flexible and wearable devices. In chapter 4, example demonstrator devices are introduced. Wearable dry ECG electrodes and safety vest with lighting systems are developed using the screen-printable C-NCP. All the devices are fabricated directly on textiles to solve the problem of partial flexibility. The devices are also washable and can be used repeatedly. A completely new fabrication method for wearable microfluidic devices and systems are developed for the first time and demonstrated successfully in chapter 5. Liquid can be controlled without contaminating the textile or experiencing significant evaporation. Lastly, both screen-printable C-NCP and the new fluidic fabrication method are combined in chapter 7. By combining screen-printable C-NCP and the fabrication method for wearable microfluidics, fully wearable active microfluidic devices are developed. An example wearable fluid conductivity sensor

device is fabricated and presented. To fabricate all the devices and systems presented in this thesis, only simple and easy techniques such as screen printing and laser cutting are used to solve the problems of complicated fabrication methods, needs for expensive equipment, and long fabrication times.

# Chapter 3.

# Screen-Printable Polymers for Wearable Microfluidics and Electronics

This chapter discusses the development of screen-printable polymers for applications in textile-based wearable fluidic and electronic devices and systems. This includes the basic characterization of a widely used screen-printable plastisol polymer to determine its stretchability, and development of a new C-NCP based on plastisol. This C-NCP primarily differs from previously developed C-NCPs in that it is designed to be easily printable on textiles for electronic routing, electrodes, and other electronic structures.

Similar techniques that are employed for already developed C-NCPs are used to develop the new C-NCP. In the Microinstrumentation Lab, the technique that we typically employ to make any C-NCP is to mix conductive particles into a non-conductive polymer so that the polymer can be rendered conductive [16, 78]. Non-conductive polymers can be converted to conductive polymers by dispersing suitable nanoparticles in the polymer matrix. In order to make a C-NCP that is easily printed (patterned) on textiles, the characteristics of the base polymer, nanoparticles, and patterning techniques are considered.

Most of this chapter outlines the development of the screen-printable C-NCP for use in flexible fluidic and electronic microdevices and systems. For the polymer base, this includes a basic analysis of the flexibility of the plastisol. For the C-NCP based on the plastisol, this includes the desired characteristics of a textile-printable C-NCP; the development of the new C-NCP that meets these requirements; and the electrical characterization of the C-NCP.

## 3.1. Plastisol for Wearable Devices and Systems

As mentioned in chapter 2, screen-printable plastisol ink is used for development of wearable and flexible devices and systems. The plastisol is non-toxic, not harmful to

ecosystems, flexible, easily printable on textiles, and easily patterned. In addition, plastisol is very inexpensive (less than $100/gallon). In this section, the stretchability of the plastisol film is characterized in order to develop wearable and flexible devices and systems. This characterization is needed to facilitate development of more complex devices and systems, including multiple layers of channels, development of the C-NCP, and integration of microfluidic channels with C-NCP electrodes and electronic routing.

To test the stretchability of the plastisol films, ninety samples of plastisol film are prepared. Each sample has the same width and length (30 mm width × 70 mm length), but has a different thickness. Samples are sorted into thirteen groups by thickness (65 to 100 μm, 100 to 135 μm, 135 to 170 μm, 170 to 205 μm, 205 to 240 μm, 240 to 275 μm, 275 to 310 μm, 310 to 345 μm, 345 to 380 μm, 380 to 415 μm, 415 to 450 μm, 450 to 485 μm, and 485 to 515 μm) with six to eight samples per group. In order to limit testing to only the plastisol films, each plastisol film is tested without a textile substrate (not printed on textile). Plastisol is printed on paper without a pattern, cured, and detached from the paper (see section 5.1 for how this is accomplished) to result in simple un-patterned samples that are not printed on textile substrates (stand-alone plastisol films). Each sample is stretched in increments of 200 μm, and the stretched length at which each sample fails is recorded.

To stretch each sample in increments of 200 μm, a micro-ruler with lines that are separated by 200 μm is prepared. Samples are attached to the ruler using adhesive tape such that only the middle of the sample (30 mm width × 40 mm length) is stretched. Figure 2 shows the ruler design and test scheme. The ruler is split into a right side and a left side with lines separated by 200 μm on both sides (see Figure 2 (a)). A laser cutter is used to engrave the lines on the PMMA testbed. Laser cutter settings of 3% of power (low power) and 90% of speed (fast speed) are used to pattern the lines with fine resolution (see Section 5.2 for a detailed discussion of resolution limits). As shown in Figure 2 (b), one side (here, labelled as the “bottom”) of the sample is fixed so that only the other side (the “top”) can be stretched. By aligning the top line of the sample with the lines on the ruler, the sample can be stretched in increments of 200 μm, and the amount of total stretch (elongation increase) measured. The stretched sample is fixed for 30 seconds and stretched again manually (which takes about 5 seconds per stretch) without recovery.

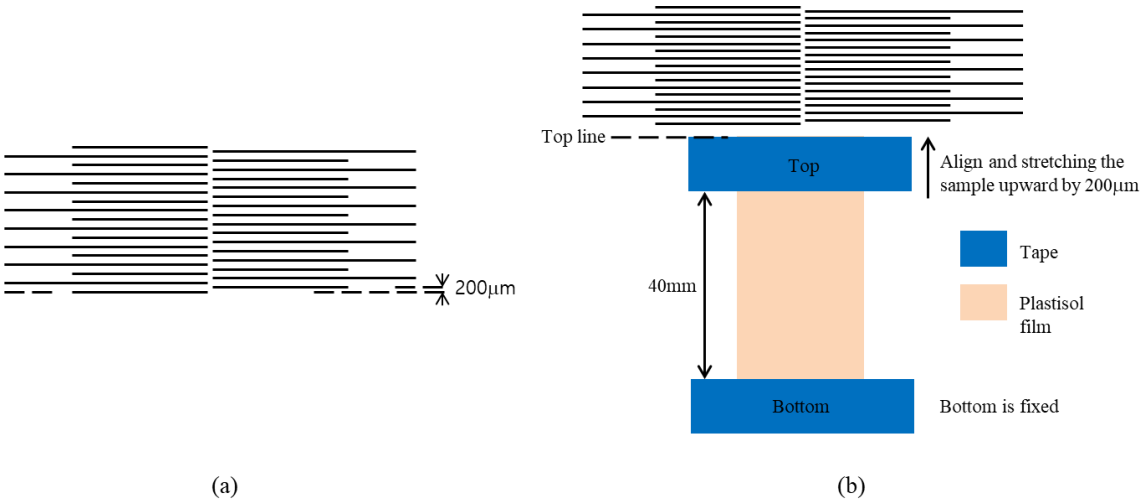


**Figure 2.** **Design of the micro-ruler, and test scheme: (a) Design of the ruler for sample stretching. Each line is separated by 200 μm to measure the stretch (elongation) of the plastisol film in increments of 200 μm. (b) Test scheme. The bottom of the sample is fixed and the top is aligned to the lines on the ruler via stretching. Samples are stretched by 200 μm increments until failure. [79]**

As each sample is stretched, the film fails (breaks) at a certain elongation distance (breaking point). Figure 3 shows the breaking point versus sample thickness for the different sample groups (thicknesses). The average film thickness for each group and the average breaking point for each group, in mm, are shown. The vertical error bars show the range of the breaking points and the horizontal bars show the range of thicknesses of each sample group. From these results, we observe that the breaking point increases as the thickness of the film increases until a certain point (around 390 μm), after which the breaking point tends to stay fairly constant (within 3%) regardless of the film thickness. For samples greater than 400 μm in thickness, the breaking point appears to level off, and compared to the initial (unstretched) length, a maximum of 37.5% of stretching (elongation) is observed before breakage. From these results, we may conclude that plastisol films less than 400 μm in thickness are optimal to maximize the stretchability of devices and to minimize the physical thickness and profile of fabricated devices. While failure point may somewhat depend on patterned dimensions (e.g., length, width of patterned structure), this test gives us a starting point for development, and shows that the films are quite flexible and promising for fabricating structures for wearable devices.

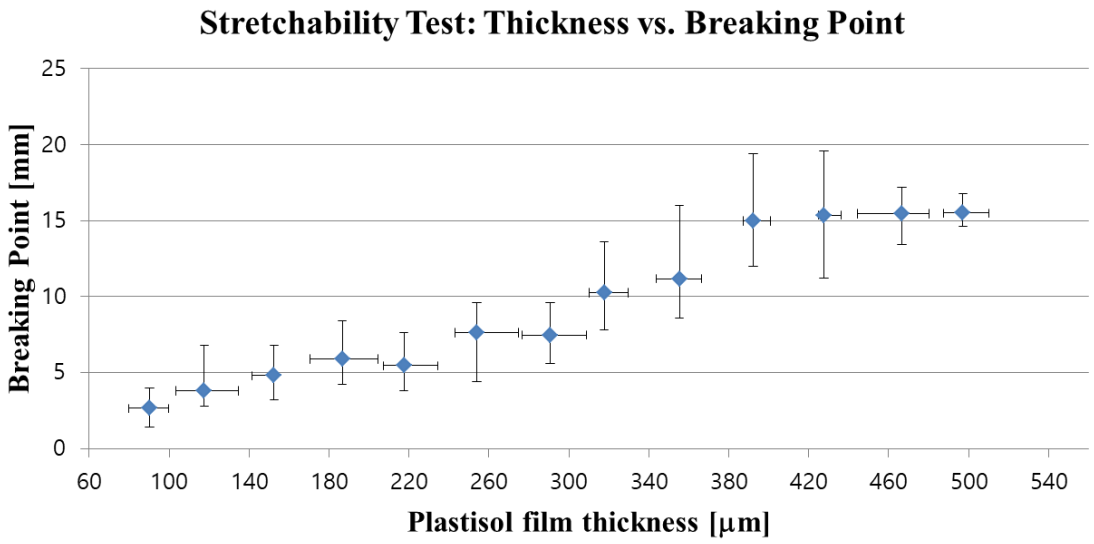


**Figure 3.** **Stretchability test results. Maximum stretchable distance increases as the thickness of plastisol film increases until certain point (around 400 μm) for films 30 mm width × 40 mm length in size. After that point, the breaking point levels off. The vertical error bars show the range of the breaking points and the horizontal bars show the range of thicknesses of each sample group. [79]**

## 3.2. Screen-Printable Silver Conductive Nanoparticle Composite Polymers (C-NCP)

In this section, development of the screen-printable C-NCP is presented. The desired properties for the C-NCP are first presented, followed by development of a C-NCP that meets the requirements and that can also be patterned on textiles.

### 3.2.1. Desired Properties

A screen-printable C-NCP for wearable devices should possess stable conductivity. By stable, we mean that the conductivity will not change with time for long term use. Also, the conductivity should be consistent under the same condition. If the conductivity changes randomly even without any condition change, it is impossible to control the conductivity and measure accurate signals. For many C-NCPs, conductive particles tend to aggregate and sink to the bottom of the mixture during the mixing and curing processes. If the conductive particles are not distributed uniformly through the polymer matrix, it will cause potential variation in conductivity. Such an unstable potential variation which cannot be controlled may hinder accurate electrical signal measurement

because electrodes or electrical routing cannot transfer the signal properly. The key point of achieving stable conductivity is the amount of conductive particles mixed with the plastisol. If the amount of particles is too high compared with the amount of base polymer, the C-NCP will lose flexibility and become brittle, as modulus of elasticity increases with particle wt-% (similarly to other nanoparticle composite polymers [80, 81]). On the other hand, if the amount of the particles is too small, the C-NCP will not be sufficiently conductive due to lack of conductive paths in the mixture.

As mentioned in section 2.3, at a certain amount of nanoparticles, the particles are sufficiently connected to form conductive pathways through the composite and the conductivity of the C-NCP increases sharply [70].To achieve stable conductivity, the amount of nanoparticles should be higher than this amount. Also, acquiring uniform conductivity depends on dispersion of nanoparticles in the plastisol. The more uniformly that the nanoparticles are dispersed, the more uniform the conductivity.

Flexibility is also a very important property for wearable devices and systems on textile substrates. One of the main advantages of screen-printable C-NCPs is their high degree of mechanical flexibility. Due to this flexibility, C-NCPs can be printed on textiles and employed for electronic components and routing without cracking or damage. Also, a flexible C-NCP can be worn without hindering the flexibility of the textile and motion of the user.

Also, the conductivity of the screen-printable C-NCP should not change with time, and should be washable without losing its conductivity for long term use. If printed C-NCP is damaged easily, or loses its electrical characteristics by washing, it is not suitable for long term use. In addition, the C-NCP is required to have consistent conductivity for long term use. If the conductivity changes with time, reliable signal measurement will be difficult.

### 3.2.2. Development of Screen-Printable C-NCP

The first step of making a C-NCP is to distribute a base polymer in an organic solvent such as heptane to loosen the tight bonds of the elastomer [69]. After the base polymer is distributed well in the solvent, conductive nanoparticles are added and distributed in the polymer-heptane mixture, and mixed manually until the organic solvent

is evaporated, resulting in a uniform distribution of conductive nanoparticles in the polymer matrix, which remains during patterning and curing. While simple mixing usually works well, ultrasonication may be used if needed [32, 82].

To prepare the screen-printable C-NCP that is developed and employed in this thesis, non-toxic plastisol ink, silver nanoparticles, and heptane are used. Plastisol provides the flexible mechanical properties of the C-NCP, and silver nanoparticles provide electrical conductivity. As stated previously, the ratio of silver particles to plastisol ink determines the flexibility and conductivity of the composite. For the example photographs shown in Figure 4, 70 wt-% of silver is used (see Section 3.3 for why this wt-% is chosen).

As mentioned, the first step of preparing screen-printable silver C-NCP is to dilute the plastisol in heptane solvent (ratio of 1:3). Plastisol is manually stirred for 30 seconds. Once the plastisol is diluted, silver nanoparticles are added and mixed manually using a stirring rod for 5 minutes until the heptane evaporates. Once the heptane is fully evaporated, the composite turns into like clay-like consistency and does not easily flow. Figure 4 shows photographs of the preparation process for screen-printable silver C-NCP (Figure 4 (a)), and an SEM image of the resulting silver C-NCP (Figure 4 (b)). After the heptane evaporates, the final C-NCP is moved to a clean container to show clear visual comparison between before heptane evaporation and after heptane evaporation. As shown is Figure 4 (a), final composite has very high viscosity which prevents aggregation of silver particles. Figure 4 (b) shows the silver nanoparticles which are connected to each other to form electrical paths in plastisol matrix.

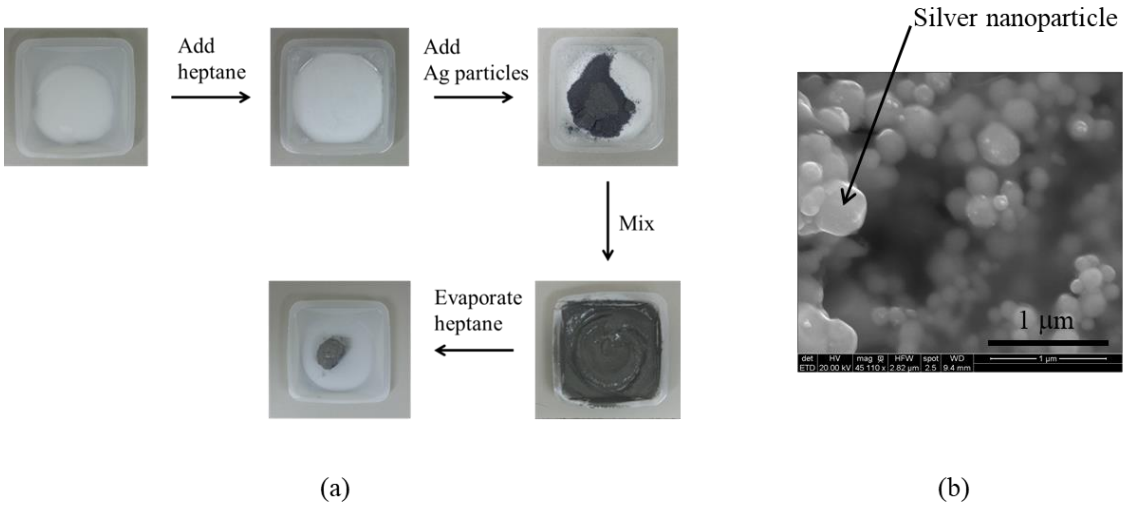


**Figure 4.** **Preparation of screen-printable silver C-NCP, and SEM image of silver particles embedded in plastisol meatrix: (a) Mixing processes for the silver C-NCP. (b) Silver particles are connected to each other to form electrical paths.**

## 3.3. Characteristics of Screen-Printable Silver C-NCP

In order to determine the suitability of the C-NCP for use in wearable electronic structures on textiles (e.g., flexible electronic circuit boards, sensor electrodes), it must first be characterized. This section includes characterizations of the silver C-NCP such as electrical resistivity, conductivity versus flexibility, suitability for long term use, and washability.

### 3.3.1. Effect of Nanoparticle/Polymer Ratio on Resistivity

Screen printable C-NCPs should possess stable conductivity under the same condition as explained in Section 3.2. For most conductive polymers developed by mixing nanoparticles with nonconductive polymers, achieving a stable conductivity has proven to be very challenging. This is primarily because it is difficult to achieve a uniform dispersion of conductive particles in a polymer matrix [16]. It is hypothesized that screen-printed C-NCPs possess more uniform and stable conductivity because of the very short curing time (5 minutes) and high viscosity of the nanoparticle composite polymer, which may help minimize nanoparticle aggregation. In addition, applied pressure during the scraping process helps in maintaining homogeneity of the patterns and uniformity of particle distribution.

In order to check the resistivity variation of the screen-printable silver C-NCP as a function of silver particle amount, samples of the silver composite polymer are prepared at 58, 61, 64, 67, and 70 wt-% of silver nanoparticles. Next, five samples (100 μm thick × 3.5 mm width × 20mm length) for each wt-% are screen printed onto fabric, and the resistance of each sample is measured using a 2-point probe measurement method and the average resistivity value is calculated at each wt-%. The 4-point probe technique is not used because high input current heats up the silver C-NCP, and the temperature variation affects the measured resistivity. Figure 5 shows the test procedure (Figure 5 (a)) and average resistivity of the conductive polymer at each wt-% with standard error deviation bars from six samples (Figure 5 (b)). Samples with 58 wt-% of particles have very unstable low conductivity, so their average resistivity cannot be calculated. This means the amount of silver particles is not enough to create a complete electrical path through the polymer matrix. At 61 wt-% of particles, the composite shows average resistivity of $1.56 \times 10^{-5}$ Ω·m with a maximum deviation of $9.46 \times 10^{-7}$ Ω·m, and the average resistivity decreases sharply at 67 wt-% to $2.33 \times 10^{-6}$ Ω·m with maximum deviation of $1.46 \times 10^{-7}$ Ω·m. The average resistivity of $2.12 \times 10^{-6}$ Ω·m is measured at 70 wt-% of silver particles with maximum deviation of $1.46 \times 10^{-7}$ Ω·m. The resistivity difference between 67 wt-% and 70wt-% is very small which means the amount of particles are saturated and enough to create electrical paths in the polymer matrix.

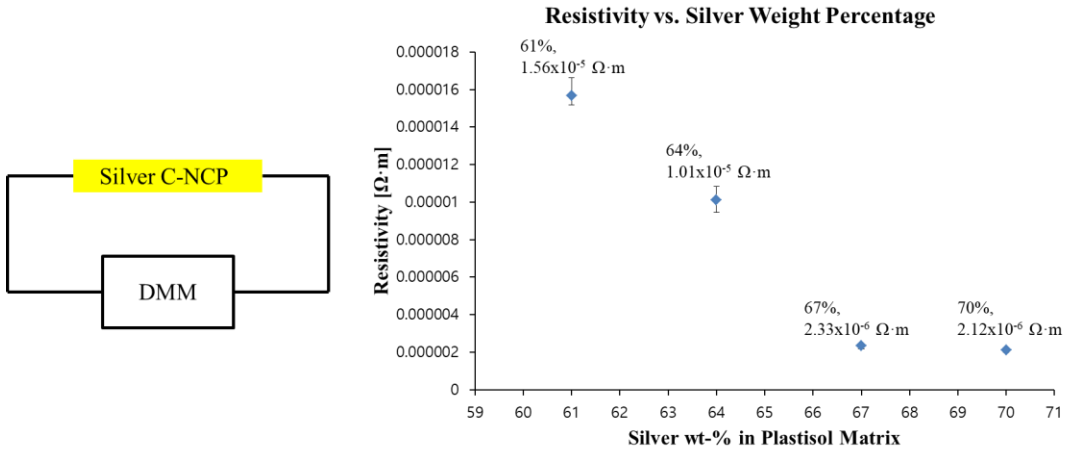


**Figure 5.** **Resistivity measurements of the screen printable silver C-NCP at different wt% of silver: (a) Test procedure. (b) Graph of resistivity of screen printable silver C-NCP vs. silver wt-%. The point at 58 wt-% is not shown because it has very low conductivity that is very unstable and can not be measured using current equipment. [77]**

### 3.3.2. Effect of Flexing on Resistivity

One of the main advantages of the screen-printable C-NCP is its mechanical flexibility. The high degree of mechanical flexibility enables development of wearable and flexible systems without hindering the textile's flexibility. C-NCPs have been shown to provide conformal contact to curved surface due to their high flexibility [77]. However, if a conductivity change occurs during user motion such bending, the C-NCP may produce an unstable output which may result in incorrect results (readings from, e.g., C-NCP based sensors or other components). In addition, the screen-printable C-NCP should not be damaged during wearer motion. To test the flexibility of the C-NCP, and to check if the C-NCP can be deformed enough to endure bending without causing any damage, the resistivity change at different bending angles is measured. Five samples at each of wt-% (61, 64, 67, and 70 wt-% of silver nanoparticles) are printed on textile (total 20 samples, 100 μm thick × 5 mm width × 20 mm length), and the resistivity change is measured at different bending angels from -90° to 90° with 10° steps. For each bending angle, the samples are recovered to 0° before being manually bent to the next angle, with each bend taking approximately 10 seconds. Figure 6 describes the measurement method (Figure 6 (a)) and shows the results (Figure 6 (b)). As can be seen from Figure 6 (b), bending does not seem to significantly affect the resistivity values for the samples of 67 and 70 wt-% because the amount of silver particles is enough to create a stable electrical path at any of these angles. For samples with 67 and 70 wt-% of silver particles, the deviations of resistivity at each angle are very small, and the overall average variation across all angles is also very small. However, as the amount of silver particles decreases, remarkable deviations are observed. At 61 wt-% of silver particles, each sample shows different resistivity even if the amount of silver particles is same. This is because consistent electrical paths cannot be formed with given amount of silver particles when the sample is bending.

Although deviations increase as the amount of silver particles decrease, the average resistivity of all samples at different bending angels is quite stable and consistent. This indicates that the samples are not damaged during the bending due to flexibility of the screen-printable C-NCP; if the samples are damaged and lost the electrical paths, they will lose its conductivity, or show very unstable varying values.

From the results from Figure 5, and 6, we conclude that required amount of silver particles should be larger than 67 wt-%.

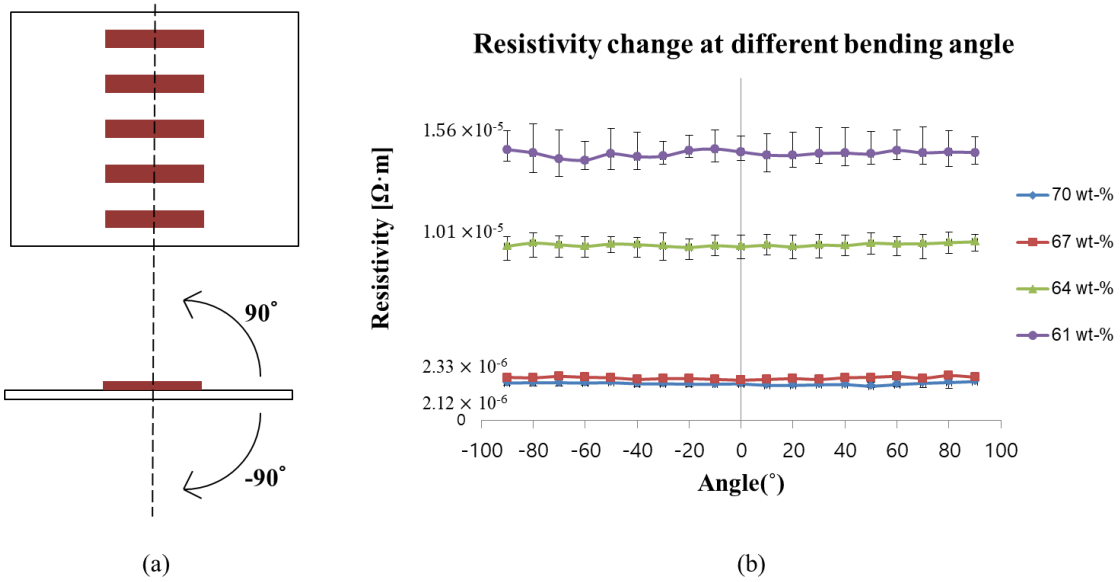


(a) (b)

**Figure 6. Resistivity measurements of the screen printable silver C-NCP at different bending angles: (a) Top view and cross view of test procedure. (b) Results showing resistivity versus bending angle for four different wt-% of silver particles (61, 64, 67, and 70 wt-%). The smallest deviation and average resistivity change at all angles are observed at 70 wt-% of silver particles. [77]**

### 3.3.3. Effect of Nanoparticle Density on Stretchability

As described in section 3.1, plastisol films are flexible and can be stretched to some degree. However, it is expected that the C-NCP samples should be less stretchable than those consisting of plastisol films alone due to the decrease in elasticity typically seen with the introduction of nanoparticles, with the elasticity being dependent on nanoparticle wt-% [80, 81]. The C-NCP is expected to become less flexible and less stretchable as the nanoparticle wt-% increases.

For the stretching experiments presented in this section, the C-NCP is patterned on a highly stretchable fabric. The textile shows about 55% of maximum stretching before the C-NCP printing. The overall goal of these tests is to determine how much the fabric can be stretched with a C-NCP pattern fabricated on it in order to not hinder movement of the wearer. To test the stretchability of the C-NCP, and check how much the C-NCP printed textile can be stretched, silver C-NCP at different wt-% of silver

particles is printed on stretchable textile samples, and the textile is stretched in the same manner used in section 3.1 until the C-NCPs are physically damaged. In addition, the degree to which the fabric/C-NCP samples can be stretched while maintaining conductivity is also measured.

Silver C-NCPs at 64, 67, 70, and 73 wt-% of silver are prepared. Four 10 cm width × 10 cm length of textiles are also prepared for printing at each wt-% of C-NCP. Five rectangular-shaped structures, which have the same size with C-NCP structures used for bending test, are screen printed on each of the textile substrates at each wt-% of silver particles (20 samples in total, 100 μm thick × 5 mm width × 20 mm length). Each textile sample is stretched in increments of 1 mm until the silver C-NCP fails (cracks). After the C-NCP is stretched beyond a certain distance (breaking point), the C-NCP fails. Figure 7 (a) shows photographs of printed C-NCP structures (70 wt-% of silver), and the close-up of a damaged structure after being stretched past its breaking point. The maximum stretchable distance before damage is recorded from each sample, and the average stretchability is shown with deviation bars that show the maximum stretchable range for each wt-% (Figure 7 (b)). As can be seen from Figure 7 (b), the stretchable distance decreases as the wt-% of silver increases. For textiles with C-NCP patterns containing 64 wt-% of silver, the highest degree of stretch (20.4% of stretch) is demonstrated, but with the largest deviation. Textiles with C-CNP containing 67 wt-% of silver can be stretched 15.2%, and Textiles with C-CNP containing 67 wt-% of silver can be stretched can be stretched 12%. However, at 73 wt-% of silver particles, the stretchable distance decreases dramatically, and only 4.6% of stretching is possible. From 73 wt-% of silver particles, the C-NCP becomes too brittle due to the high amount of particles, and cannot be applied to flexible applications. From the results, it is shown that the amount of silver particles should be less than 73 wt-% for stetchability without C-NCP pattern failure. Although, large sizes of C-NCP patterns are used for this test, micro-sized patterns also can be printed (see next section 3.4.). When the micro-sized patterns are used, these should affect the stretchability of the textile much less, although the robustness of the patterns may be lower.

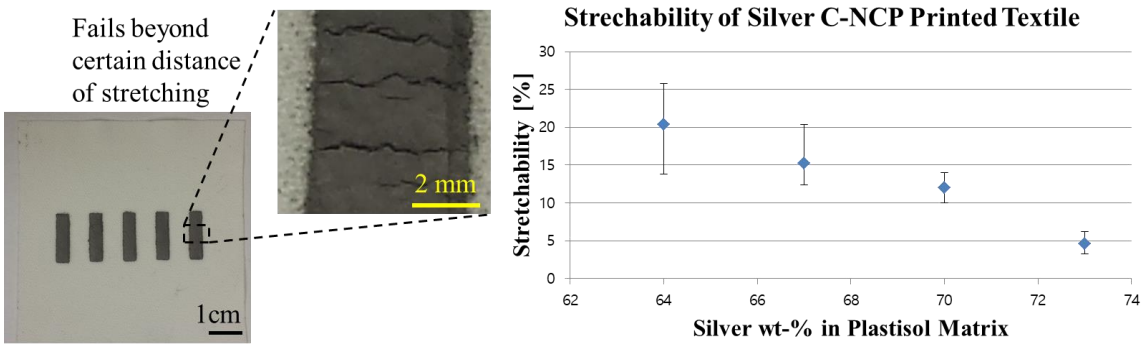


(a) (b)

**Figure 7. Stretchability test of silver C-NCP: (a) Photographs of the silver C-NCP structures (70 wt-%) and close-up of damaged structure after breaking point is reached. Physical damage occurs when the C-NCP is stretched beyond a certain distance. (b) Results from C-NCPs with different wt-% of silver. Strechable distance decreases as the amount of silver particle increases.**

During the textile stretching, the printed C-NCP structures are also stretched, and show a similar pattern of failure versus nanoparticle wt-% as shown in Figure 7 (b). For samples with 64 wt-% of silver, the structures are stretched about 20.4% before failure, and 15.2% of stretching is observed for structures with 67 wt-% of silver. The structures with 70 wt-% of silver are stretched about 4.6%. As the amount of silver particles increases, the stretchable distance of the C-NCP structures is decreased.

The conductivity change with stretching is also measured using the structures. For the structures with 67 wt-% of silver, consistent conductivity is measured until about 9% of stretching; after that, the conductivity is decreased because the electrical paths in the plastisol matrix become disconnected due to stretching. For samples with C-NCP patterns containing 70 wt-% of silver, consistent conductivity ($2.12 \times 10^{-6}$ Ω·m) is measured until the structures fails. Conductivity change is not observed during the stretching (4.6% of stretching). While the failure point may depend on patterned dimensions (e.g., length, width of patterned structure), based on this result and the results shown in Figure 5 and 6, we conclude that 70 wt-% of silver C-NCP is likely the best for wearable and flexible applications because of its high conductivity, high flexibility (to bending and conforming to curved surfaces), and consistency in conductivity under stretching. It should also be noted that under stretching, the textile tends to easily stretch around the C-NCP patterns even though the textile under the patterns tends to stress

less due to the excellent adhesion of the C-NCP to textile substrates. Thus, when typical electrodes and electronic routing for most applications are patterned, where the ratio of patterned C-NCP surface to fabric surface of a garment is minimized, a typical garment should retain much of its flexibility and not hinder the user.

### 3.3.4. Suitability for Long Term Use and Washability

It is shown in previous sections that the screen-printable silver C-NCP is flexible and highly conductive. However, ideally the C-NCP's conductivity should not change with time for long term use, and should also be washable in order to be applicable for wearable devices and systems on clothing.

To evaluate the screen-printable silver C-NCP for long term monitoring, 7 square samples (2mm × 2mm, 70 wt-% of silver) are prepared and monitored for 10 full days of typical activity as seen by a person wearing the electrodes, including exercise, bath, and sleep. The average resistivity of the screen printed conductive structures is measured twice a day. Figure 8 (a) shows the resistivity change of 7 samples with time, including deviation bars. The deviation is very small on the first day, but it increases over time. The average resistivity decreases 12.2% over the 10 day period. A possible reason is sodium and chloride ions in sweat. Because the samples are attached on skin for 240 hours, ions from sweat may result in a decrease in the resistivity. The change may be also caused by measurement error of the multimeter, but this change is expected to be relatively small because the initial average resistivity is very low ($2.12 \times 10^{-6}$ Ω·m). However, these results indicate that the flexible conductive polymer should be usable for wearable long term monitoring, although this change in conductivity may need to be better characterized and accounted for in the measurement system.

To test the capability of the screen-printable C-NCP for wearable systems, the washability of silver C-NCP structures on fabric is also tested. A total of 20 square structures (2mm x 2mm, 70 wt-% of silver) are screen printed on fabric and washed by hand twice a day with soap for 9 days, and the average resistivity is measured twice per day after each washing and after being allowed to dry. Figure 8 (b) shows the resistivity of the 20 samples with (single) standard deviation bars. Similarly to Figure 8 (a), the average resistivity decreases slightly as the sample structures are hand washed. A 10.8 %

change in resistivity is observed; however, this change is small and, as with the previous test, may be attributed to measurement error of the multimeter. These results show that fabric samples with screen printed C-NCP structures can be hand washed without causing damage to the conductive structures.

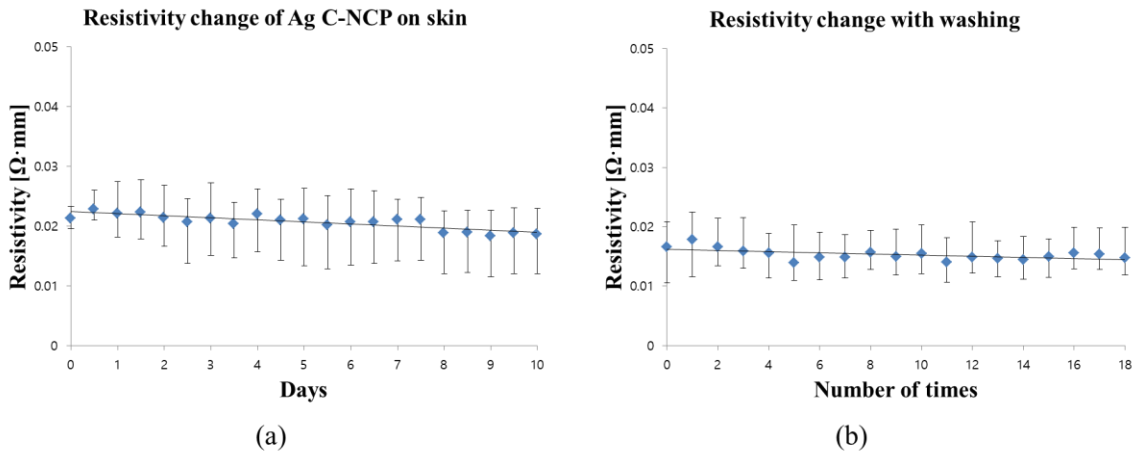


**Figure 8. Resistivity change of silver composite polymer: (a) Resistivity change over 10 day period of typical wear and tear on electrodes. (b) Resistivity change with hand-washing. [77]**

## 3.4. Screen Printed Silver C-NCP

As mentioned in chapter 2, screen printing techniques are used in this thesis to develop wearable devices and microfluidics. Figure 9 shows photographs of an example screen printed silver C-NCP patterns on textile (65% polyester + 35% cotton). Once the C-NCP is prepared, the composite is screen printed manually and cured at 150°C for 5 minutes on a hotplate. Figure 9 (a) shows a pattern of 2 mm diameter circle electrodes, and Figure 9 (b) shows an example printed circuit board (PCB) on fabric. Because of the high viscosity and short curing time of the nanocomposite polymer, it is possible to produce very homogeneous conductive patterns with uniformly dispersed silver particles in the plastisol, which in turn results in more reliable performance and lower energy consumption.

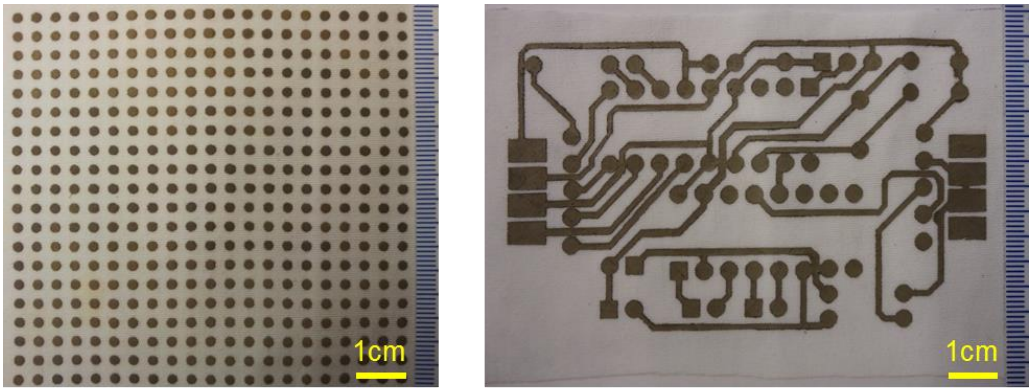


(a) (b)

**Figure 9. Screen printed C-NCP on fabric: (a) 2mm diameter circle electrode array pattern. (b) example printed circuit board (PCB) pattern. [77]**

Using the screen printing technique on the silver C-NCP, many different patterns can be printed on different textiles. However, the resolution of the printed pattern depends on the resolution of the laser cutter machine because the screen is prepared using the laser cutter machine. The finest dimension is 76 μm for the laser machine, with an actual resolution of larger than 76 μm because the laser melts the surface of the screen material and transfers heat to adjacent areas. Figure 10 shows photographs of the smallest pattern achieved for this thesis work. A straight line with width of 76 μm (as designed), and an array of circle electrodes with diameter of 76 μm (as designed) are screen printed on fabric with an thickness of about 100 μm , and actual resolution of about 100 μm is observed for both patterns. Figure 10 (c) shows close-up of the circle electrodes. To achieve this resolution, a plastisol-based C-NCP with 70 wt-% of silver particles is used, which is patterned via a Scotch® Magic™ tape screen. However, achieving smaller feature size with screen printing is challenging, and silver C-NCP may not be applied to applications which require sub-micron feature size with screen printing.

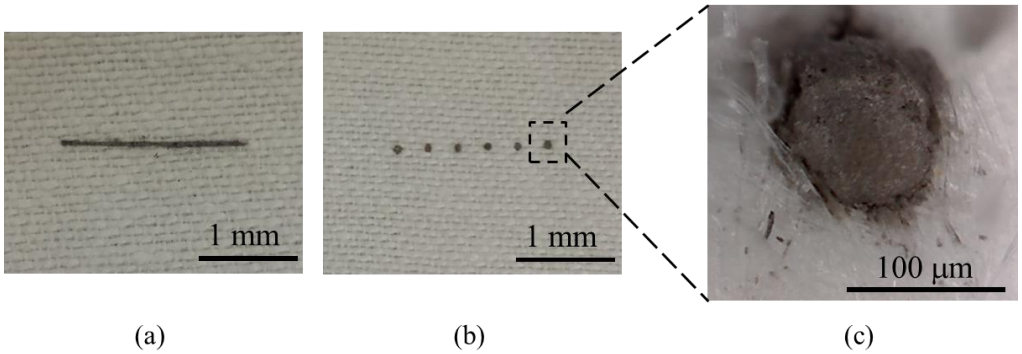


**Figure 10.** **Printing resolution: (a) A straight line with a 100 μm width is printed on fabric. (b) An array of circle electrodes each with 100 μm diameter is printed on fabric. (c) Close-up of a circle electrode.**

# Chapter 4.

# Applications of Screen-Printable C-NCP to Wearable Electronics for Health and Safety

Wearable electronics have the potential to offer the next major step in the evolution of electronic systems. The production of flexible electronic components on textiles will enable the low-cost manufacturing of more compact, lightweight systems with improved performance and reliability. In addition, wearable and flexible electronics can eliminate bulky wiring and expand the limits of design for a myriad of devices. All of these benefits will open up new applications that are not previously possible, including flexible sensors and lighting systems.

In this chapter, the screen-printable C-NCP developed in chapter 3 is applied to a health application and a safety application to demonstrate its potential for wearable textile-based devices and systems. This includes detailed fabrication processes and test results for each system. The C-NCP is used as active electrical components such as sensing electrodes and electrical routing without hindering the flexibility of the textile. By using screen printing techniques for the C-NCP, fully wearable devices are developed and demonstrated. First, the screen-printable silver C-NCP is applied to a biomedical application. Wearable dry Ag/AgCl ECG electrodes are developed on textiles, tested, and compared to commercial ECG electrodes. By screen printing C-NCP on textiles, reusable ECG electrodes without electrolyte gel are developed. Also, screen-printable silver C-NCP is applied to a safety application. The C-NCP is screen printed on a commercial safety vest to form electrical routing, and lighting systems are developed using surface mount light emitting diodes (LEDs).

This chapter demonstrates actual applications of the screen-printable C-NCP to various fields. By applying the C-NCP, fully flexible devices which can be used repeatedly are developed using only simple and easy techniques.

## 4.1. Application 1: Screen Printed Wearable Electrocardiogram (ECG) Electrodes

One major focus of research into wearable technologies is health applications, especially as the population ages [83]. Measurements of bio-signals are critical to patients requiring long-term monitoring or the elderly to prevent or detect unexpected medical emergencies or accidents. Traditionally, bio-signals such as ECG or respiration rate have been measured at the hospital with specialized equipment. However, wearable sensors, combined with wireless communication technology, offer the ability to measure bio-signals, in particular bioelectric signals, to enable individualized continuous health monitoring regardless of the individual's location.

In this section, a new type of electrode is developed using screen-printable silver C-NCP and screen printing techniques. Traditional electrodes that are used to measure bio-signals require electrolyte gel that often causes skin irritation. Furthermore, conventional electrodes are not flexible. To solve these problems, flexible dry Ag/AgCl electrodes are developed using the materials and techniques explained in chapter 2 and 3, and applied to ECG signal measurements. Silver C-NCP is employed to develop textile-based non-polarizable electrodes with good flexibility and conductivity. Flexible plastisol provides flexibility, and highly conductive silver nanoparticles enable fabrication of non-polarizable electrodes with good conductivity. Also, a simple screen printing technique simplifies the fabrication process and shortens fabrication time. The developed electrodes are tested with a simple ECG circuit, and compared to commercial Ag/AgCl electrodes.

### 4.1.1. Development of Wearable Dry ECG Electrodes

The wearable dry ECG electrodes consist of two parts: the sensing electrode and electrical routing. The sensing electrode (circular, 3mm in diameter) is patterned on the front side of the fabric. The sensing electrode contacts the skin to measure the ECG signal. On the back side of the fabric, electrical routing is screen printed using the same silver C-NCP. Cables or wires from the ECG acquisition equipment are connected through the back side for testing. Eventually, the routing on the back side of the electrodes and wire interfaces could be eliminated if a proper wireless system could be implemented together on the fabric with the electrodes using, e.g., surface mount

technology (SMT) components. A partial area of the back side pattern is passivated using non-conductive plastisol to minimize oxidation of silver particles and to prevent physical damage to the conductive pattern. The exposed area of the front side pattern is chloridized to form non-polarizable Ag/AgCl electrodes. For the chlorination, an electrochemical chlorination is performed.

Figure 11 shows the fabrication process of wearable dry ECG electrodes, which makes use of the general screen-printing process discussed in Section 2.3. The fabric is manually punched with a needle (1.27 mm of outer diameter) for electrical connection between the sensing electrodes on the front side and the routing pattern on the back side (Figure 11 (a)). The fabric is then placed on the plate of the screen printing equipment, and the screen is aligned with the hole in the fabric. Next, silver C-NCP (70 wt-% of silver) is prepared and printed on the front side of the fabric to pattern the sensing electrode and cured for 5 minutes at 150°C using a hotplate (Figure 11 (b)). After this curing process, the back side of the fabric is aligned with the screen, and the silver C-NCP is printed and cured to pattern the electrical routing (Figure 11 (c)). Finally, non-conductive plastisol ink is screen printed on the back side for passivation, and the sensing electrode is chloridized to form non-polarizable Ag/AgCl electrodes using bleach (6% of sodium hypochlorite) (Figure 11 (d)). The electrode is soaked in the bleach for 3 minutes, and washed using DI water. We use 70 wt-% of silver particles because, as outlined in Chapter 3, plastisol with 70 wt-% of silver particles possess stable and relatively high conductivity. Figure 12 shows photographs of the front side (Figure 12 (a)) and back side (Figure 12 (b)) of the fabricated flexible ECG electrodes on fabric. The flexible ECG electrodes are patterned on a long strip of fabric so that the strip can be wrapped on wrist and ankle.

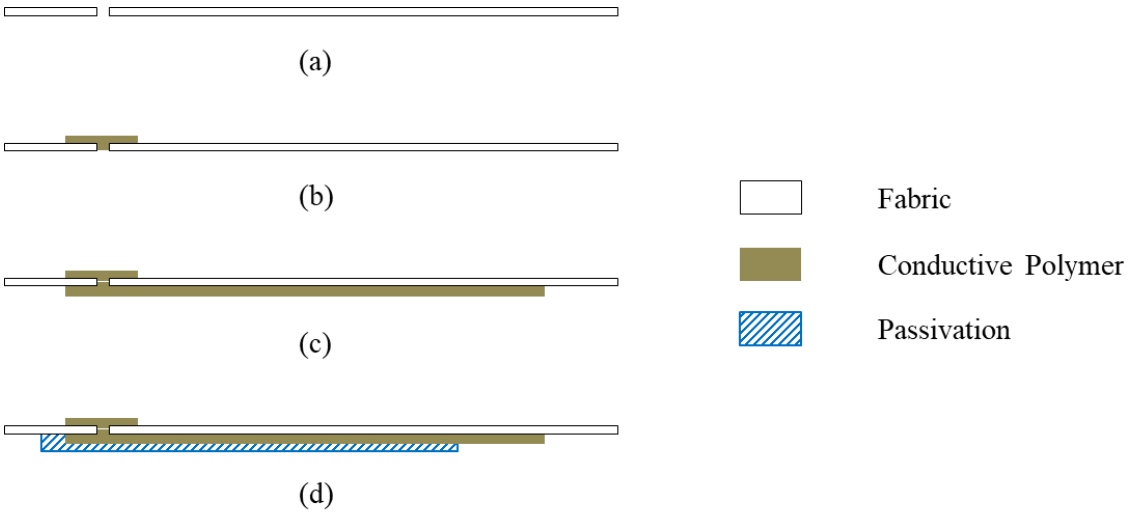


**Figure 11.** **Fabrication process for flexible, wearable ECG electrodes: (a) Punch the fabric for electrical connection between the sensing electrode and electrical routing. (b) Print silver C-NCP on the front side first and cure it. (c) Print the back side and cure it. (d) Encapsulate partial area on the back side and chloridize the front side to make Ag/AgCl electrodes. [77]**

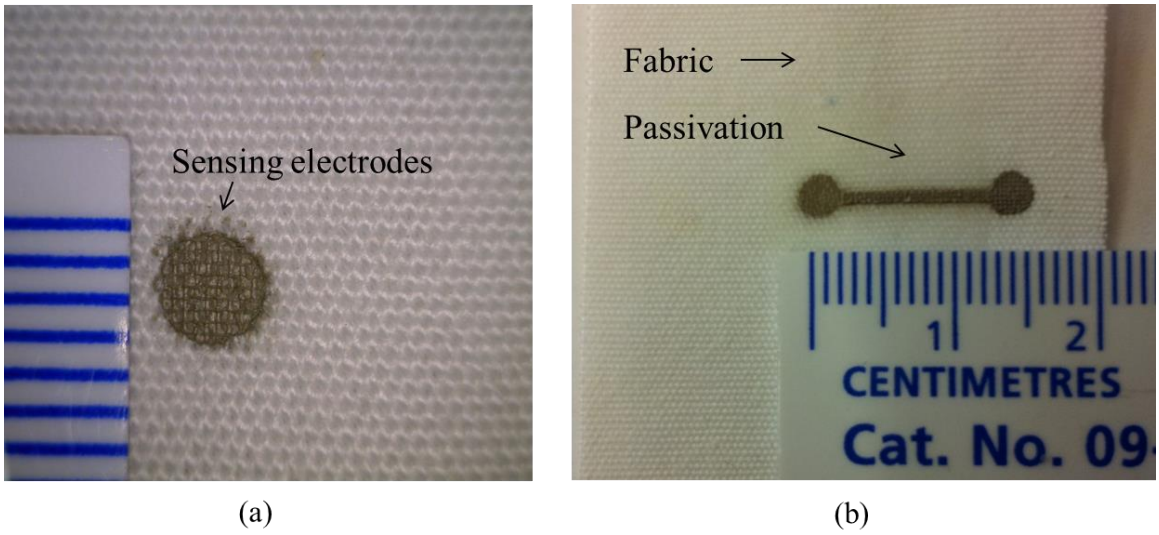


**Figure 12.** **Photos of wearable dry ECG electrode: (a) Front side, showing sensing electrode. (b) Back side, showing electrical routing. [77]**

### 4.1.2. Experiments and Test Results

The ECG signal amplifier circuit is built using an instrumentation amplifier and a band pass filter to test the fabricated wearable ECG electrodes. The instrumentation amplifier amplifies the signal difference between the two inputs. To remove unwanted

signal and increase the overall gain of the tiny ECG signals, a band pass filter is added. A right leg drive circuit is used to achieve a clearer signal with less noise, and three wearable electrodes are placed on both wrists and the right leg. Figure 13 shows the schematic design of the ECG signal amplifier circuit. The circuit can operate off of batteries. The circuit is designed to have a gain of 1024 with common mode rejection ratio (CMRR) of 82. The desired lower cut-off frequency is 1.59Hz and higher cut-off frequency is 1061Hz. Such a simple circuit is chosen so it could instead be integrated into a microelectronic chip that could be integrated onto the textile substrate (see next section on circuit board using SMT LEDs).

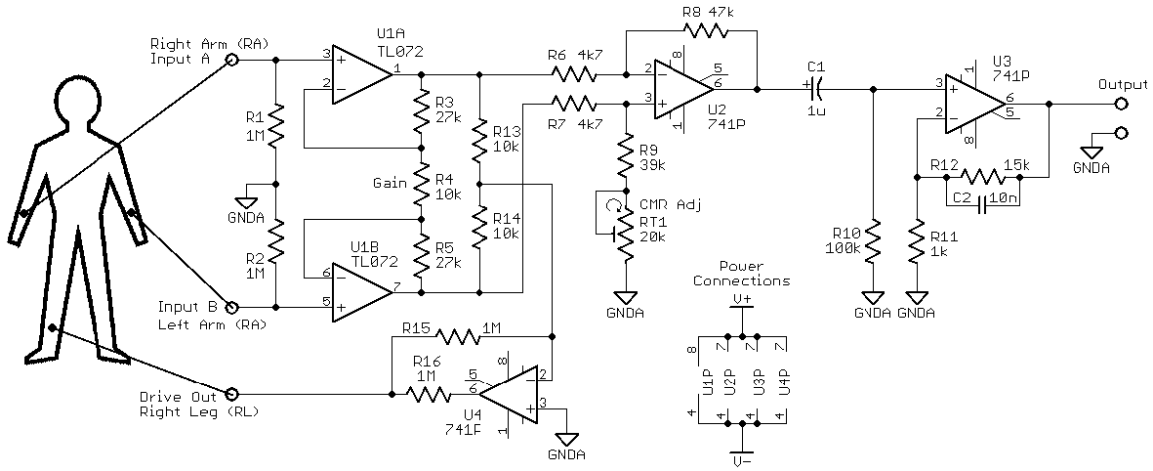


**Figure 13. ECG instrumentation right leg driven signal amplifier. [77]**

After the circuit is prepared, typical normal ECG signals are acquired through a commercially available ECG signal simulator (PS420 multiparameter simulator, Fluke) using the circuit. Next, actual ECG signals are acquired through both commercially available Ag/AgCl ECG electrodes and the new C-NCP electrodes for comparison. For the simulator, three inputs of the circuit are connected to the simulator and the output is displayed on an oscilloscope. The results are shown in Figure 14 (a). Because the simulator produces a consistent signal without any motion or electrode artifacts, the acquired signal is very clean and clear. We could easily distinguish the heart signals (P waves, QRS peaks, and T waves) very clearly. Next, both commercially available Ag/AgCl electrodes and flexible wearable ECG electrodes are employed to measure real-time ECG signals under the same conditions. Figure 14 (b) shows the ECG signal acquired from commercially available Ag/AgCl electrodes. Compared with the signal from the simulator, the signal is much noisier: the P waves are barely distinguished, but

the QRS peaks and T waves are very clear. Figure 14 (c) shows the ECG signal using the new flexible wearable electrodes. Similarly to Figure 14 (b), noise is also observed. Although the QRS peaks show about 11.8% decrease compared with Figure 14 (a), and 6.7% decrease compared with Figure 14 (b), they are still clearly recognized. In addition, the T waves are clearly distinguishable.

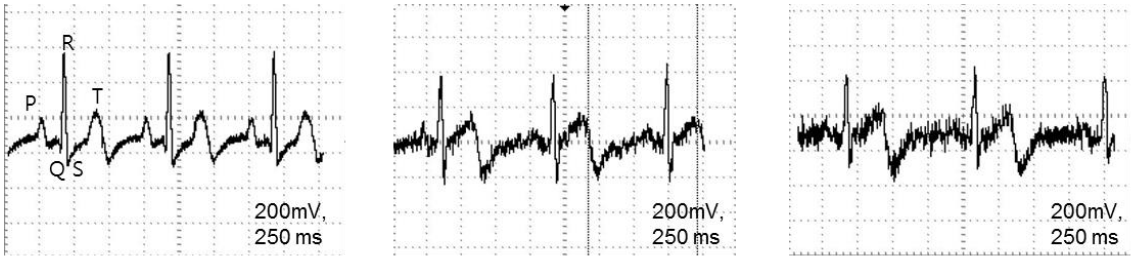


(a) ECG simulator (b) Commercial Ag/AgCl ECG electrodes (c) Flexible dry Ag/AgCl ECG electrodes

**Figure 14. ECG signal acquired using simple driven right leg circuit with input from: (a) ECG simulator. (b) Commercial macro-scale ECG electrodes. (c) Fabricated flexible dry ECG C-NCP electrodes. [77]**

It should be noted that the commercially available ECG electrodes are floating gel electrodes designed to minimize motion artifact, while the flexible, wearable ECG electrodes are employed dry. Given the relative quality of the signals, we may conclude that the flexible dry electrodes may be suitable for basic long-term monitoring where gel cannot be employed. Furthermore, the electrodes are washable, and can be used repeatedly. The results could potentially be improved if commercially available ECG acquisition equipment and shielded cables are used for data acquisition. However, we also note that there could be practical problems, such as if sweat were to bridge the back side of the silver contact.

## 4.2. Application 2: Screen Printed Safety Vest with LEDs

In this section, a new type of safety vast with lighting system is developed using screen-printable C-NCP. Commercially available safety vests are made up of reflective materials so that the vest can be seen by others very easily. Wearing a safety vest is important for those who operating heavy equipment or driving in construction. However, the vest may not retain high visibility at night, foggy days, or rainy days because of lack of enough light to be reflected. To improve the vest and increase the safety of user

under low light conditions, surface mount LEDs are attached on the commercially available safety vest using the screen-printable silver C-NCP as electrical routing. This is made possible through application of the silver C-NCP developed for this thesis, and this application shows that the C-NCP can be employed for a circuit board of SMT components and battery holder to realize fully wearable textile-based electronic devices. Flexible electrical routing which can be printed on textile, and require low power for operation can be used for development of textile-based wearable microelectronic chips by combining with SMT components.

### 4.2.1. Flexible Electrical Routing on Textile

It is already shown that C-NCP can be printed on textiles. To test that the adaptability of the silver C-NCP, silver C-NCP with 70 wt-% of silver is printed on different types of textiles, and tested as electrical routing between single or multiple LEDs and a power source. Figure 15 shows a single LED on stretchable fabric (polyester + elastam) as a proof-of-concept device to show that the C-NCP can be employed as a simple printed circuit board. The C-NCP is patterned on the fabric and cured on a hotplate at 130°C for 5 minutes, and the LED is connected to the conductive pattern by simply piercing the pattern with the LED. For this simple text, an external power supply machine is used. The LED lights up successfully; however, this sample has limitations of the LED being too large and employs an external power supply.

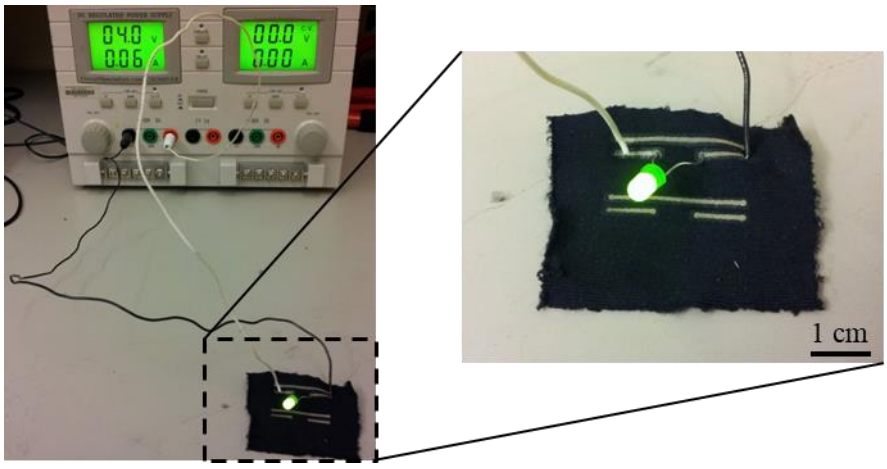


**Figure 15. A Single LED on fabric connected to power supply equipment to show proof-of-concept of the C-NCP for electronic routing between components.**

To solve these limitations, an improved sample is fabricated with battery and surface mount LEDs. The number of LEDs is increased to five, and a 3.6V battery and switch are used. For this sample, the lines of silver C-NCP are patterned on a fabric (polyester + cotton) using the screen printing technique. Figure 16 shows the sample device. Similar with the fabrication process explained in section 4.1, the fabric is punched with needle for electrical connection between front side and back side, and conductive lines are patterned on both front and back sides of the fabric. Only the switch and LEDs are seen on front side (Figure 16 (a)), with the electrical routing on the back side (Figure 16 (b). The surface mount LEDs are attached to the conductive lines by soldering, and the battery is connected to the back side of the sample with wires. The LEDs light successfully when the switch is pushed (Figure 16 (c)). However, metal wire, large size of battery, and large size of switch, which hinder the development of fully flexible devices, are still used.

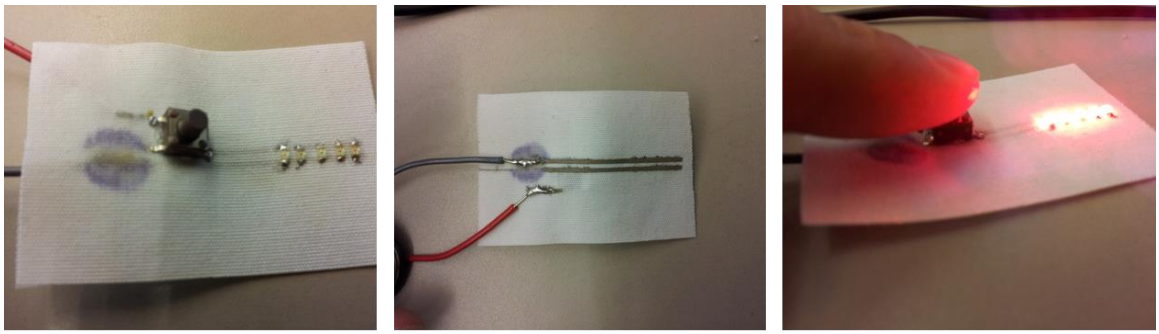

(a) (b) (c)

**Figure 16. Five surface mount LEDs on fabric with battery: (a) Front side with switch and LEDs. (b) Back side with silver C-NCP routing. The battery is connected to the C-NCP routing through the wires. (c) powered LEDS.**

## 4.2.2. Fabrication of Safety Vest with LEDs

To realize the safety vest with lighting system, the system is next realized on a commercial safety vest with some further improvements. First, the wires are eliminated by using a battery holder, and a coin cell battery (3V, Panasonic) is used to reduce the size of the battery. The number of surface mount LEDs is also increased to 30, and the LEDs are actually attached to the commercially available safety vest. Figure 17 shows the fabrication process of the vest. First, the vest is punched to make holes for electrical connection between front side and back side (Figure 17 (a)). Then the silver C-NCP is

patterned on both sides, and cured on a hotplate at 150°C for 5 minutes (Figure 17 (b) and (c)). Next, non-conductive plastisol is printed on the back side to protect the electrical routing (Figure 17 (d)), and LEDs are attached on the front side of the vest by soldering after patterning the conductive polymers (Figure 17 (e)). The battery holder and one variable resister are attached on the back side of the vest (Figure 17 (f)). The variable resistor is used to control the current flowing through the LEDs. Lastly, the front side is also coated with non-conductive plastisol for protection (Figure 17 (g)). Figure 18 shows photographs of both sides of the safety vest with lighting system. Both sides are passivated with non-conductive plastisol ink. Lastly, Figure 19 shows the powered LEDs in daylight and in the dark when the battery is connected to the battery holder. The LEDs are powered for around 24 hours with a single 3V coin battery.

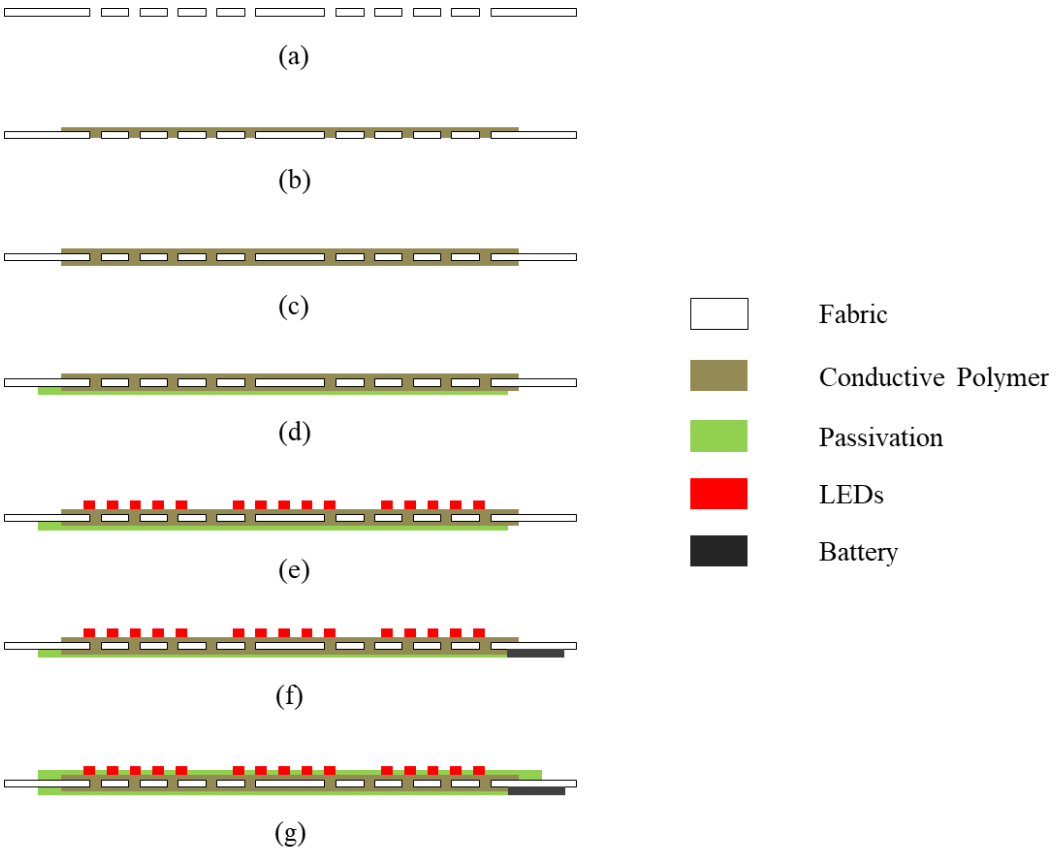


**Figure 17.** **Fabrication process of the safety vest with lighting system: (a) Punch the fabric for electrical connection between front side and back side of the fabric. (b) Screen print silver C-NCP on the front side first and cure it. (c) Screen print the back side and cure it. (d) Encapsulate the back for physical protection of the electrical routing. (e) Attach LEDs by soldering. (f) Attach the Battery holder. (g) Encapsulate the front side for physical protection.**


**Figure 18.** **Photographs of the safety vest with LEDs: (a) Front side with LEDs. (b) Back side with electrical routing, a coin battery, and a resistor.**

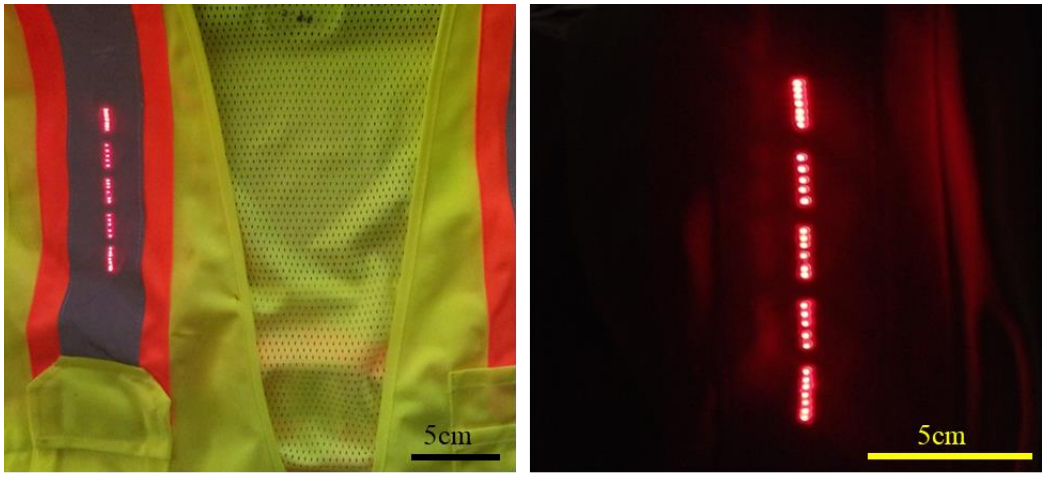


**Figure 19.** **Lighted LEDs on the safety vest: (a) in daylight. (b) in the dark.**

# Chapter 5.

# Wearable and Flexible Microfluidic Systems

In this chapter, a whole new printing-based fabrication process for the development of fully wearable and flexible microfluidic devices is presented. We develop a new method of fabricating flexible and durable microfluidic channels and devices on fabric using the screen-printable plastisol polymer, and sheets of paper are used as a sacrificial substrate. The fabrication method is simple, fast, and inexpensive. Microfluidic devices can be made within an hour using simple processes and inexpensive equipment. Also, the fluids can be isolated in the device without evaporation.

This chapter explains the basic concept of the fabrication method and optimization for each process are explained in detail. In addition, stretchability and flexibility of the devices are also characterized. With the fabrication method, wearable single-layered microfluidic channels, multi-layered channels, and a simple microfluidic mixer are fabricated on textile and demonstrated.

## 5.1. Fabrication of Wearable Microfluidic Devices

The fabrication process is based on the separate patterning of multiple layers of a device which are subsequently bonded together. Figure 20 shows the fabrication process for simple flexible and wearable microfluidic channels as an example. Three different plastisol layers (bottom layer, channel layer, and top layer) are prepared separately, and bonded together to form the microfluidic channel.

First, the plastisol polymer ink is manually applied and printed on two sheets of paper to form thin plastisol films on each piece of paper. One thin layer of plastisol forms the microfluidic channel layer and the other forms the top of the microfluidic channels. The thickness of the channels can be controlled by the thickness of the coated plastisol ink. The plastisol-coated paper sheets are cured on a hotplate at 110°C (Figure 20 (a)) and planarization is performed by pressing the plastisol films with flat glass slide using approximately 10kPa. Next, microfluidic channels are patterned in one layer of plastisol

film using the laser cutter machine (Figure 20 (b)). The dimensions of the channels are determined by the power and speed of the laser cutter. The bottom layer of the channel is screen printed on textile using the same plastisol polymer ink, and the channel-layer is then bonded to the bottom layer using thermal fusion bonding (Figure 20 (c)). Thermal fusion bonding is an easy and simple technique that is widely used for sealing microfluidic channels [84], and can be used in our process because the plastisol ink is a thermoplastic. After bonding, the sacrificial paper substrate is manually detached from the channel structure (Figure 20 (d)). Both inlet and outlet are patterned on the top layer using laser ablation before the top layer is bonded on the channel layer. Lastly, the top layer with inlet and outlet is bonded on the channel layer (Figure 20 (e)), and the second piece of sacrificial paper is also removed (Figure 20 (f)). Polyethylene tubes with diameters of 0.86 mm (#427425, Intramedic) are connected using a silicone sealant (Dow Corning 732) to allow liquid injection during testing. Figure 20 shows the fabrication process for a simple example microfluidic channel, but depending on the device design and purpose, multiple layers can be fabricated with different shapes of patterns to result in multi-layered devices.

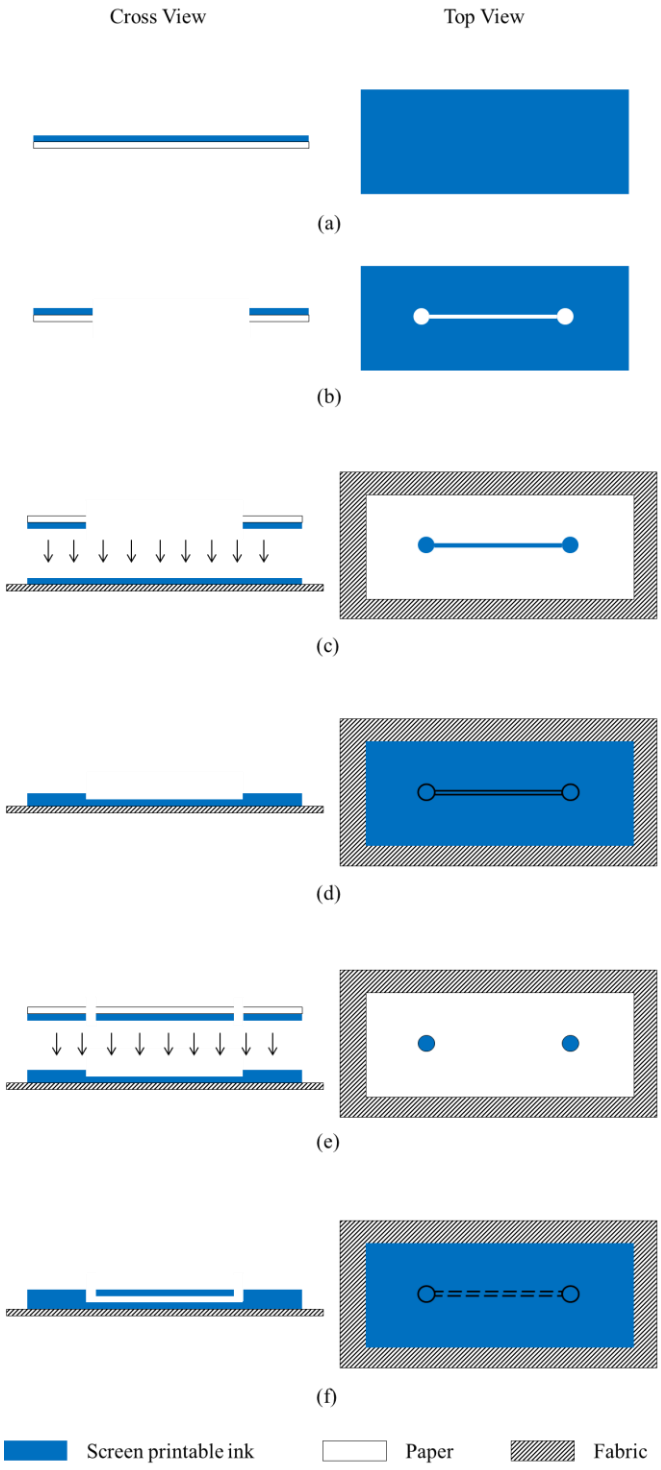


**Figure 20.** **Fabrication procedure for wearable microfluidic devices: (a) Coat the screen printable plastisol ink on a sheet of paper. (b) Pattern channels on the ink-coated paper with laser cutter. (c) Print the bottom layer on fabric, and bond channel layer. (d) Detach the paper. (e) Prepare the top layer and bond it. (f) Detach the paper. [85]**

## 5.2. Key Processes for Optimization of the Fabrication

In this section, fabrication process are optimized and explained in detail. Because the fabrication method prepares each layer of the device separately and bonds them together, the thickness of each plastisol film determines the total thickness of the device. So, thickness control is optimized first, and then planarization process to achieve flat surface profile is explained. Next, thermal fusion bonding technique is explained, and pattern resolution for the device is measured. After the optimization for each process is explained, example single-layered and multi-layered microfluidic channels are fabricated.

### 5.2.1. Plastisol Coating and Control of the Thickness of the Plastisol Film

Coating the plastisol ink on a sheet of paper manually without any screen or mask may result in an uneven thickness of the polymer film. A squeegee, which is a conventional tool in screen-printing for controlling the spread of ink on a screen, is used to spread the plastisol into a thin film. The higher the applied pressure of the squeegee, the thinner the film would be. A uniform thickness of plastisol film cannot be easily applied with manual coating. To solve this problem, Scotch® Magic™ Tape with a thickness of 63 μm is used as an example open mask. Figure 21 shows the coating process. First, a sheet of 8.5 x 11 inch paper is cut into quarters (4.25 x 5.5 inches) for convenience in coating. Next, the tape is attached on the right and left sides of the paper, and the plastisol ink is coated using a common screen-printing squeegee. Because the tape had a thickness of 63 μm, the ideal thickness of the coated plastisol ink is also 63 μm. A 126-μm-thick layer of plastisol film can be obtained by stacking two layers of the tape mask. While simple tape is used in this example, the thickness can be tailored using other materials depending on the desired thickness of the masking layer.

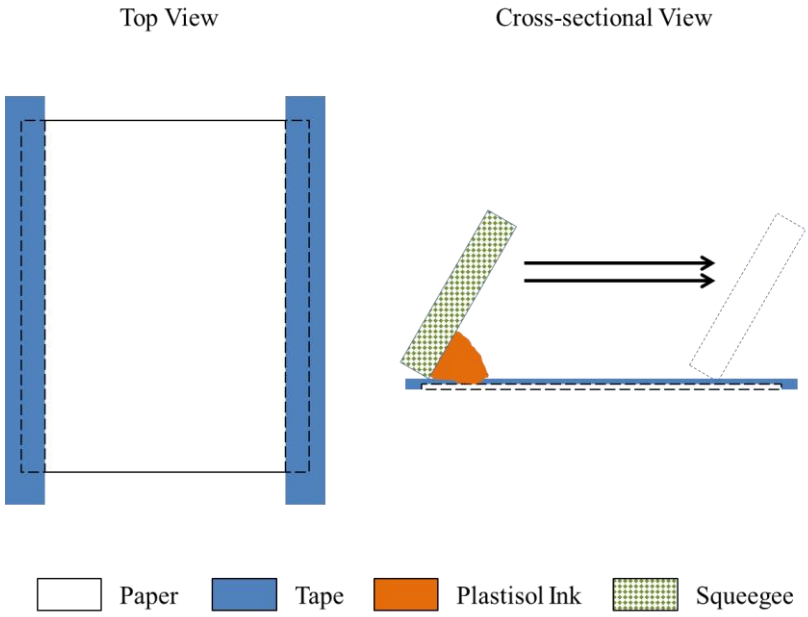


**Figure 21. Plastisol ink coating process on paper. Tape is used as an example mask to control the thickness of the plastisol film, and conventional screen-printing squeegee is used to spread the ink. [85]**

To measure the actual thicknesses of printed plastisol films, 20 sheets of paper (4.25 x 5.5 inches) are prepared with the two different mask thicknesses (63 μm and 126 μm). Ten samples are prepared using a single layer of tape (63 μm) to form the mask, and the other ten are formed using two layers (126 μm). The plastisol ink is coated on all twenty sheets of paper and cured on a hotplate at 110°C. The temperature has an effect on the process. If the temperature is not high enough, it takes longer to cure the plastisol ink, and the plastisol film becomes tacky and does not cure. However, if the curing temperature is too high, the solvent that controls the viscosity of the plastisol evaporates too fast and bubbles are formed on the surface. The recommended curing temperature supplied by the manufacturer is 170 – 180 °C for the plastisol; however, that recommendation is for thicker plastisol layers that are more common to screen-printing of artistic designs and lettering. For the thin-film microfluidic devices presented here, a very small amount of plastisol ink is used (e.g., tens of ml to print a sheet of 4.25 x 5.5 inches paper) and the film thickness is comparatively very shallow (measured in micrometers as opposed to millimeters). At 110°C, the ink is cured thoroughly after 15 seconds with no evidence of bubbles. After curing, the thickness of the each plastisol film on paper is measured before planarization at nine different positions using a micrometer. Figure 22 (a) shows the positions where the thickness is measured.

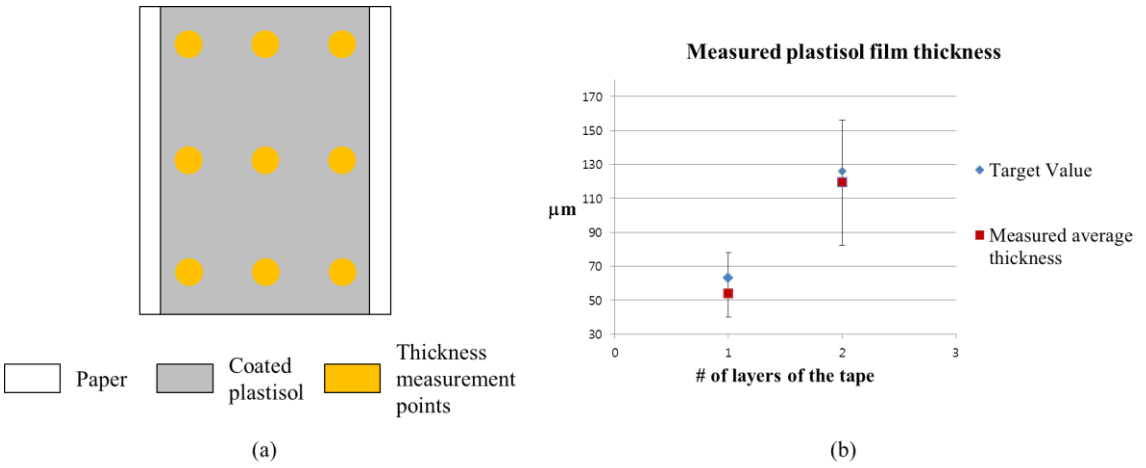


**Figure 22. Details for thickness measurement and results: (a) Showing approximately where the nine points for thickness measurements are performed on each film. (b) Comparison between target thickness and measured average thickness with maximum deviation (vertical bars shows the range of values). [85]**

A total of 90 measurements from 10 samples are performed for each mask thickness (63 μm and 126 μm), and the average thickness for plastisol films is calculated. Figure 22 (b) shows the results. For the mask thickness of 63 μm, an average thickness of 54.08 μm is measured with a standard deviation of 11.09 μm. The average measured thickness is 8.92 μm thinner than the target value, and the range of the film thickness is from 40 μm to 78 μm (maximum deviation of +23.92 μm, and -14.07 μm). For the mask that is 126 μm thick, the average measured thickness of the film is 116.18 μm with a standard deviation of 20.2 μm. The range of the film thickness is from 79 μm to 153 μm (maximum deviation of +36.82 μm, and -37.17 μm). Overall thickness non-uniformity resulted from two different film non-uniformities: variation of film thickness on each individual sample, and variation from sample to sample. Across an individual sample of plastisol film, where measurements are taken as shown in Figure 22 (a), films have a maximum variation of 13 μm. From sample to sample, the variation is higher, with a maximum of 18 μm difference in average thickness between samples. These variations are likely due to manual placement of the masks and the manual plastisol film coating process. It is also possible that the variation in thickness of the masking tape caused the variation in the thickness of the plastisol film. When a tape mask is attached to paper and measured for thickness, the thickness varies only slightly (1 – 3 μm for a tape mask 63 μm in thickness, and 2 – 5 μm for 126 μm tape mask). It is expected that all of these

variations can be minimized with a custom-made masking layer with more controlled thickness and using a more automated film deposition process (e.g., automated screen-printer).

### 5.2.2. Planarization of the Plastisol Films

Although the plastisol is carefully coated using a manual squeegee, the surface of coated plastisol film is not completely flat. Grooves are observed that appear to be due to the edge of the conventional screen-printing squeegee not being completely flat. This is not surprising, given that the squeegee is usually used for artistic designs where the thickness and resolution of the resulting pattern is not as critical. Figure 23 (a) shows an uneven edge of a typical squeegee. Micro-scale grooves that can result in uneven surface profile are observed. Figure 23 (b) shows the surface of the coated plastisol film before planarization. Grooved patterns are visually observed due to uneven edges of the squeegee, and an approximately 9 – 13 μm gap is measured via profilometer. In addition to affecting surface profile for fluid flowing along the film surface, the uneven surface of the film could hinder bonding between plastisol films. The air gaps between two films potentially cause weak adhesion, high chance of leakage, and poor performance of the devices.

To minimize this problem, a planarization process is performed. For planarization, the film is placed on the hotplate at 110°C, and pressurized using flat glass slides for 15 seconds. Figure 23 (c) shows a photograph of a plastisol film surface after planarization, which appears much smoother. Groove patterns are not observed visually, and a gap of only 3 – 6 μm is measured after planarization. Another possible solution would be to develop a custom squeegee with a very straight and smooth edge; however, a planarization step may still be beneficial for the smoothest possible film.

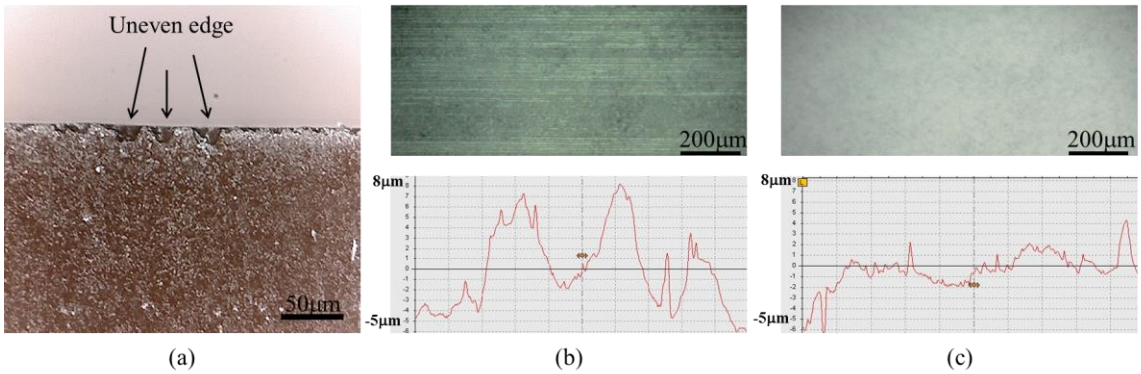


**Figure 23. Photographs showing the effect of squeegee edge roughness: (a) Uneven edge of a squeegee. (b) Photo of uneven surface of coated plastisol film before planarization, and its surface profile as measured by profilometer. (c) Photo of flattened surface of coated plastisol film after planarization, and its improved surface profile. [85]**

The average thickness of the plastisol films is also measured after planarization with the same method as discussed previously at the same points shown in Figure 22 (a). Figure 24 presents the results. For a mask 63 μm in thickness, the film thickness decreases from 54.08 μm to 45.38 μm (16% decrease) with a standard deviation of 11.7 μm, and a 25 μm to 80 μm range (deviation of +34.62 μm, and -20.38 μm). For a mask thickness of 126 μm, the thickness of the film decreases from 116.18 μm to 112.97 μm (2.8% decrease) with a standard deviation of 25.33 μm, and a 65 μm to 156 μm range (deviation of +43.02 μm, and -47.97 μm). The average thickness thus slightly decreases for both cases because the films are pressurized during the planarization process. The thickness variation between samples is increased after planarization due to manual pressing process, but automated pressing can be used to minimize the variation.

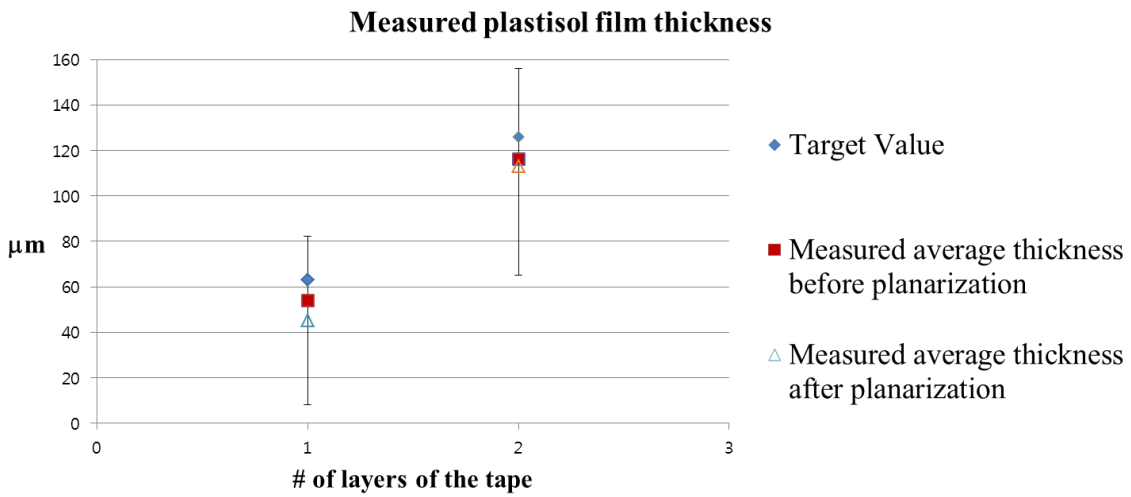


**Figure 24. Measured average thickness of the plastisol film after planarization. The average thickness is decreased due to the applied pressurization of the squeegee during planarization. Vertical bars show the measured ranges of the film thicknesses. [85]**

### 5.2.3. Thermal Fusion Bonding

The bonding of the plastisol films is a very important process for successful fabrication of both single and multi-level microfluidic devices. Weak bonding or imperfect bonding causes malfunction of the devices such as leakage or collapse. Many different methods can be used to bond two thermoplastic polymer surfaces, such as solvent bonding, vibration welding, ultrasonic welding, and laser beam welding [86]. We employ thermal fusion bonding because the bonding process is simple and easy to perform and does not require a cleanroom facility. Solidified plastisol can be melted and bonded to another plastisol film via one or more thermal cycle(s) of heating and cooling. First, two plastisol films printed on paper are heated up again to make the plastisol film soften at 110°C. The two films are then bonded by pressurizing the films. Lastly, the bonded films are cooled to room temperature. In order to bond the two films using thermal fusion, a laminating machine (Apache, AL13P) is used as purchased, which provides a uniform pressure and temperature to enable proper thermal fusion bonding.

Once the plastisol films are bonded together, the paper substrate must be removed. The paper substrate is easily detached from the film since the adhesion between the bonded plastisol films is much stronger than the adhesion between the plastisol and the paper substrate. The paper may tear if separated manually, resulting in

a residue remaining on the film surface. However, the residue is removed easily with water, which does not affect the cured thermoplastic plastisol film.

### 5.2.4. Pattern Resolution

The achievable dimensions of structures and channels patterned in each plastisol film depend mainly on the power and speed of the laser cutting machine. When the power is too high and the speed is too low, the paper may burn and/or the plastisol melt more than desired, resulting in larger dimensions than expected. On the contrary, if the power is too low and the speed is too high, the plastisol film remains unpatterned. To test the effects of laser power and speed on pattern dimensions, two sets of lines with the same width are prepared. This width is the thinnest width that can be achieved from the laser machine (hair line setting, 76 μm). For the first set of lines, the power is fixed at 50% and the speed is changed from 90% to 10%. Figure 25 (a) shows the design as input into the laser cutter, and Figure 25 (b) shows a photograph of fabricated patterned lines showing the effect of different laser speeds. The patterned lines show different line widths as expected. At fixed power, line width becomes thicker as the speed decreases; this is because the heat of the laser had greater (longer) influence on the plastisol film as the speed is lower. Table 5.1 shows the results. The biggest difference occurs when speed is decreased from 90% to 70%. From this data, we may conclude that a laser speed higher than 70% should be used in order to minimize pattern dimensions, i.e., improve resolution (smallest achievable pattern).

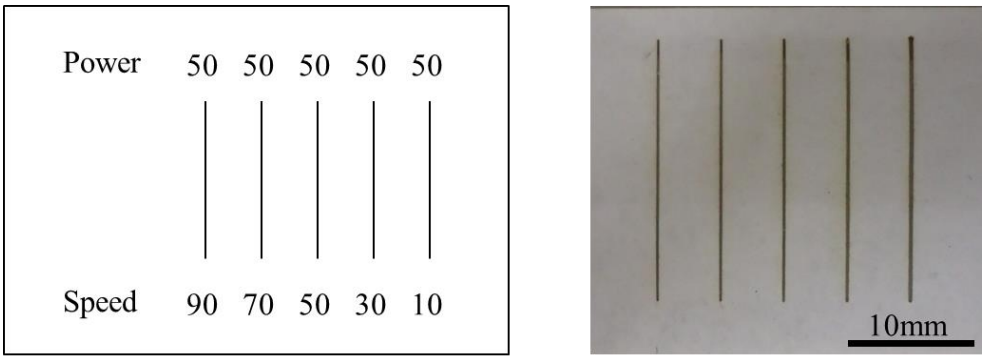


(a) (b)

**Figure 25. Dimension difference as a result of different laser speeds: (a) Expected design showing as-designed dimension for each line width of 76 μm. (b) Patterned lines. The width for each line is different since a different laser setting is used for each line: higher speeds of the laser result in narrower widths. [85]**

**Table 5.1. Achievable widths as measured at different laser speeds with design of 76 μm (the finest) channel width. These results are for a single experiment at each width. [85]**

| **Power** | 50% | | | | |
|---|---|---|---|---|---|
| **Speed** | 90% | 70% | 50% | 30% | 10% |
| **Patterned width** | 136 μm | 208 μm | 218 μm | 240 μm | 264 μm |

For the second set of lines, the speed is fixed at 50% and the power is changed from 10% to 90%. Figure 26 (a) shows the design, and Figure 26 (b) shows a photo of the resulting laser-patterned lines where power is varied. At a fixed speed, line width becomes thicker as the power increases; this is because higher powers of the laser increase melting of the plastisol. Table 5.2 shows the results. The biggest difference occurs when power is increased from 30% to 50%. From this data, we may conclude that a laser power lower than 50% should be used in order to minimize pattern dimensions (i.e., increase resolution).

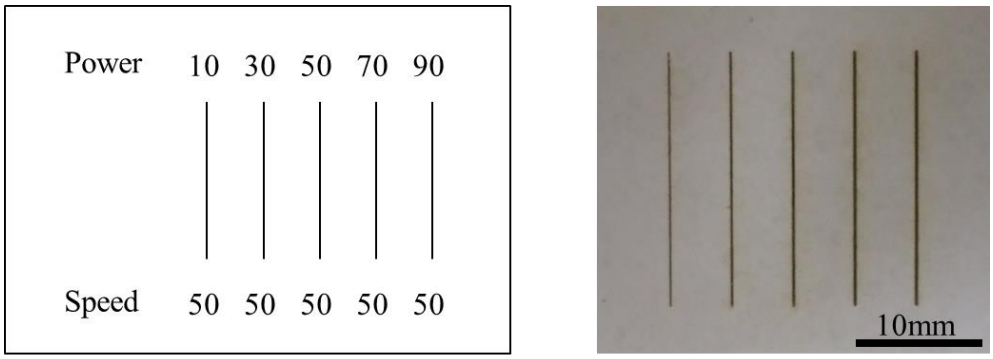


**Figure 26.** **Dimension difference with different laser powers: (a) showing as-designed dimension for each line of 76 μm. (b) Patterned lines. The width for each line is different since a different laser setting is used for each line. Higher power of the laser results in thicker line width. The resulting widths as-fabricated are shown in Table 2. [85]**

**Table 5.2.** **Achievable widths as measured at different laser power with design of 76 μm (the finest) channel width. These results are for a single experiment at each width. [85]**

| **Speed** | 50% | | | | |
|---|---|---|---|---|---|
| **power** | 10% | 30% | 50% | 70% | 90% |
| **Patterned width** | 156 μm | 188 μm | 228 μm | 252 μm | 272 μm |

To minimize melting of the plastisol film and in order to keep the dimension of each channel as small as possible, it is required to use fairly low power and high speed, and repeat the cutting process until the plastisol film is fully patterned. The proper power and speed of the laser differs depending on the thickness of plastisol film, and desired width of the structure. Based on the data from Tables 1 and 2, a setting of 30% of maximum power and 90% of maximum speed is used for optimal laser patterning. It is also possible to use settings of 10% of maximum power and 90% of maximum speed, but it took a longer time to make a pattern due to the low power of the laser. The patterning process should be repeated many times.

Although the laser ablation machine is a convenient and easy tool that can pattern over a large surface area, it has some disadvantages. One of the main disadvantages is that the patterned structures have a V-shape patterning profile because the laser melts the surface of the material and transfers heat to adjacent areas.

It is impossible to make structures with perfectly vertical walls. Figure 27 (a) shows a photograph of a cross-sectional view of microfluidic channel patterned on a substrate of solid polymethyl methacrylate (PMMA), and Figure 27 (b) shows a cross-sectional view of laser-patterned channel in a thin plastisol film that has been coated on a paper substrate. For both cases, a V-shaped profile for the channel is evident.

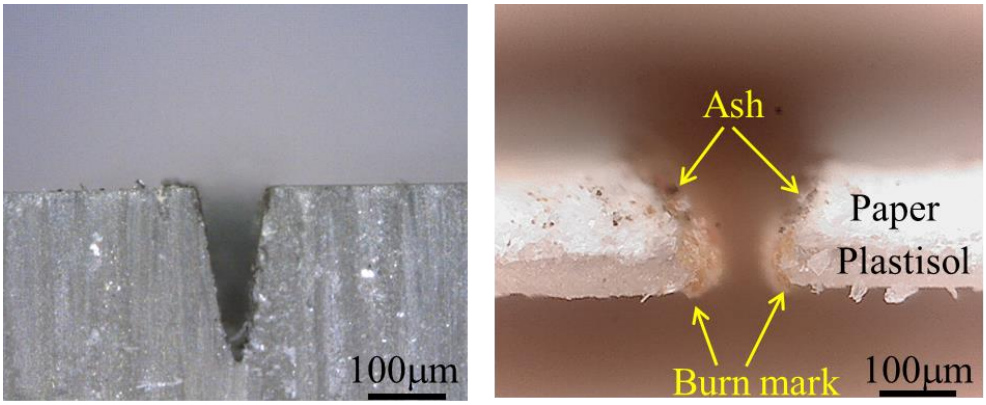


**Figure 27. Cross-sectional view of example laser-patterned materials: (a) V-shaped profile on solid polymethyl methacrylate (PMMA) substrate. (b) V-shaped profile on plastisol-coated paper film. [85]**

The dimension of a patterned channel also changes with the bonding process. When the bonding temperature is too high, the plastisol layer melts and deforms easily during the pressurization for thermal fusion bonding. The best way of bonding two plastisol films without deformation is to perform multiple lamination steps (repetitions) at a moderate temperature until the plastisol films are fully bonded. To measure the actual width of patterned channels, and how each changes with the bonding process, five samples are prepared. Each sample is designed to have seven channels with the same depth (about 100 μm) but with different width (76 μm, 100 μm, 200 μm, 400 μm, 600 μm, 800 μm, and 1000 μm). Each sample is bonded to a flat plastisol layer using lamination, and the widths of the channels are measured via profilometer. Due to the V-shaped cross-sectional profile, widths for both top and bottom of each channel are measured separately. The measured widths of the tops of the patterned channels before bonding are: 182 μm, 210 μm, 266 μm, 408 μm, 622 μm, 824 μm, 1018 μm. For the designed widths of 76 μm, 100 μm, and 200 μm channels, the actual channel widths are much larger than the design; however, widths from 400 μm have actual patterned widths that are similar to the designed widths. Each sample is bonded at 145°C with a different

number of laminating cycles (one to five times). Table 5.3 shows the results. Data is only provided for three lamination process steps and greater since at least three repetitions of the lamination process must be performed in order to ensure good bonding of plastisol films. For each channel, only one measurement is performed for the top and bottom of each V-shaped cross-sectional profile.

**Table 5.3. Width change measurements at different numbers of bonding repetitions (repeat cycle). Data is only provided for three lamination process steps and greater since at least three repetitions of the lamination process must be performed in order to ensure good bonding of plastisol films. [85]**

| Laminating Repeat Cycle | Measured Position | Width (μm) | | | | | | |
|---|---|---|---|---|---|---|---|---|
| | | 76 | 100 | 200 | 400 | 600 | 800 | 1000 |
| Before Bonding | Top | 182 | 210 | 266 | 408 | 622 | 824 | 1018 |
| 3 times | Top | 216 | 272 | 376 | 540 | 752 | 944 | 1084 |
| | Bottom | 118 | 120 | 236 | 348 | 544 | 748 | 982 |
| 4 times | Top | 244 | 284 | 384 | 600 | 764 | 952 | 1144 |
| | Bottom | 108 | 120 | 220 | 336 | 524 | 736 | 968 |
| 5 times | Top | 176 | 211 | 276 | 464 | 620 | 920 | 1063 |
| | Bottom | N/A | N/A | N/A | N/A | N/A | 672 | 903 |

As can be seen from Table 5.3, all the bottom widths are narrower than the top widths due to the V-shaped profile characteristic, and all of the top widths are wider than their designed dimensions as expected from experiments presented previously. For each bottom width of the channel, the measured width is wider than the designed width when the design width is below 200 μm. This means that no matter how small the designed dimension is, the actual patterned dimension is larger than the expected design at given conditions used for this thesis (145°C of bonding temperature, 100 μm thickness of the plastisol film, and $CO_2$ laser with 30% of power and 90% of speed). The smallest channel size (e.g., 108 μm for the as-designed 76 μm channel width) is obtained with four repetitions of the lamination process.

As the laminating process is repeated, the top layer channel widths become wider and the bottom layer channel widths become narrower due to the pressure applied during lamination. In addition, when the laminating process is repeated five times, the plastisol films are melted and the channel is blocked due to deformation of the pattern. Only for designed channel widths larger than 800 μm can be maintained with five lamination steps.

### 5.2.5. Sample Microfluidic Channels

Using the new fabrication method, simple microfluidic channels are fabricated. Figure 28 shows a cross-sectional view of the microfluidic channel showing the different layers. Each layer is firmly bonded via thermal fusion bonding, creating a micro-scaled flexible fluidic channel (120 μm width × 60 μm thickness) on the flexible fabric substrate.

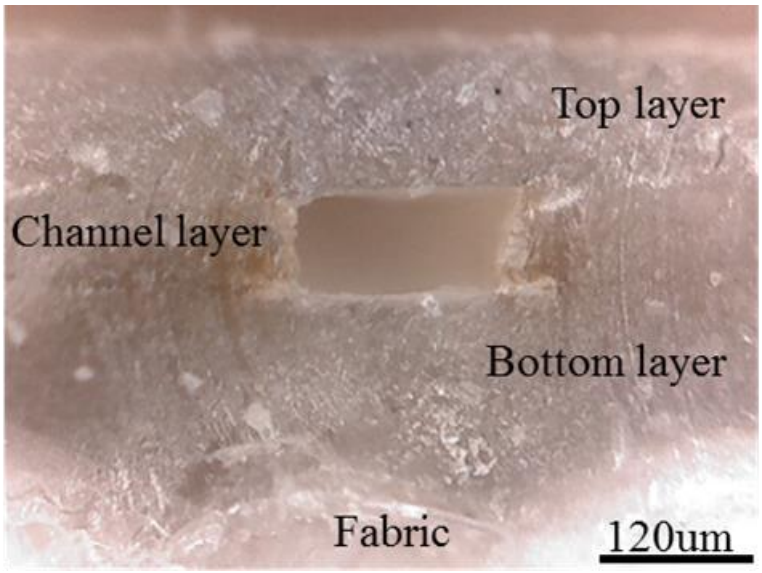


**Figure 28. Cross-sectional view of the sample microfluidic channel showing the different plastisol polymer layers used to make the channel. [85]**

Also, one of the advantages of the fabrication method is that multi-layered structures can be easily fabricated by simply bonding more layers. Additional layers can be prepared with a laser cutter machine and bonded to form multi-layered structures. Figure 29 shows the design of an example microfluidic structure with multiple layers of microfluidic channels and interconnecting via holes. One sample has two channels in parallel on different levels (Figure 29 (a)), and consists of a bottom layer, first channel layer, second channel layer, and top layer (Figure 29 (b)). Each channel is designed to

be 100 μm in width and height. A second sample has two channels that intersect at their centers, with the channels at right angles to each other (Figure 29 (c)). Both channels are designed to have a height of 100 μm and a width of 400 μm (Figure 29 (d)), and are interconnected via a hole (200 μm high × 100 μm width × 400 μm length). Even when the channel width is four times wider than the height, the top layer neither collapses nor deforms to block the channel as shown in Figure 29 (d). This is important as other flexible devices, such as those made in PDMS, can also collapse or sag when high aspect ratios of width to height are employed [87].

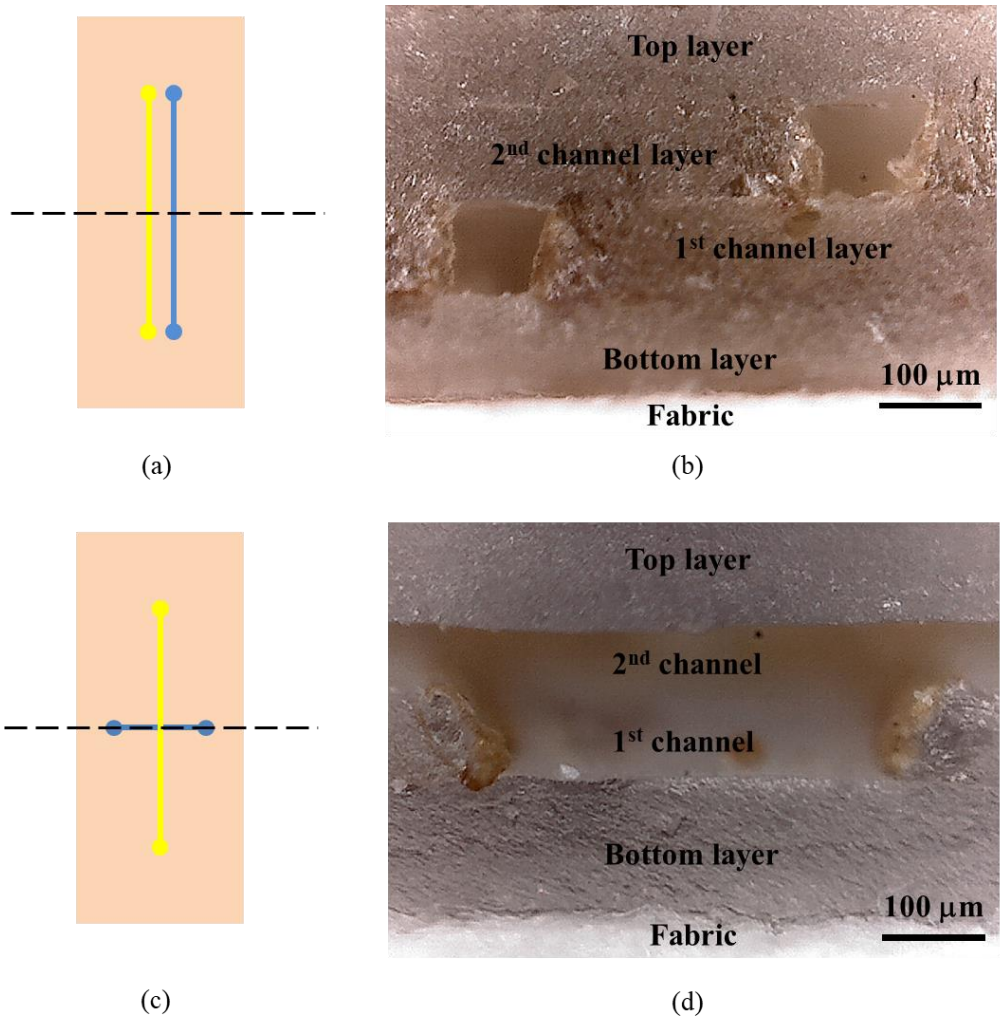


**Figure 29. Designs and photographs of multi-layer microfluidic channels: (a) Design of parallel channels. Two channels are in parallel on different levels. (b) Photo of a cross-section of the parallel channels. (c) Design of two channels on different levels that intersect. (d) Photograph of cross-section of the device at the microfluidic channels' intersection point. [79]**

## 5.3. Characterization of the Flexible Microfluidic Devices

In this section, characterization of the plastisol-based flexible microfluidic devices is presented. Stretchability and flexibility of the microfluidic channels are characterized, and optimal dimension for wearable microfluidic devices is determined. Also, passive microfluidic mixer is fabricated and demonstrated as an example device.

### 5.3.1. Stretchability of Plastisol-based Microfluidic Channels

As demonstrated in section 3.1, plastisol film is stretchable. However, to check mechanical property and optimize the dimension of the wearable microfluidic devices, the stretchability of microfluidic structures is also tested. In order to test the stretchability of microfluidic structures in plastisol, two simple microfluidic channels 500 μm in width, 15 mm in length, and approximately 100 μm in thickness, are prepared. As with the un-patterned plastisol samples, the channel devices are not patterned on fabric in order to test the stretchability of the devices alone. Figure 30 shows the design of the channels. One sample has a vertical channel (Figure 30 (a)), and another sample has a horizontal channel (Figure 30 (b)). For both channels, the bottom and top layers are designed to be approximately 150 μm in thickness, so that the total thickness of each device is designed to be 400 μm in order to maximize sample stretchability as previously discussed. The actual measured averaged thicknesses are around 426 μm for both samples. The variation is caused by the manual coating of the plastisol. The inlet and outlet each has a diameter of 2 mm. Each sample is stretched in increments of 500 μm until failure, with the width and length change of each channel also measured.

For the test, five additional distance rulers are prepared on a PMMA substrate. Figure 31 shows the design of the rulers. One ruler is designed for sample stretching similarly to that shown in Figure 2 (a) for un-patterned samples, but the lines are separated by 500 μm instead of 200 μm. The other four rulers are designed to measure the dimension change of the channels. For these rulers, the length of the lines on the ruler is increased or decreased by 50 μm for adjacent ruler markings. Arrays of lines in different lengths are made as shown in Figure 31.

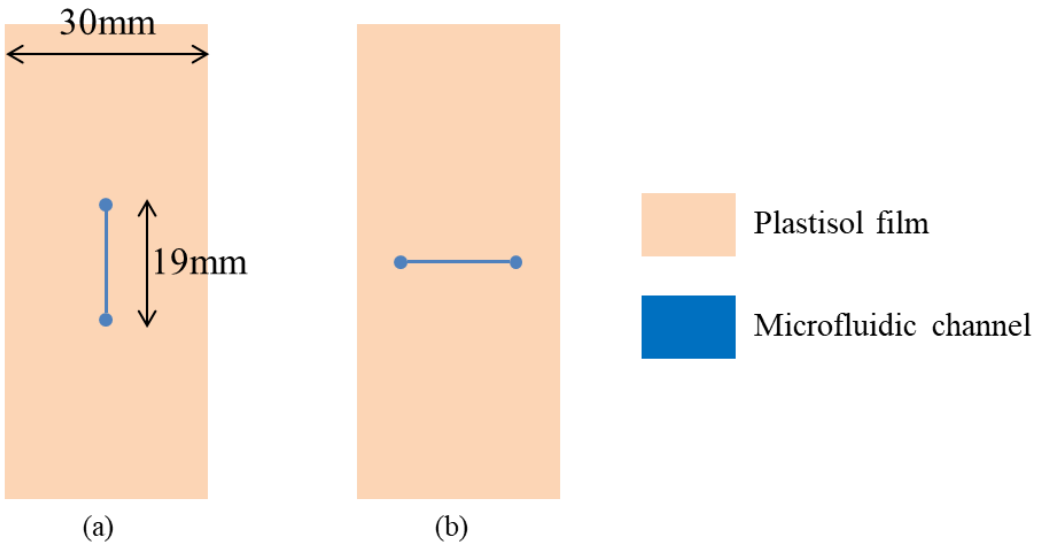


**Figure 30.** **Design of sample channels for stretchability test: (a) Vertical channel. (b) Horizontal channel. Both channels have the same dimensions including thickness. [79]**

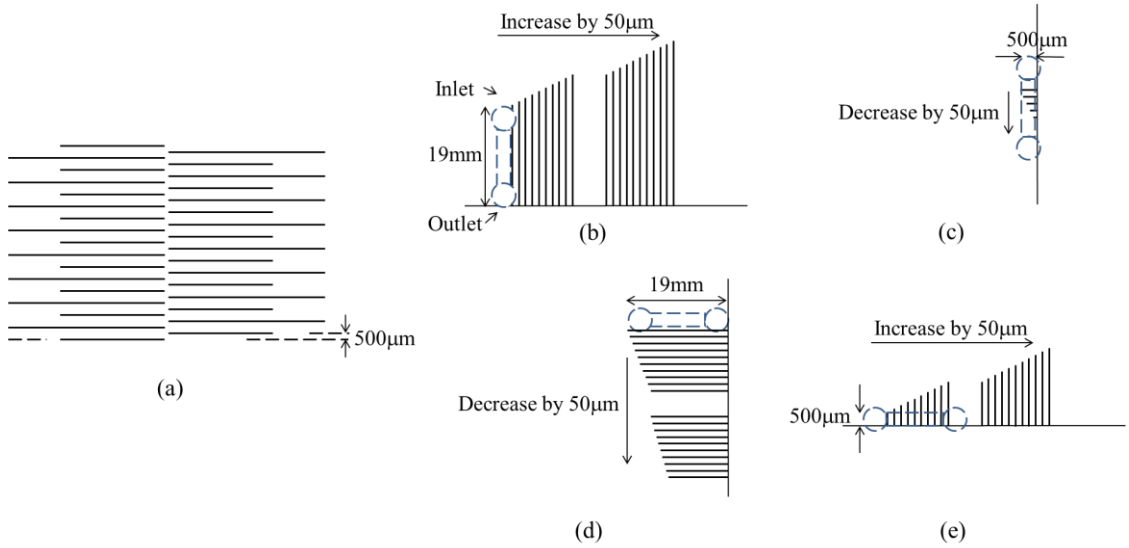


**Figure 31.** **Design of micro-rulers for stretchability test of microfluidic channels: (a) Ruler for microfluidic channel stretching. The microfluidic channel device is attached and aligned to the ruler, and stretched in increments of 500 μm. (b) Ruler for measurement of length increase for the vertical channel. The channel is aligned to the ruler and change in length is observed. (c) Ruler for measurements of width decrease for the vertical channel. (d) Ruler for measurements of length decrease for the horizontal channel. (e) Rulers for measurement of width increase for the horizontal channel. The channel is aligned to the ruler and change in width is observed. [79]**

In order to measure change in each channel's dimensions, the two microfluidic channels are attached and aligned on the PMMA micro-rulers, and stretched in increments of 500 μm, similarly to the method shown in Figure 2 (b). For each channel, the changes in length and width are measured. For example, to measure the increase in width of the horizontal channel, the channel is aligned to the left end line (500 μm) of the ruler shown in Figure 31 (e). Then as the channel width increases due to stretching, the line which contacts the channel's edge is observed and the length of the line is recorded. Increased distance is calculated by subtracting 500 μm from the length of the line which makes contact to the channel edge. Figure 32 shows photographs of the testing method for the horizontal channel and a microscopic image of the channel width measurement. Figure 32 (a) shows the horizontal channel before stretching, and Figure 32 (b) shows elongated channel under stretching prior to the breaking point. Figure 32 (c) shows the channel at the breaking point. Figure 32 (d) shows how the channel width is measured by the micro-ruler as described in Figure 31 (e). The initial width of the channel is 500 μm, and the width is increased upon stretching. The photograph shows that the channel width is stretched approximately 150 μm because the fourth line (650 μm) makes contact to the channel edge. The channel width change is measured in increments of 50 μm. For the horizontal channel, the length decreases and the width increases upon stretching. The maximum length decrease before breakage is 7.55% (from 19.2 mm to 17.75mm) and the maximum width increase is 45.45% (from 0.55 mm to 0.8mm). On the other hand, for the vertical channel, the length increases and the width decreases upon stretching. The maximum length increase is 15% (from 19.05 mm to 21.95mm) and the maximum width decrease is 20% (from 0.5 mm to 0.4 mm). Compared to the stretchability of the un-patterned plastisol films, the microfluidic channel device could not be stretched as far before failure. Specifically, un-patterned 400 μm-thick plastisol films could be stretched approximately 15 mm (37.5%), but the channel devices could only be stretched approximately 7 mm (17.5%) before failure. This is likely because the channel device is composed of three separate plastisol films that are bonded with empty space in the middle to form the channel, creating a less robust structure. As Figure 32 (c) shows, the damage caused by stretching occurs at the location of the channel.

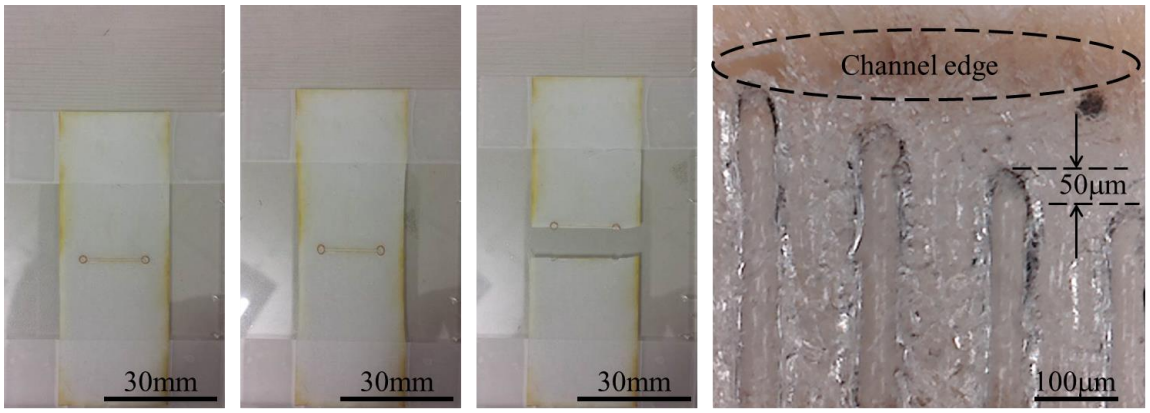


**Figure 32. Photographs of the sample and channel width measurement: (a) Horizontal channel before stretch. (b) Stretched channel. (c) Broken sample at breaking point. (d) Measurement of the increase in width of the horizontal channel. The initial channel width is 500 μm, and the width is increased upon stretching. It is shown that the width is increased by 150 μm. [79]**

### 5.3.2. Flexibility of Microfluidic Channels

To demonstrate that the fabrication method is suitable for flexible and wearable devices and systems, the flexibility of microfluidic devices is also tested. A plastisol microfluidic device consisting of a single channel (150 μm thickness × 1 mm width × 70 mm length) is fabricated using the new fabrication method and tested for operation when flexed. The channel is fabricated without fabric so that only the plastisol device is tested in the absence of a textile substrate. The device is tested by wrapping it around five pillars with different diameters (diameters of 5 cm, 4 cm, 3 cm, 2 cm, and 1 cm) that are each prepared by rolling a sheet of paper. Figure 33 shows photographs of the paper pillars with different diameters (Figure 33 (a)) and the test set-up (Figure 33 (b)). The channel is attached on each paper pillar and fixed using adhesive tape. Polyethylene tubes with diameters of 0.86 mm are connected to the channel, and red ink is injected to the channel through the tube using a syringe pump (Harvard Apparatus, 11 plus) at a flow rate of 5 ml/min, which is a typical (although relatively high) flow rate used for applications in our laboratory. Figure 34 shows photographs of the working flexible microfluidic channel. The channel works without any leakage or clogging even when the channel is wound twice on the pillar of 1 cm diameter (Figure 34 (a)). Also, in another test the channel is bent alternately and tested using four ball-point pens each with a

diameter of 0.8 cm (Figure 34 (b)). Even when the channel is bent and flexed in such a complex manner, the ink flows without clogging or leakage in the channel at the same flow rate (5 ml/min).

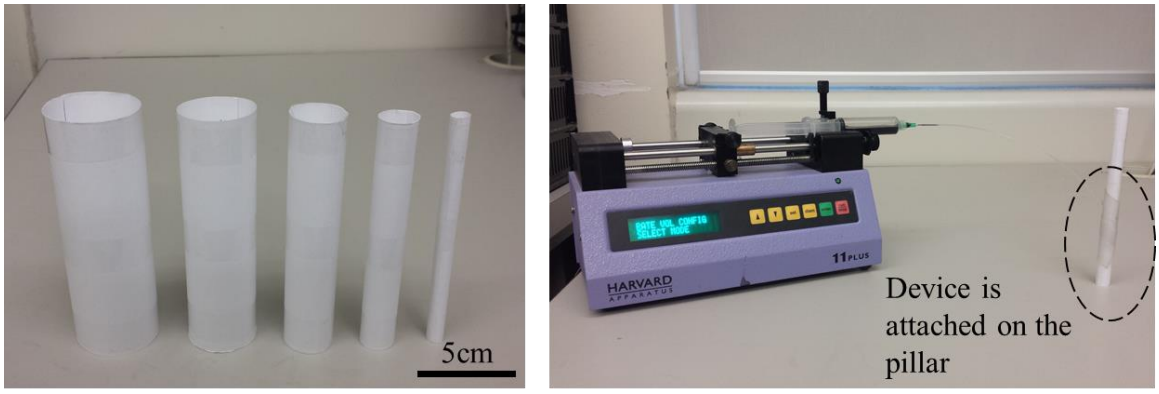


**Figure 33. Photographs of the paper pillars and the testing of microfluidic channel flexibility: (a) Paper pillars with different diameters (5 cm, 4 cm, 3 cm, 2 cm, 1 cm). (b) Test set-up. The flexible channel is attached on the paper pillar, and red ink is injected through the channel using a syringe pump at volumetric flow rate of 5 ml/min. [79]**

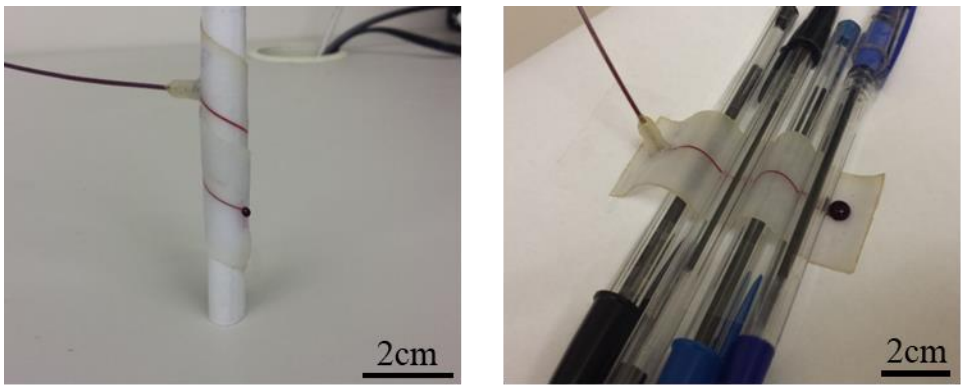


**Figure 34. Working flexible microfluidic channel (plastisol only, no textile substrate): (a) Working channel wrapped twice around a paper pillar 1 cm in diameter. (b) Using ball-point pens to demonstrate flexibility that can be achieved yet still result in a working device. [79]**

## 5.4. Wearable Microfluidic Mixer

In order to demonstrate that the fabrication process can be employed for microfluidic devices, a simple example Tee-mixer is fabricated and its basic operation both on flat and curved surfaces is performed. The flexible microfluidic mixer (480 μm thickness × 40 mm width × 70 mm length) consists of two inlets, one outlet, and single-layered channel, and is designed such that two different liquids entering each inlet are combined at a Tee-shaped junction to flow and mix along a single channel to the outlet. Figure 35 (a) shows the design of the example microfluidic mixer, and Figure 35 (b) shows a photograph of a fabricated mixer. Close-ups from the top of the inlet channel intersection, microfluidic channel for mixing, and outlet section of the device, are shown in Figure 35 (b).

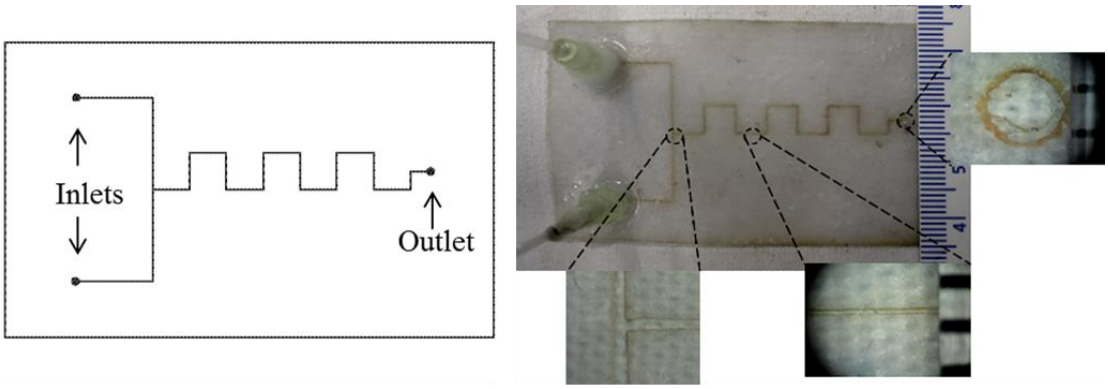


**Figure 35. Microfluidic mixer: (a) Design of the mixer from top view. (b) Photograph of fabricated mixer with close-ups. [85]**

Figure 36 shows the mixer in operation. The mixer is tested on both a flat surface (Figure 36 (a)) and on a curved surface (Figure 36 (b)) using green and red fluid. Close-ups in Figure 36 (a) show that the green fluid and the red fluid are clearly separated at the intersection of the two inlet channels, but the fluids are mixed as they flow through the channel. The mixer is next attached to a cylinder with a diameter of 48 mm in order to demonstrate operation on a curved surface. No absorption of liquids into the plastisol polymer is observed (due to its hydrophobicity) for both cases. The mixer is also tested with an injected volumetric flow rate from 5.5 ml/min to 46 ml/min. The mixer works properly without any leakage of liquid over this range of volumetric flow. This range was chosen to be on the upper end of what may be expected for many microfluidic systems.

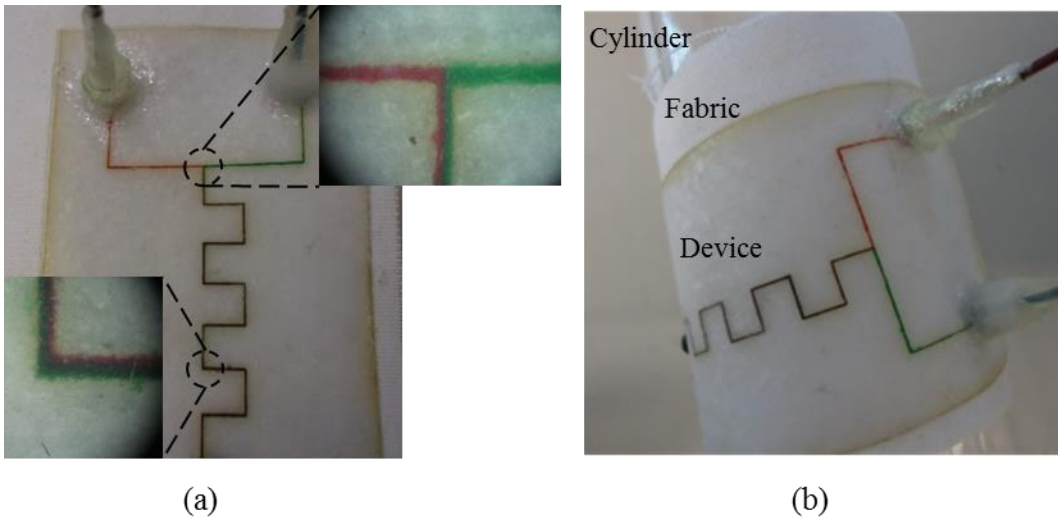


**Figure 36. Testing of the flexible fluidic mixer: (a) Test on a flat surface showing mixing. (b) Test on a curved cylinder showing unaltered mixing operation. No leakage is observed in either case. [85]**

# Chapter 6.

# Active Wearable Microfluidic Device Combined with Screen-Printable Silver C-NCP

In order to demonstrate that fully flexible and wearable active microfluidic devices can be developed using the new integrated fabrication method, a simple example microfluidic device which measures the conductivity through the fluid between two electrodes in response to a voltage across the electrodes is designed, fabricated, and tested.

Screen-printable silver C-NCP for wearable systems is presented in chapter 3 and 4. As previously shown, normally non-conductive plastisol ink can be rendered conductive by mixing conductive silver nanoparticles, resulting in a resistivity of $2.12 \times 10^{-6}$ Ω·m at 70 wt-% of silver particles. This silver C-NCP is now combined with the new fabrication method for wearable microfluidic devices as active components to develop a fully flexible active microfluidic device on a textile substrate.

## 6.1. Design and Fabrication Method

Figure 37 shows the design of the device. Figure 37 (a) shows the cross-sectional view, and Figure 37 (b) shows the top-down view of the device. The device consists of a single layer channel (300 μm thickness × 1 mm width × 60 mm length), one pair of commercial silver epoxy electrodes, and one pair of silver C-NCP electrodes. Each electrode has the same design and dimension, and is connected to electrical routing made from the same material as its electrode to transfer the signal. The electrical routing is also connected to contact pads for connection to measurement equipment. silver epoxy (CW2640 conductive epoxy, Circuitworks) with resistivity of $1 \times 10^{-6}$ ~ $10 \times 10^{-6}$ Ω·m is used for the conductive epoxy electrodes, and silver C-NCP is used for the other set of electrodes. Though silver epoxy is much less flexible that the silver C-NCP, the epoxy is employed for one set of electrodes in order to compare the epoxy's characteristics with those of the silver C-NCP electrodes. This is done to compare the two materials, as silver epoxy is a commonly used screen-printable material when

conductivity is required. Figure 37 (c) shows the design of the electrodes, electrical routing, and contact pads. The same silver epoxy is used to form electrical routing and contact pads for the epoxy electrodes. However, silver C-NCP is used to form electrical routing and contact pads for the silver C-NCP electrodes. Each electrode (150 μm thickness × 800 μm width × 3 mm length) is inside the channel, thus making contact to the fluid. The electrical routing (150 μm thickness × 1.5 mm width × 4.5 mm length) is embedded in the device outside the channel for electrical isolation. Each contact pad (400 μm thickness × 2.5 mm width × 2.5 mm length) is open for connection to the digital multimeter. Thus, only the contact pads are exposed to air, with the electrodes and electrical routing all embedded in the device, either in the microfluidic channel (electrodes) or between polymer layers (routing). Fluid is injected into the channel by syringe pump, flows through the channel, and the current through the fluid is measured using the digital multimeter with a voltage applied between each set of electrodes (silver epoxy or silver C-NCP electrode pair).

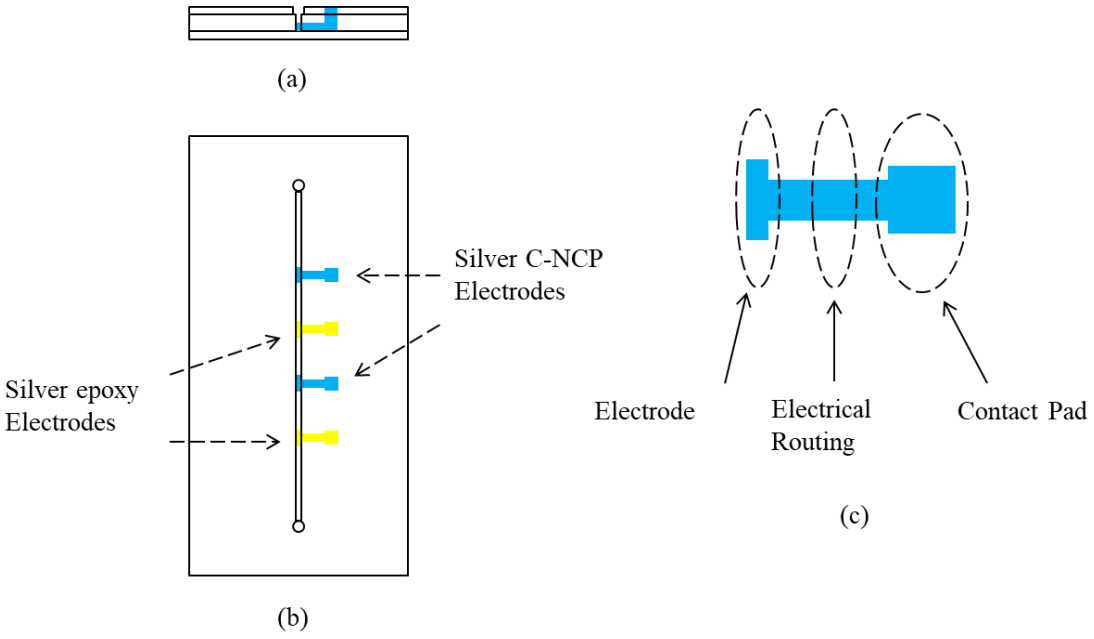


**Figure 37.** **Flexible and wearable fluid conductivity sensor design: (a) Cross-sectional view of the device showing one electrode, its electrical routing, and contact pad. The electrode is inside the channel, and the electrical routing is embedded in the device. (b) Top-down view of the device. A pair of silver C-NCP electrodes and a pair of conductive epoxy electrodes are aligned with a microfluidic channel. (c) Detail of the electrodes' design. Each electrode is connected to the contact pad through the electrical routing. [79]**

Figure 38 outlines the fabrication process of the device. First, the bottom layer is screen printed on fabric, and C-NCP electrodes, electrical routing, and contact pads are screen printed on the bottom layer using silver C-NCP (Figure 38 (a)). We use 70 wt-% of silver particles to prepare the screen-printable silver C-NCP. The adhesion between the bottom layer and C-NCP electrodes is very strong (as tested via tape test using techniques similar to other researchers [88]), likely because the same plastisol ink forms the base polymer for each structure. Commercial silver epoxy is next screen printed to pattern silver epoxy electrodes, electrical routing, and contact pads (Figure 38 (b)). The first channel layer is then patterned using a laser cutter and bonded to the bottom layer on the same level with the electrodes (Figure 38 (c)). Next, contact pads for the two different types of electrodes are screen printed again and a second channel layer is prepared and bonded (Figure 38 (d)). The second channel layer is designed to have both the channel and contact pad patterns so that electrical routing is covered by the second channel layer, thus embedding the electrical routing between the bottom layer and second layer. However, the contact pads are on the same level as the second channel layer because they are printed twice. Finally, contact pads are printed again, and the top layer is prepared and bonded to seal the channel (Figure 38 (e)). The top layer is designed to have inlet, outlet, and contact pad openings so that the channel is sealed by the top layer, with only the contact pads exposed (not embedded between polymer layers in the device). As shown in Figure 38, the final device consists of four layers. The second channel layer is needed because the electrodes are on the same level with the first channel layer. Without the second channel layer, the channel would be blocked by the electrodes and injected fluid could not flow through the channel. Figure 39 shows photographs of a fabricated device with close-up and microscopic images. Figure 39 (a) shows the top view of the device and close-up of the active components (electrodes, electrical routing, and contact pads). Figure 39 (b) shows a cross-sectional view of the silver C-NCP contact pad, and Figure 39 (c) shows the cross-sectional view of the channel on the silver C-NCP electrode.

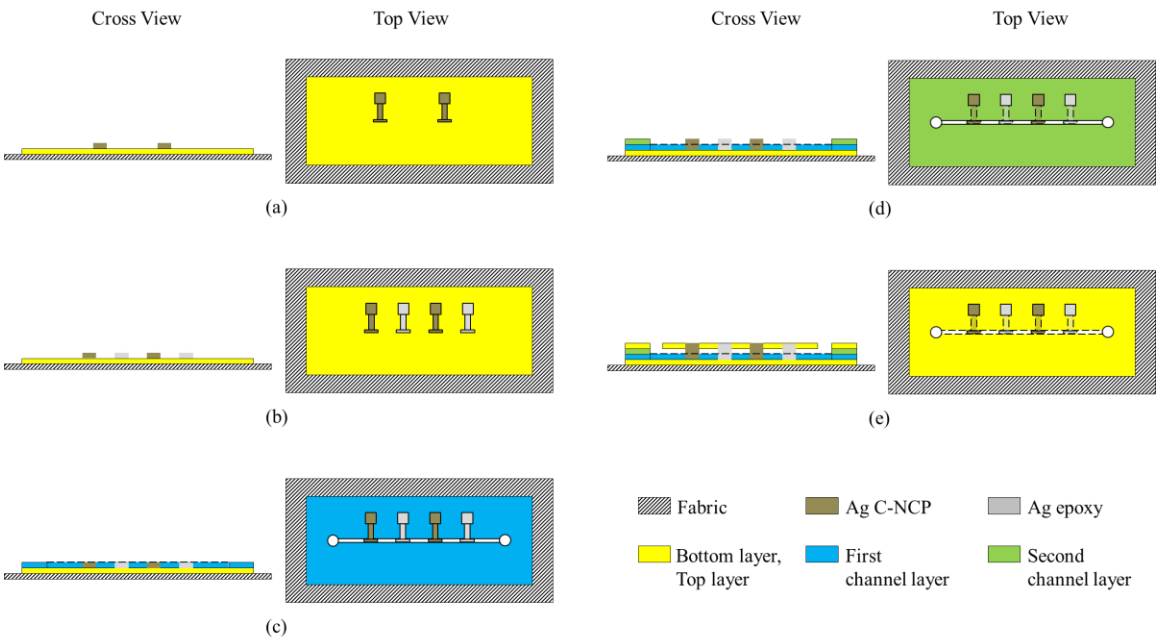


**Figure 38.** **Integrated fabrication process for flexible and wearable conductivity sensor: (a) Print the bottom layer on fabric, and print C-NCP electrodes, electrical routing, and contact pads on the bottom layer. (b) Print conductive epoxy electrodes, electrical routings, and contact pads using silver epoxy ink. (c) Prepare the first channel layer, align the channel to the electrodes, and bond to the bottom layer on the same level with electrodes. (d) Print contact pads for both types of electrodes, and prepare and bond the second channel layer. Contact pads are on the same level with the second channel layer. (e) Print the contact pads again, and prepare and bond the top layer. Only the contact pads and inlet/outlet holes are exposed on the device, with all other structures (electrodes, channel, etc.) embedded in the device. [79]**

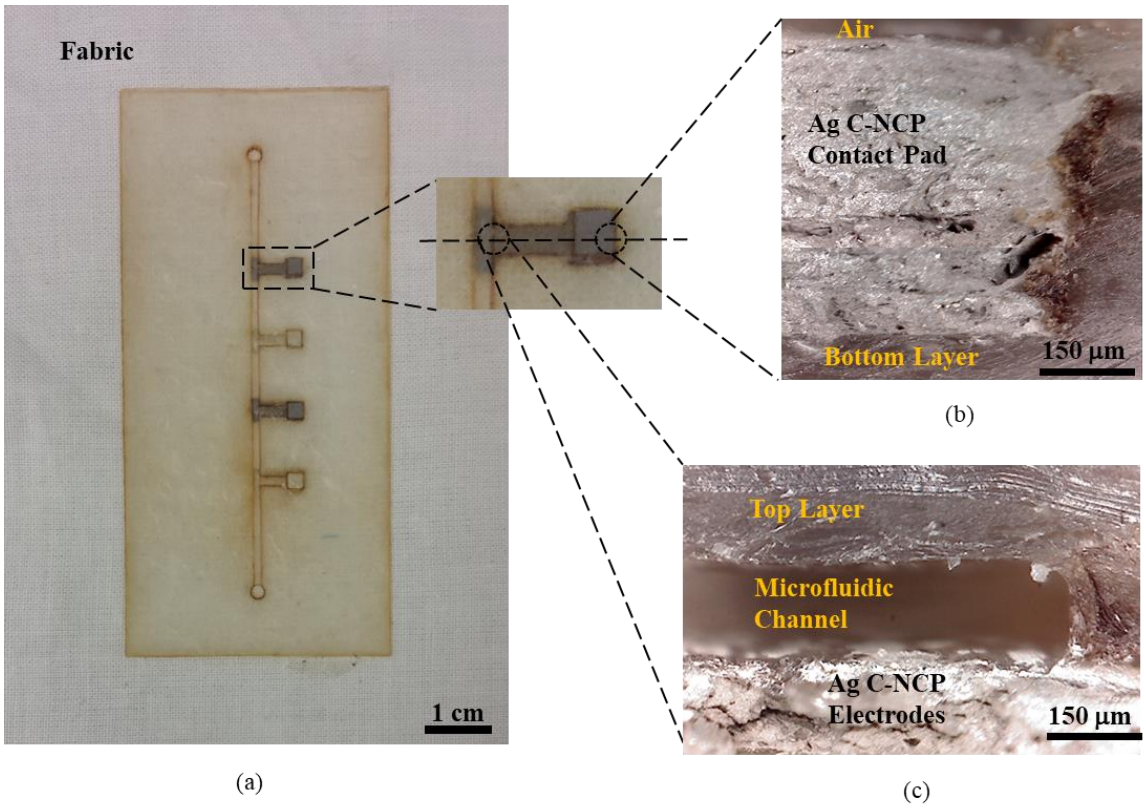


**Figure 39. Photographs of the device with close-ups and microscope images: (a) Top view of the device and close-up of the conductive active component. The close-up shows a C-NCP electrode in the microfluidic channel so that fluids can flow on the electrode. (b) Cross-sectional view of the silver C-NCP contact pad. (c) Cross-sectional view of the channel on the silver C-NCP electrode. [79]**

## 6.2. Experimental Methods and Results

Saline solution samples with different concentrations of salt are employed to test the flexible microfluidic device. Polyethylene tubes with diameters of 0.86 mm are connected to both the inlet and outlet of the device using a silicone sealant to allow liquid saline injection and waste removal during testing. Ten saline solutions are prepared at different salt concentrations (0.2 wt-%, 0.4 wt-%, 0.6 wt-%, 0.8 wt-%, 1.0 wt-%, 1.2 wt-%, 1.4 wt-%, 1.6 wt-%, 1.8 wt-%, and 2 wt-%). An alternating current (AC) voltage at 10KHz is applied between each type of electrodes separately to allow for comparison. For each saline concentration, the applied AC voltage is varied from 0.3V peak-to-peak to 3V peak-to-peak by 0.3 V peak-to-peak increments (thus, a total of 10 increments). A DC voltage is not used to prevent chloridization of both silver C-NCP and silver epoxy

electrodes. While producing Ag/AgCl non-polarizable electrodes may be desirable from the standpoint of producing sensors that operate across a wide range of frequencies [78], in order to simplify our initial characterization experiments, we prevent the formation of AgCl formation on the electrode surface. Figure 40 shows the test set-up. An AC voltage is applied between the two different sets of electrodes of the same type (silver epoxy or silver C-NCP), and a multimeter is connected in series to measure the current. First, to check the correlation between applied voltage and the measured current, the current is measured through silver C-NCP electrodes by changing the applied voltage but keeping the saline solution concentration the same. Next, the same measurement is repeated at different salt concentrations, but the same applied voltage to check the correlation between salt concentrations and measured current. Silver epoxy electrodes are then tested with the same procedure. The current measurements are performed three times for all saline concentrations at each applied voltage, and the channel is washed between measurements of each saline concentration to minimize the effect of fouling for the proof-of-concept devices. From these measurements, the average current is calculated for both silver C-NCP electrodes and silver epoxy electrodes. Figure 41 (a) shows the results from the silver C-NCP electrode pair, and Figure 41 (b) shows the results from the silver epoxy electrode pair.

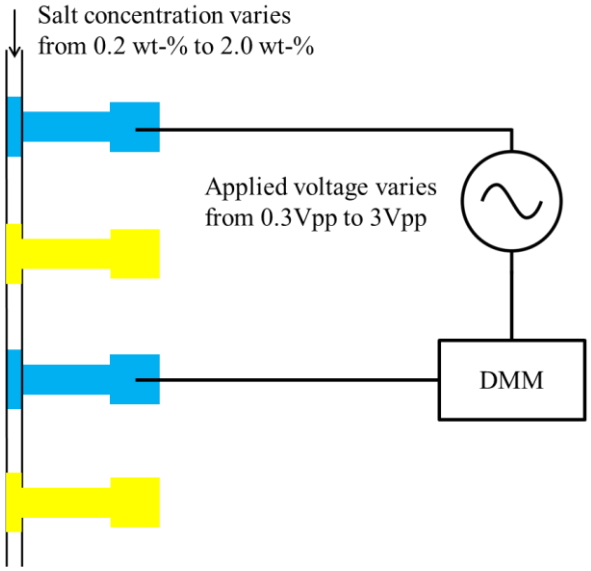


**Figure 40. Device test set-up. AC voltage is applied between same type of electrodes, and multimeter is connected in serial to measure the current. The current measurements are performed for all saline concentrations at each applied voltage. [79]**

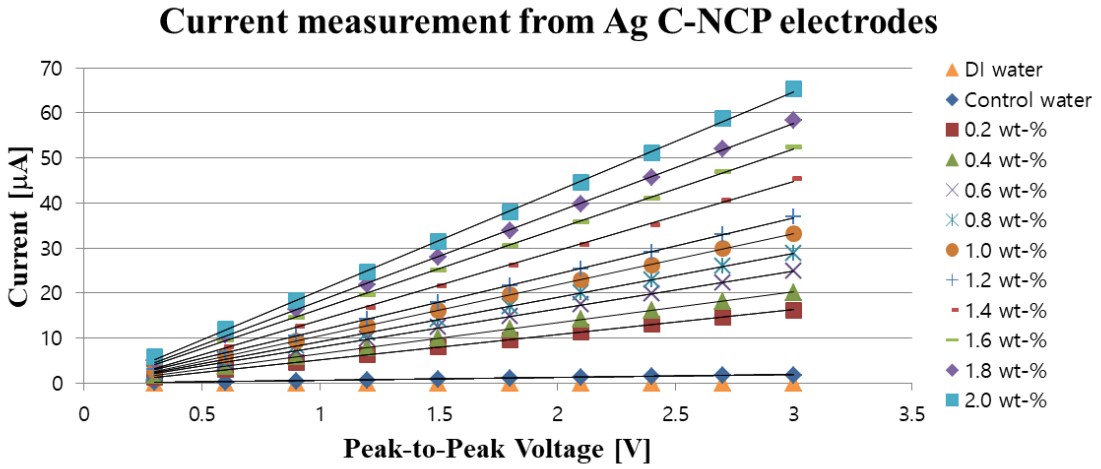


(a)

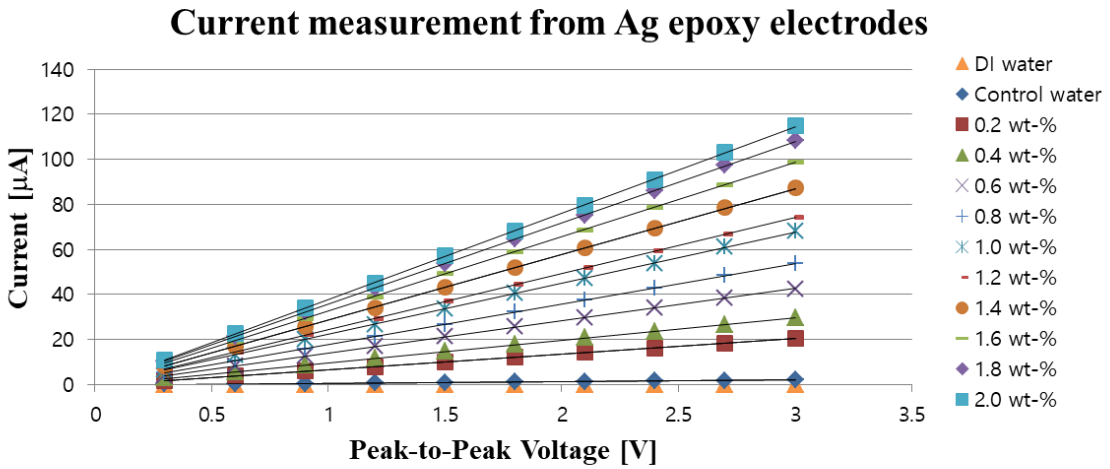


(b)

**Figure 41. Current measurement results: (a) Results from silver C-NCP electrodes. As expected, the current appears to increase linearly as the applied voltage increases. In addition, also as expected, the current increases as the concentration of salt increases. (b) Results from silver epoxy electrodes. The current increases linearly as the concentration of salt increases and applied voltage increases. [79]**

For the saline solutions, filtered water (control water) is used, but a small current is measured due to a small amount of minerals in the control water. When de-ionized water is used, no current is measured as shown in Figure 41. For both cases, the current appears to increase linearly with the applied voltage, and the variations for each measurement are very small (< 0.8%). The error bars are not shown in the Figure 41 because they are not visible at the scale of the figures (too small). In addition, the current increase as the salt concentration increases, as expected due to the higher

conductivity with increasing sodium ion concentration. As the salt concentration increases in increments of 0.2 wt-%, the current increases approximately by 1.17 times for the silver C-NCP electrodes and by 1.22 times for the silver epoxy electrodes. Furthermore, for a salt concentration increase from 0.2 wt-% to 2.0 wt-%, the current increases approximately 3.98 times for the silver C-NCP electrodes and approximately 5.57 times for the silver epoxy electrodes. From these results, we may conclude that both types of electrodes function properly for current measurements across all concentrations of saline solution tested, but the epoxy electrodes' sensitivity to the sodium ions' concentration change is higher than that of the C-NCP electrodes.

Figure 42 shows a comparison between silver C-NCP electrodes and silver epoxy electrodes. The current change at a fixed salt concentration and the current change at a fixed voltage are compared. When the salt concentration is same, the current increases linearly as the applied voltage increases for both types of electrodes (Figure 42 (a)). However, the measured current from the silver epoxy electrodes is 1.4 times higher than the current from the silver C-NCP electrodes. The current also increases linearly as the salt concentration increases when a fixed voltage is employed (Figure 42 (b)) for both types of electrodes. However, the current from the silver C-NCP electrodes is smaller than the current from the silver epoxy electrodes. In all cases, the currents from the silver C-NCP electrodes are smaller than those of silver epoxy electrodes. This is because silver C-NCP is less conductive than silver epoxy. From the tests in Figure 41 and Figure 42, it is observed that the conductivity and sensitivity of silver C-NCP electrodes are lower compared with the silver epoxy electrodes. However, the silver C-NCP electrodes function in a similar manner, and are much more flexible than silver epoxy electrodes, which is beneficial to wearable and flexible systems.

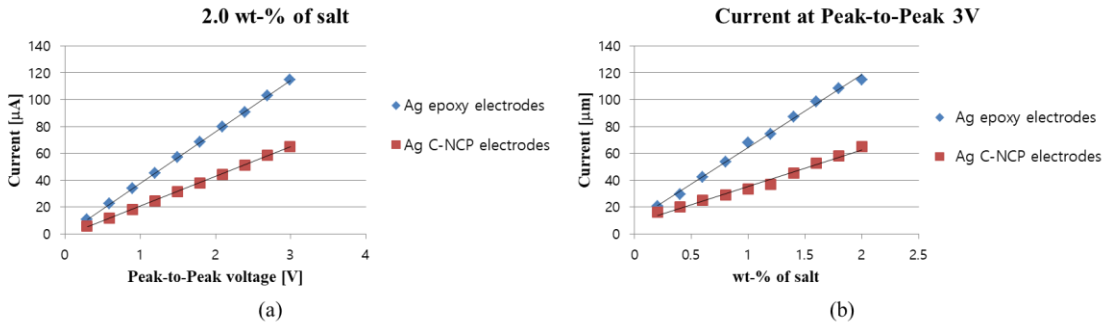


**Figure 42. Comparison between silver C-NCP electrodes and silver epoxy electrodes: (a) Results at 2.0 wt-% of salt concentration with change of applied voltage. (b) Results at 3V of voltage with change of salt concentration. Though the conductivity and sensitivity of silver C-NCP are lower than those of silver epoxy, silver C-NCP electrodes still work in a similar manner with silver epoxy electrodes. [79]**

# Chapter 7.

# Future Work and Conclusions

In this chapter, several possible improvements are identified for future work, and the achievements of this thesis are summarized. Future work in terms of material and fabrication methods and measurement techniques are discussed. In addition, limitations of prior works and how this thesis addresses or does not address these limitations, are also discussed, along with a critical view of the limitations of the work presented in this thesis. In addition, the contributions that this thesis makes to the advancement of the field of textile-based wearable systems are presented.

## 7.1. Future Work

Future work can be divided into two different types: future work that extends the characterization of the materials and fabrication methods already developed, and future work that more fully explores the general concepts developed in this thesis as applied to new materials, devices and applications.

### 7.1.1. Additional Characterization

In this thesis, many tests are performed to characterize the silver C-NCP and developed fabrication methods for microfluidics. However, additional characterization is required in order to understand the capability and limitations of both the silver C-NCP and the fabrication methods for wearable microfluidics. First, the silver C-NCP should be characterized more fully with automated equipment. Most of the characterizations performed in this thesis are manually tested. For example, the bending tests and stretchability tests of silver C-NCP should be automated to check how many bending and stretching cycles can be repeated under various conditions (temperature, humidity) without causing damage. In addition, due to direct contact to different kinds of fluids, the silver particles on the surface may be easily oxidized or corroded, which may reduce device lifetime. Thus, the lifetime of the silver C-NCP for a microfluidic application, in the presence of different fluids, should be tested. In addition, the resistivity of silver C-NCP

can also be affected by ions in fluids. The surface change of silver C-NCP electrodes, and its effect on resistivity and performance, should be tested more thoroughly using X-ray photoelectron spectroscopy (XPS). Lastly, correlation between silver C-NCP and temperature should be studied. The effect of temperature change on resistivity, stretchability, and flexibility should be characterized.

The new fabrication methods for wearable microfluidics also should be better characterized and the fabrication processes optimized. The process whereby the plastisol is coated on paper, as well as the planarization process, should be automated to minimize the variation across the coated film and result in a more uniform thickness. In addition, the laser cutting process and bonding process should also be optimized. The reproducibility of the laser cutter with the same setup should be tested, and the reproducibility of bonding repetition should also be tested. Lastly, more tests of the conductivity sensor are also required in order to make a practical sensor. In this thesis, the applied violated is changed from 0.3 Vpp to 3 Vpp at each fixed salt concentration, and the process is repeated three times without changing the salt concentration. However, in the future, the salt concentration will be changed at a fixed applied voltage, and test will be repeated to verify how little error occurs after changing the salt concentration. This would more closely mimic the use of such a sensor in perspiration measurement.

### 7.1.2. Development of New Materials and Devices

One of the main goals of this thesis is the development of a new conductive material for textile-based wearable applications. Screen-printable C-NCP is prepared using screen printable plastisol ink and conductive silver nanoparticles, and applied to various applications to show its advantages and benefits. In the future, different kinds of nanomaterials can also be used to develop plastisol-based screen-printable C-NCPs and composite nanopolymers, including nanopowders, nanowires, and nanoflakes. For example, gold or platinum nanoparticles could be investigated for other biomedical applications. Using the C-NCPs, a textile-based circuit board for ECG circuitry can be developed and combined with the wearable ECG electrodes developed in this thesis. Also, complex conductive patterns for the lighting system could be designed and optimized. Patterns like a company’s logo, or even the name of the person wearing the

lighting system, can be designed for identification at a distance. Flexible solar cells or energy harvesting devices could also be incorporated into such systems on a C-NCP based textile circuit board.

The other main goal is the development of new fabrication methods for wearable microfluidic systems. The new processes are characterized, and example passive and active microfluidic devices are demonstrated. In the future, more various active devices can be fabricated and tested. New fabrication methods combined with C-NCP can be used to develop bio-sensors such as flexible perspiration sensors for, e.g., pH, lactate, and amount of perspiration. In addition, methods to collect and deliver fluidic biosamples to the sensors within the enclosed microsamples must be developed in order to take advantage of the use of enclosed channels for sample isolation and preservation (protection against evaporation). In addition, different types of NCPs may be used to develop such fluid manipulation and other active microfluidic devices. For example, flexible microfluidic valves are developed using magnetic NCP [16]. Using similar methods, screen-printable magnetic NCP can be developed and applied to textile-based microfluidic devices, or wicking pumps could be demonstrated, enabling the possibility of full complex microfluidic systems with fluid pumping and routing components on a textile substrate. By combining with different kinds of flexible conductive or magnetic polymer, or polymer nanocomposites with other functionality, fully operational textile-based wearable devices and systems may be realized.

## 7.2. Conclusions

Wearable microfluidic technologies that can be combined with garments for collecting and analyzing of body fluids with simultaneous measurement of bioelectrical signals, enable development of portable and lightweight real-time health monitoring devices without hindering the flexibility of the garments. This thesis makes significant progress towards the improvement of textile-based wearable technologies by developing screen-printable C-NCP and new fabrication methods for wearable microfluidic devices and systems. Prior works for wearable technologies have limitations such as complicated fabrication methods, use of expensive equipment, long fabrication times, low conductivity of conductive materials, weak adhesion between the material and the flexible substrate, and lack of reusability. Furthermore, technologies for textile-based

wearable microfluidic devices are not fully explored due to difficulty in direct fabrication on textiles. In this thesis, a new screen-printable C-NCP is developed as an alternative material for wearable devices and systems by using screen-printable plastisol ink and conductive silver nanoparticles. The plastisol used in this thesis has advantages such as being non-toxic, not harmful to ecosystems, flexible, easily printable on textiles, designed for adhesion to textiles, and easily patternable. The plastisol is normally used for artistic printing on cloth, but can also be used as electrical components by mixing with conductive nanoparticles, or for microfluidic structures using the fabrication processes outlined in this thesis.

Using plastisol and silver nanopowders, screen-printable silver C-NCP is developed, and properties such as flexibility, stretchability, and electrical behavior are characterized. The new screen-printable silver C-NCP possesses good conductivity and mechanical flexibility, and has a great potential in wearable and flexible technology. A resistivity of $2.12 \times 10^{-6}$ Ω·m is achieved at 70 wt-% of silver particles, and the conductivity changes only minimally with bending from -90° to 90°. Also, the silver C-NCP is washable and suitable for long term use. The silver C-NCP is showcased in two applications, one biomedical application and one safety applications. For the biomedical application, wearable dry ECG electrodes are developed on a textile. Silver C-NCP is directly printed on fabric to form sensing electrodes and electrical routing, and sensing electrodes are chloridized to form non-polarizable Ag/AgCl electrodes. A right leg driven ECG circuit is used to test the electrodes, and the results are comparable with results from commercial ECG electrodes. For the safety application, a lighting system is developed on a safety vest. Silver C-NCP is printed directly on a commercial safety vest and used as electronic routing. Silver C-NCP is printed on both the front and back sides of the vest to form conductive lines, and surface mount LEDs are attached on the front side of the vest. A coin battery is connected to the silver C-NCP lines on back side to supply power. The safety vest works in both daylight and the dark, and the LED light maintains about 24 hours with single coin battery. By using SMT and coin battery, it is shown that silver C-NCP can be used for integrated microelectronic wearable devices and systems that require low power.

The plastisol is also used for the first time for fabrication of wearable microfluidic devices on textile. A whole new printing-based fabrication process for fully wearable and

flexible microfluidic devices is developed using flexible and stretchable properties of the plastisol. The fabrication process is based on the separate patterning of multiple layers of a device which are subsequently bonded together. For the fabrication method, only fast, inexpensive, and simple screen printing, laser cutting, and thermal bonding techniques are used. All the processes are optimized, and micro-scaled sample passive microfluidic channels are fabricated. A microfluidic mixer that mixes two different kinds of liquid is also developed and demonstrated under both flexed and non-flexed conditions. The new microfluidic fabrication method and screen-printable silver C-NCP are also combined to develop fully wearable active microfluidic devices. A fluid conductivity sensor that measures the current through the fluid between two electrodes in response to a voltage across the electrodes is developed. Both silver C-NCP electrodes and silver epoxy electrodes (for comparison) show similar behavior, but the current-voltage relationship from the silver C-NCP electrodes are lower compared with the relationship from electrodes fabricated in silver epoxy silver C-NCP because silver C-NCP is less conductive and less sensitive to the sodium ions' concentration change than the silver epoxy. However, the results for both types of electrodes are qualitatively similar, with silver C-NCP electrodes having the advantage of greater flexibility.

This thesis addresses limitations of prior works for flexible and wearable systems as follows:

1. Materials:

    1a. Weak adhesion between metal films and polymer substrates is addressed by using the same plastisol inks for both conductive and non-conductive components

    1b. Low conductivity of composite polymers is addressed by using silver nanoparticles for higher conductivity than, e.g., CNTs

    1c. Problems of electrodes' polarizability are addressed by developing flexible non-polarizable Ag/AgCl electrodes

2. Fabrication process:

2a. Problems of complicated fabrication methods, need for expensive equipment, and long fabrication times are addressed by using simple, easy, and fast methods such as screen printing, laser cutting, and thermal bonding

2b. Inflexibility of devices, which can hinder human motion or activity, are addressed by developing fully flexible devices on textiles

2c. Difficulties in fabricating devices on textiles are addressed by developing new fabrication methods based on screen-printable polymers which enable direct fabrication on textiles

3. Performance:

3a. Lack of reusability is addressed by developing devices which can be used repeatedly and laundered

3b. Problems of fluid evaporation, which may cause changes in signal, are addressed by fabricating microfluidic devices that can isolate the sample fluid

However, while the techniques and materials developed for this thesis work address many of the limitations of prior art, the contributions also have some limitations. Specifically, the resolution of printable structures remains similar to those of other printed structures, and methods to improve resolution, and determination of resolution limit, must be determined. It is difficult to print silver C-NCP of 50 μm or less using the laser cutter machine. The minimum feature size is 76 μm for the laser cutter machine, which results in an actually patterned size which is even larger. In addition, the current contributions have limitations in how high of a temperature that the devices can be used, and the potential oxidation or corrosion of silver particles. Due to the thermoplastic property of plastisol polymer, it is difficult to use the devices for high temperature applications (> 100°C). The plastisol will soften and deform above these temperatures. Furthermore, for microfluidic applications, fluid that easily transforms the silver particles may not be used. The change of silver particles may result in inaccurate measurements. Thus, performance of specific devices in practical setting may have additional limitations.

This thesis makes substantial contributions of new methods and new materials to realize textile-based wearable systems. The methods enables fast and easy fabrication for wearable devices on textiles, and the materials can be applied to various applications including bio-medical applications, safety applications, and microfluidic applications. The contributions that this thesis makes to the field of wearable microsystems on textiles are as follows:

1. Development of fabrication processes for flexible wearable devices and systems on textile substrates featuring a plastisol polymer that is intended for screen-printing based patterning on textiles:

    1a. Development of a screen printable C-NCP, together with a screen-printing based fabrication method, for patterning on textiles.

    1b. Development of a multi-level wearable microfluidic technology using paper as a sacrificial substrate.

    1c. Combined wearable microfluidic and C-NCP electronic fabrication process on textiles for active microfluidic devices.

2. Demonstration of various devices that showcase the new material and fabrication processes. Each of these new devices not only showcases the new materials and fabrication technologies, but makes significant contributions to the fields of wearable health and safety devices:

    2a. Wearable dry ECG electrodes for measuring heart signals, showing comparable performance to commercially available electrodes.

    2b. Wearable safety vest lighting system that operates in flexed and non-flexed conditions with user-defined pattern.

    2c. Wearable passive microfluidic device (microfluidic mixer) that operates in flexed and non-flexed conditions.

    2d. Wearable active microfluidic devices (fluid conductivity sensors) with integrated microfluidic and C-NCP electronic structures.

# References


[1] P. Bonato. (2010, Augst). Advances in Wearable Technology and Its Mmedical Applications. *2010 Annual International Conference of the IEEE Engineering in Medicine and Biology*, 2021-2024. doi:10.1109/iembs.2010.5628037.

[2] S. Patel, H. Park, P. Bonato, L. Chan, M. Rodgers. (2012). A Review of Wearable Sensors and Systems with Application in Rehabilitation. Journal of NeuroEngineering and Rehabilitation, 9 (1), 21. doi:10.1186/1743-0003-9-21.

[3] B. Holschuch, D. Newman. (2015). Two-spring Model for Active Compression Textiles with Integrated NiTi Coil Actuators. *Smart Materials and Structures, 24* (3), 035011. doi:10.1088/0964-1726/24/3/035011.

[4] G. Matzeu, L. Florea, D. Diamond. (2015). Advances in Wearable Chemical Sensor Design for Monitoring Biological Fluids. Sensors and Actuators B: Chemical, 211, 403-418. Doi:10.1016/j.snb.2015.01.077.

[5] J. Yeo, K. Kenry, C. Lim. (2016). Emergence of microfluidic wearable technologies. Lab on a Chip, 16 (24), 4082-4090. doi:10.1039/c6lc00926c.

[6] W. Gao, S. Emaminejad, H. Y. Nyein, S. Challa, K. Chen, A. Peck, H. M. Fahad, H. Ota, H. Shiraki, D. Kiriya, D. Lien, G. A. Brooks, R. W. Davis, A. Javey. (2016). Fully Integrated Wearable Sensor Arrays for Multiplexed in situ Perspiration Analysis. Nature, 529 (7587), 509-514. doi:10.1038/nature16521.

[7] A. J. Bandodkar, W. Jia, C. Yardımcı, X, Wang, J.Ramirez, J. Wang. (2014). Tattoo-Based Noninvasive Glucose Monitoring: A Proof-of-Concept Study. *Analytical Chemistry, 87* (1), 394-398. doi:10.1021/ac504300n.

[8] A. W. Martinez, S. T. Phillips, M. J. Butte, G. M. Whitesides. (2007). Patterned Paper as a Platform for Inexpensive, Low-Volume, Portable Bioassays. *Angewandte Chemie, 119* (8), 1340-1342. doi:10.1002/ange.200603817.

[9] H. Nagai, M. Matsubara, K. Chayama, J. Urakawa, Y. Shibutani, Y. Tanaka, S. Takeda, S. Wakida. (2009). Fabrication of Electrophoretic PDMS/PDMS Lab-on-a-chip Integrated with Au Thin-Film Based Amperometric Detection for Phenolic Chemicals. Atmospheric and Biological Environmental Monitoring, 275-284. doi:10.1007/978-1-4020-9674-7_19.

[10] S. Xiao, L. Che, X. Li, Y. Wang. (2007). A Cost-effective Flexible MEMS Technique for Temperature Sensing. Microelectronics Journal, 38 (3), 360-364. doi:10.1016/j.mejo.2007.01.022.

[11] A. Zulfiqar, A. pfreundt, W. Svendsen, M. Dimaki. (2015). Fabrication of Polyimide Based Microfluidic Channels for Biosensor Devices. Journal of Micromechanics and Microengineering, 25 (3), 035022. doi:10.1088/0960-1317/25/3/035022.

[12] S. Wang, S. Yu, M. Lu, L. Zuo. (2017). Microfabrication of Plastic-PDMS Microfluidic Devices Using Polyimide Release Layer and Selective Adhesive Bonding. Journal of Micromechanics and Microengineering, 27 (5), 055015. doi:10.1088/1361-6439/aa66ed.

[13] U. M. Attia, S. Marson, J. R. Alcock. (2009). Micro-Injection Moulding of Polymer Microfluidic Devices. Microfluidics and Nanofluidics, 7 (1), 1-28. doi: 10.1007/s10404-009-0421-x.

[14] M. Liu, C. Zhang, F. Liu. (2015). Understanding Wax Screen-Printing: A Novel Patterning Process for Microfluidic Cloth-Based Analytical Devices. Analytica Chimica Acta, 891, 234-246. doi:10.1016/j.aca.2015.06.034.

[15] C. Carlborg, T. Haraldsson, K. Öberg, M. Malkoch, W. van der Wijngaart. (2011). Beyond PDMS: Off-stoichiometry thiol–ene (OSTE) Based Soft Lithography for Rapid Prototyping of Microfluidic Devices. Lab on a Chip, 11 (18), 3136. doi:10.1039/c1lc20388f.

[16] A. Khosla, B. L Gray. (2010). Preparation, Micro-patterning and Electrical Characterization of Functionalized Carbon-nanotube Polydimethylsiloxane Nanocomposite Polymer. Macromolecular Symposia, 297 (1), 210-218. doi: 10.1002/masy.200900165.

[17] M. Rahbar, L. Shannon, B. L. Gray. (2016). Design, Fabrication and Characterization of an Arrayable All-Polymer Microfluidic Valve Employing Highly Magnetic Rare-Earth Composite Polymer. Journal of Micromechanics and Microengineering, 26 (5), 055012. doi:10.1088/0960-1317/26/5/055012.

[18] Wearable technology. En.wikipedia.org. https://en.wikipedia.org/wiki/Wearable_technology. Published 2018. Accessed July 20, 2018.

[19] M. Chan, D. Estève, J. Fourniols, C. Escribe, E. Campo. (2012). Smart Wearable Systems: Current Status and Future Challenges. Artificial Intelligence in Medicine, 56 (3), 137-156. doi:10.1016/j.artmed.2012.09.003.

[20] H. Jung, J. Moon, D. Baek, J. Lee, Y. Choi, J. Hong, S. Lee. (2012). CNT/PDMS Composite Flexible Dry Electrodesfor Long-Term ECG Monitoring. IEEE Transactions on Biomedical Engineering, 59 (5), 1472-1479. doi:10.1109/tbme.2012.2190288.

[21] R. Zhang, K. Moon, W. Lin, C. Wong. (2010). Preparation of Highly Conductive Polymer Nanocomposites by Low Temperature Sintering of Silver Nanoparticles. Journal of Materials Chemistry, 20 (10), 2018. doi:10.1039/b921072e.

[22] L. Hu, M. Pasta, F. La Mantia, L. Cui, S. Jeong, H. Deshazer, J. Choi, S. Han, Y. Cui. (2010). Stretchable, Porous, and Conductive Energy Textiles. Nano Letters, 10 (2), 708-714. doi:10.1021/nl903949m.

[23] H. Kudo, T. Sawada, E. Kazawa, H. Yoshida, Y. Iwasaki, K. Mitsubayashi. (2006). A Flexible and Wearable Glucose Sensor Based on Functional Polymers with Soft-MEMS Techniques. Biosensors and Bioelectronics, 22 (4), 558-562. doi:10.1016/j.bios.2006.05.006.

[24] B. Shim, W. Chen, C. Doty, C. Xu, N. A. Kotov. (2008). Smart Electronic Yarns and Wearable Fabrics for Human Biomonitoring made by Carbon Nanotube Coating with Polyelectrolytes. Nano Letters, 8 (12), 4151-4157. doi:10.1021/nl801495p.

[25] J. L. Delaney, C. F. Hogan, J. Tian, W. Shen. (2011). Electrogenerated Chemiluminescence Detection in Paper-Based Microfluidic Sensors. Analytical Chemistry, 83 (4), 1300-1306. doi:10.1021/ac102392t.

[26] P. Lukowicz, T. Kirstein, G. Tröster. (2004). Wearable Systems for Health Care Applications. *Methods of Information in Medicine, 43*, 232-238.

[27] D. Maji, S. Das. (2014). Analysis of Plasma-induced Morphological Changes in Sputtered Thin Films Over Compliant Elastomer. *Journal of Physics D: Applied Physics, 47* (10), 105401. doi:10.1088/0022-3727/47/10/105401.

[28] C. Chen, C. Chang, T. Chien, C. Luo. (2013). Flexible PDMS Electrode for One-Point Wearable Wireless Bio-Potential Acquisition. *Sensors and Actuators A: Physical, 203*, 20-28. doi:10.1016/j.sna.2013.08.010.

[29] R. Matsuzaki, K. Tabayashi. (2015). Highly Stretchable, Global, and Distributed Local Strain Sensing Line Using GaInSn Electrodes for Wearable Electronics. *Advanced Functional Materials, 25* (25), 3806-3813. doi:10.1002/adfm.201501396.

[30] T. Guinovart, A. J. Bandodkar, J. R. Windmiller, F. J. Andrage, J. Wang. (2013). A Potentiometric Tattoo Sensor for Monitoring Ammonium in Sweat. *The Analyst, 138* (22), 7031. doi:10.1039/c3an01672b.

[31] Tattoo. En.wikipedia.org. https://en.wikipedia.org/wiki/Tattoo. Published 2018. Accessed Sept 21, 2018.

[32] A. Giuliani, M. Placidi, F. Di Francesco, A. Pucci. (2014). A New Polystyrene-Based Ionomer/MWCNT Nanocomposite for Wearable Skin Temperature Sensors. *Reactive and Functional Polymers, 76*, 57-62. doi:10.1016/j.reactfunctpolym.2014.01.008.

[33] S. Deng, J. Zhang, L. Ye. (2009). Halloysite–Epoxy Nanocomposites with Improved Particle Dispersion through Ball Mill Homogenisation and Chemical Treatments. *Composites Science and Technology, 69* (14), 2497-2505. doi:10.1016/j.compscitech.2009.07.001.

[34] R. Andrews, D. Jacques, M. Minot, T. Rantell. (2002). Fabrication of Carbon Multiwall Nanotube/Polymer Composites by Shear Mixing. *Macromolecular Materials and Engineering, 287* (6), 395. doi:10.1002/1439-2054(20020601)287:6<395::aid-mame395>3.0.co;2-s.

[35] J. Lee, S. Lee, H. Byeon, J. Hong, K. Park, S. Lee. (2014). CNT/PDMS-Based Canal-Typed Ear Electrodes for Inconspicuous EEG Recording. *Journal of Neural Engineering, 11* (4), 046014. doi:10.1088/1741-2560/11/4/046014.

[36] Q. Li, J. Li, D. Tran, C. Luo, Y. Gao, C. Yu, F. Xuan. (2017). Engineering of Carbon Nanotube/Polydimethylsiloxane Nanocomposites with Enhanced Sensitivity for Wearable Motion Sensors. *Journal of Materials Chemistry C, 5* (42), 11092-11099. doi:10.1039/c7tc03434b.

[37] Webster, J. G. (2009). *Medical Instrumentation (4th ed., Chapter 5).* New York, NY: Wiley.

[38] B. You, C. Han, Y. Kim, B. Ju, J. Kim. (2016). A Wearable Piezocapacitive Pressure Sensor with a Single Layer of Silver Nanowire-Based Elastomeric Composite Electrodes. *Journal of Materials Chemistry A, 4* (27), 10435-10443. doi:10.1039/c6ta02449a.

[39] S. Choi, J. Park, W. Hyun, J. Kim, J. Kim, Y. Lee, C. Song, H. Hwang, J. Kim, T. Hyeon, D. Kim. (2015). Stretchable Heater Using Ligand-Exchanged Silver Nanowire Nanocomposite for Wearable Articular Thermotherapy. *ACS Nano, 9* (6), 6626-6633. doi:10.1021/acsnano.5b02790.

[40] nanoamor. https://www.nanoamor.com/home. Published 2018. Accessed Sept 23, 2018.

[41] G. Paul, R. Torah, K. Yang, S. Beeby, J. Tudor. (2014). An investigation into the durability of screen-printed conductive tracks on textiles. *Measurement Science and Technology, 25* (2), 025006. doi:10.1088/0957-0233/25/2/025006.

[42] Z. Stempien, T. Rybicki, E. Rybicki, M. Kozanecki, M. I. Szynkowska. (2015). In-situ Deposition of Polyaniline and Polypyrrole Electroconductive Layers on Textile Surfaces by the Reactive Ink-Jet Printing Technique. *Synthetic Metals, 202*, 49-62. doi:10.1016/j.synthmet.2015.01.027.

[43] J. Han, B. Kim, J. Li, M. Meyyappan. (2013). A Carbon Nanotube Based Ammonia Sensor on Cotton Textile. *Applied Physics Letters, 102* (19), 193104. doi:10.1063/1.4805025.

[44] B. K. Little, Y. Li, V. Cammarata, R. Broughton, G. Mills. (2011). Metallization of Kevlar Fibers with Gold. *ACS Applied Materials & Interfaces,* 3 (6), 1965-1973. doi:10.1021/am200193c.

[45] F. Ochanda, W. E. Jones. (2005). Sub-Micrometer-Sized Metal Tubes from Electrospun Fiber Templates. *Langmuir, 21* (23), 10791-10796. doi:10.1021/la050911s.

[46] X. Liu, H. Chang, Y. Li, W. T. S. Huck, Z. Zheng. (2010). Polyelectrolyte-Bridged Metal/Cotton Hierarchical Structures for Highly Durable Conductive Yarns. *ACS Applied Materials & Interfaces, 2* (2), 529-535. doi:10.1021/am900744n.

[47] G. Gioberto, L. E. Dunne. (2013). Overlock-Stitched Stretch Sensor: Characterization and Effect of Fabric Property. *Journal of Textile and Apparel, Technology and Management, 8* (3), 1-14.

[48] G. Whitesides. (2006). The Origins and the Future of Microfluidics. Nature, 442 (7101), 368-373. doi:10.1038/nature05058.

[49] Z. Nie, C. A. Nijhuis, J. Gong, X. Chen, A. Kumachev, A. W. Martinez, M. Narovlyansky, G. M. Whitesides. (2010). Electrochemical Sensing in Paper-based Microfluidic Devices. Lab on a Chip, 10 (4), 477-483. doi:10.1039/b917150a.

[50] Y. Lu, W. Shi, L. Jiang, J. Qin, B. Lin. (2009). Rapid Prototyping of Paper-based Microfluidics with Wax for Low-Cost, Portable Bioassay. ELECTROPHORESIS, 30 (9), 1497-1500. doi:10.1002/elps.200800563.

[51] X. Li, J. Tian, G. Garnier, W. Shen. (2010). Fabrication of Paper-Based Microfluidic Sensors by Printing. *Colloids and Surfaces B: Biointerfaces, 76* (2), 564-570. doi:10.1016/j.colsurfb.2009.12.023.

[52] Y. Lu, W. Shi, L. Jiang, J. Qin, B. Lin. (2009). Rapid Prototyping of Paper-Based Microfluidics with Wax for Low-Cost, Portable Bioassay. *ELECTROPHORESIS, 30* (9), 1497-1500. doi:10.1002/elps.200800563.

[53] W. Dungchai, O. Chailapakul, C. S. Henry. (2011). A Low-Cost, Simple, and Rapid Fabrication Method for Paper-Based Microfluidics Using Wax Screen-Printing. *The Analyst, 136* (1), 77-82. doi:10.1039/c0an00406e.

[54] M. Sher, R. Zhuang, U. demirci, W. Asghar. (2017). Paper-based Analytical Devices for Clinical Diagnosis: Recent Advances in the Fabrication Techniques and Sensing Mechanisms. *Expert Review of Molecular Diagnostics, 17* (4), 351-366. doi:10.1080/14737159.2017.1285228.

[55] D. Liana, B. Raguse, J. Gooding, E. Chow. (2012). Recent Advances in Paper-Based Sensors. *Sensors, 12* (9), 11505-11526. doi:10.3390/s120911505.

[56] K. Tenda, R. Ota, K. Yamada, T. Henares, K. Suzuki, D. Citterio. (2016). High-Resolution Microfluidic Paper-Based Analytical Devices for Sub-Microliter Sample Analysis. *Micromachines, 7* (5), 80. doi:10.3390/mi7050080.

[57] R. S. P. Malon, k. Y. Chua, D. H. B. Wicaksono, E. P. Córcoles. (2014). Cotton Fabric-Based Electrochemical Device for Lactate Measurement in Saliva. *The Analyst, 139* (12), 3009-3016. doi:10.1039/c4an00201f.

[58] A. Nilghaz, D. H. B. Wicaksono, D. Gustiono, F. A. Abdul Majid, E. Supriyanto, M. R. Abdul Kadir. (2012). Flexible Microfluidic Cloth-Based Analytical Devices Using a Low-Cost Wax patterning Technique. *Lab on a Chip, 12* (1), 209-218. doi:10.1039/c1lc20764d.

[59] X. Xu, B. Yan. (2018). A Fluorescent Wearable Platform for Sweat Cl− Analysis and Logic Smart-Device Fabrication Based on Color Adjustable lanthanide MOFs. *Journal of Materials Chemistry C, 6* (7), 1863-1869. Doi:10.1039/c7tc05204a.

[60] S. Anastasova, B. Crewther, P. Bembnowicz, V. Curto, H. Ip, B. Rosa, G. Yang. (2017). A Wearable Multisensing Patch for Continuous Sweat Monitoring. *Biosensors and Bioelectronics, 93,* 139-145. doi:10.1016/j.bios.2016.09.038.

[61] J. Heikenfeld. (2014). Let Them See You Sweat. *IEEE Spectrum, 51* (11), 46-63. doi:10.1109/mspec.2014.6934933.

[62] A. Koh, D. Kang, Y. Xue, S. Lee, R. M. Pielak, J. Kim, T. Hwang, S. Min, A. Banks, P. Bastien, M. C. Manco, L. Wang, K. R. Ammann, K. I. Jang, P. Won, S. Han, R. Ghaffari, U. Paik, M. J. Slepian, G. Balooch, Y. Huang, J. A. Rogers. (2016). A Soft, Wearable Microfluidic Device for the Capture, Storage, and Colorimetric Sensing of Sweat. Science *Translational Medicine, 8* (366), 366ra165. doi:10.1126/scitranslmed.aaf2593.

[63] J. Choi, Y. Xue, W. Xia, T. R. Ray, J. T. Reeder, A. J. Bandodkar, D. Kang, S. Xu, Y. Huang, J. A. Rogers. (2017). Soft, Skin-Mounted Microfluidic Systems for Measuring Secretory Fluidic Pressures Generated at the Surface of the Skin by Eccrine Sweat Glands. Lab on a Chip, 17 (15), 2572-2580. doi:10.1039/c7lc00525c.

[64] Plastisol. En.wikipedia.org. https://en.wikipedia.org/wiki/Plastisol. Published 2018. Accessed July 21, 2018.

[65] N. Nakajima, E. R. Harrell. (2001). Rheology of PVC Plastisol. Journal of Colloid and Interface Science, 241 (2), 492-496. doi:10.1006/jcis.2001.7733.

[66] G. M. Spirou, A. A. Oraevsky, I. A. Vitkin, W. M. Whelan. (2005). Optical and Acoustic Properties at 1064 nm of Polyvinyl Chloride-Plastisol for Use as a Tissue Phantom in Biomedical Optoacoustics. Physics in Medicine and Biology, 50 (14), N141-N153. doi:10.1088/0031-9155/50/14/n01.

[67] A. K. Singh, R. K. singh, B. Sharma, A. K. Tyagi. (2017). Characterization and Bbiocompatibility Studies of Lead Free X-ray Shielding Polymer Composite for Healthcare Application. Radiation Physics and Chemistry, 138, 9-15. doi:10.1016/j.radphyschem.2017.04.016.

[68] C. Buzea, I. Pacheco, K. Robbie. (2007). Nanomaterials and Nanoparticles: Sources and Toxicity. *Biointerphases, 2* (4), MR17-MR71. doi:10.1116/1.2815690.

[69] A. Khosla, (2011). Micropatternable Multifunctional Nanocomposite Polymers for Flexible Soft MEMS Applications. Ph.D thesis, Simon Fraser University, Burnaby, BC, 2011.

[70] J. D. Sudha, S. Sivakala, R. Prasanth, V. L. Reena, P. R. Nair. (2009). Development of Electromagnetic Shielding Materials from the Conductive Blends of Polyaniline and Polyaniline-clay Nanocomposite-EVA: Preparation and Properties. Composites Scienece and Technology, 69, 358-364. doi:10.1016/j.compscitech.2008.10.026.

[71] A. N. Lagarkov, A. K. Sarychev. (1996). Electromagnetic Properties of Composites Containing Elongated Conducting Inclusions. Physical Review B, 53 (10), 6318-6336. doi:10.1103/physrevb.53.6318.

[72] Percolation threshold. En.wikipedia.org. https://en.wikipedia.org/wiki/Percolation_threshold. Published 2018. Accessed July 31, 2018.

[73] P. K. Prabhakar, S. Raj. P. R. Anuradha, S. N. Sawant, M. Doble. (2011). Biocompatibility Studies on Polyaniline and Polyaniline-silver Nanoparticle Coated Polyurethane Composite. Colloids and Surfaces B: Biointerfaces, 86 (1), 146-153. doi:10.1016/j.colsurfb.2011.03.033.

[74] L. Oropeza-Ramos, A. Macias, S. Juarez, Z. Falcon, A. Torres, M. Hautefeuille, H. Gonzalez. (2011). Low Cost Micro-platform for Culturing and Stimulation of Cardiomyocyte Tissue. 2011 IEEE 24th International Conference on Micro Electro Mechanical Systems. doi:10.1109/memsys.2011.5734574.

[75] H. Hung, H. Hsu. (2007). Biological Performances of Poly(ether)urethane-silver Nanocomposites. Nanotechnology, 18 (47), 475101. doi:10.1088/0957-4484/18/47/475101.

[76] A. Teichler, J. Perelaer, U. S. Schubert. (2013). Inkjet Printing of Organic Electronics-comparison of Deposition Techniques and State-of-the-art Developments. Journal of Materials Chemistry C, 1, 1910-1925. doi:10.1039/c2tc00255h.

[77] D. Chung, A. Khosla, B. L. Gray. (2014). Screen Printable Flexible Conductive Nanocomposite Polymer with Applications to Wearable Sensors. Nanosensors, Biosensors, and Info-Tech Sensors and Systems 2014. doi:10.1117/12.2046548.

[78] D. Chung, A. Khosla, B. Gray, A. Parameswaran, R. Ramaseshan, K. Kohli. (2014). Investigations of Flexible Ag/AgCl Nanocomposite Polymer Electrodes for Suitability in Tissue Electrical Impedance Scanning (EIS). Journal of the Electrochemical Society, 161 (2), B3071-B3076. Doi:10.1149/2.018402jes.

[79] D. Chung, and B. L. Gray. (2018). Development of Conductive Nanoparticle Composite Polymers and its Application for Fully Flexible Microfluidic Devices. Journal of Micromechanics and Microengineering, Manuscript sumbitted for publication

[80] B. D. Leahy, L. Pocivavsek, M. Meron, K. Lam, D. Salas. P. J. Viccaro, K. C. Lee, B. Lin. (2010). Geometric Stability and Elastic Response of a Supported Nanoparticle Film. Physical Review Letters, 105 (5). doi:10.1103/physrevlett.105.058301.

[81] I. Kim, Y. Jeong. (2010). Polylactide/exfoliated Graphite Nanocomposites with Enhanced Thermal Stability, Mechanical Modulus, and Electrical Conductivity. *Journal of Polymer Science Part B: Polymer Physics, 48* (8), 850-858. doi:10.1002/polb.21956.

[82] J. Li, J. Kim, M. L. Shan. (2005). Conductive Graphite Nanoplatelet/epoxy Nanocomposites: Effects of Exfoliation and UV/ozone Treatment of Graphite. Scripta Materialia, 53 (2), 235-240. doi:10.1016/j.scriptamat.2005.03.034.

[83] Y. Hao, R. Foster. (2008). Wireless Body Sensor Networks for Health-monitoring Applications. Physiological Measurement, 29 (11), R27-R56. doi:10.1088/0967-3334/29/11/r01.

[84] C. Tsao, D. DeVoe. (2009). Bonding of Thermoplastic Polymer Microfluidics. Microfluidics and Nanofluidics, 6 (1), 1-16. doi:10.1007/s10404-008-0361-x.

[85] D. Chung, B. L. Gray. (2017). Printing-based Fabrication Method Using Sacrificial Paper Substrates for Flexible and Wearable Microfluidic Devices. Journal of Micromechanics and Microengineering, 27 (11), 115009. doi:10.1088/1361-6439/aa8b21.

[86] A. Yousefpour, M. Hojjati, J. Immarigeon. (2009). Fusion Bonding/Welding of Thermoplastic Composites. *Journal of Thermoplastic Composite Materials, 17* (4), 303-341. doi:10.1177/0892705704045187.

[87] J. Lee, Y. Yun, Y. K, K. Jo. (2009). PDMS Nanoslits without Roof Collapse. *Bulletin of the Korean Chemical Society, 30* (8), 1793 -1797. doi:10.5012/bkcs.2009.30.8.1793.

[88] C. Peng, Z. Chen, M. K. Tiwari. (2018). All-organic Superhydrophobic Coatings with Mechanochemical Robustness and Liquid Impalement Resistance. *Nature Materials, 17* (4), 355–360. doi:10.1038/s41563-018-0044-2.

# Appendix A.

# List of Publications

**Refereed Journal Papers:**

1. D. Chung, A. Khosla, B. L. Gray, A. M. Parameswaran, R. Ramaseshan, and K. Kohli, "Investigations of Flexible Ag/AgCl Nanocomposite Polymer Electrodes for Suitability in Tissue Electrical Impedance Scanning (EIS)", Journal of The Electrochemical Society 161 (2), B3071-B3076, 2014.

2. D. Chung, and B. L. Gray, “Printing-based fabrication method using sacrificial paper substrates for flexible and wearable microfluidic devices”, Journal of Micromechanics and Microengineering, vol. 27, No. 11, 115009, 2017.

3. D. Chung, and B. L. Gray, “Development of conductive nanoparticle composite polymers and its application for fully flexible microfluidic devices”, Journal of Micromechanics and Microengineering, Manuscript sumbitted for publication (29, June, 2018).

**Refereed Conference Papers:**

1. D. Chung, A. Khosla, and B. L. Gray, "Screen printable flexible conductive nanocomposite polymer with applications to wearable sensors", Proc. SPIE 9060, Nanosensors, Biosensors, and Info-Tech Sensors and Systems 2014, 90600U.

2. D. Chung, and B. L. Gray, “Fabrication of wearable plastisol microfluidic devices on fabric using sacrificial paper substrates”, MicroTAS2015, 2015.

**Conference Poster:**

1. D. Chung , and B. L. Gray, “Conductive nanoparticle composite polymers (C-NCPs) for wearable electronics and microfluidic systems”, Canadian Printable Electronics Symposium 2018, 2018.

**Conference Abstracts:**

1. B. L. Gray, and D. Chung, “(Invited) Wearable microfluic and electronic frameworks for miomedical applications”, The Electrochemical Society, 2018.

2. B. L. Gray, and D. Chung, “(Keynote) Wearable devices and systems on textiles for biomedical monitoring and safety”, The Electrochemical Society, 2018.

**Patent Application:**

1. D. Chung, and B. L. Gray, “Process and method for fabricating wearable and flexible microfluidic devices and systems”, U.S. Patent App. 15/331,665, 2017.

# Appendix B.

# Data of Plastisol Film Stretchability Test

**Table B1. Data sheet of plastisol film stretchability test shown in Figure 3.**

| Film thickness [μm] | Average Thickness [μm] | Average Breaking point [mm] | (+) Thickness Deviation [μm] | (-) Thickness Deviation [μm] | (+) Breaking Point Deviation [mm] | (-) Breaking Point Deviation [mm] |
|---|---|---|---|---|---|---|
| **Group 1 (65 - 100)** | 90.267 | 2.640 | 9.400 | 10.600 | 1.360 | 1.240 |
| **Group 2 (100 - 135)** | 117.600 | 3.800 | 17.067 | 14.267 | 3.000 | 1.000 |
| **Group 3 (135 - 170)** | 152.429 | 4.800 | 0.000 | 10.762 | 2.000 | 1.600 |
| **Group 4 (170 - 205)** | 186.636 | 5.891 | 17.697 | 15.970 | 2.509 | 1.691 |
| **Group 5 (205 - 240)** | 217.467 | 5.460 | 16.867 | 10.467 | 2.140 | 1.660 |
| **Group 6 (240 - 275)** | 253.944 | 7.633 | 20.722 | 10.944 | 1.967 | 3.233 |
| **Group 7 (275 - 310)** | 290.722 | 7.467 | 18.278 | 14.056 | 2.133 | 1.867 |
| **Group 8 (310 - 345)** | 317.750 | 10.250 | 11.917 | 7.417 | 3.350 | 2.450 |
| **Group 9 (345 - 380)** | 355.333 | 11.171 | 11.000 | 11.667 | 4.829 | 2.571 |
| **Group 10 (380 - 415)** | 392.190 | 14.971 | 8.810 | 4.857 | 4.429 | 2.971 |
| **Group 11 (415 - 450)** | 427.611 | 15.367 | 8.389 | 2.611 | 4.233 | 4.167 |
| **Group 12 (450 - 485)** | 466.556 | 15.467 | 13.778 | 22.222 | 1.733 | 2.067 |
| **Group 13 (485 - 520)** | 497.167 | 15.500 | 12.833 | 9.833 | 1.300 | 0.900 |

# Appendix C.

# Data of silver C-NCP resistivity

**Table C1. Data sheet of resistivity measurement of silver C-NCP shown in Figure 5.**

| wt-% of Ag | Average Resistivity [Ω·m] | (+) Resistivity Deviation [Ω·m] | (-) Resistivity Deviation [Ω·m] |
|---|---|---|---|
| **58** | N/A | N/A | N/A |
| **61** | 1.567E-05 | 9.466E-07 | 5.029E-07 |
| **64** | 1.012E-05 | 7.016E-07 | 6.748E-07 |
| **67** | 2.334E-06 | 1.194E-07 | 1.469E-07 |
| **70** | 2.123E-06 | 1.065E-07 | 1.389E-07 |

# Appendix D.

# Data of Resistivity Change with Different Bending

**Table D1. Data sheet of resistivity change test with different bending angle shown in Figure 6.**

| | Average Resistivity [Ω•m] | | | | |
|---|---|---|---|---|---|
| **Bending Angle (°)** | **58 wt-% of Ag** | **61 wt-% of Ag** | **64 wt-% of Ag** | **67 wt-% of Ag** | **70 wt-% of Ag** |
| **-90** | N/A | 1.581E-05 | 1.016E-05 | 2.501E-06 | 2.166E-06 |
| **-80** | N/A | 1.562E-05 | 1.035E-05 | 2.479E-06 | 2.189E-06 |
| **-70** | N/A | 1.528E-05 | 1.025E-05 | 2.555E-06 | 2.189E-06 |
| **-60** | N/A | 1.520E-05 | 1.016E-05 | 2.503E-06 | 2.166E-06 |
| **-50** | N/A | 1.556E-05 | 1.029E-05 | 2.479E-06 | 2.192E-06 |
| **-40** | N/A | 1.539E-05 | 1.026E-05 | 2.388E-06 | 2.126E-06 |
| **-30** | N/A | 1.542E-05 | 1.017E-05 | 2.430E-06 | 2.123E-06 |
| **-20** | N/A | 1.576E-05 | 1.010E-05 | 2.430E-06 | 2.103E-06 |
| **-10** | N/A | 1.585E-05 | 1.019E-05 | 2.382E-06 | 2.101E-06 |
| **0** | N/A | 1.567E-05 | 1.012E-05 | 2.334E-06 | 2.123E-06 |
| **10** | N/A | 1.549E-05 | 1.022E-05 | 2.379E-06 | 2.039E-06 |
| **20** | N/A | 1.547E-05 | 1.012E-05 | 2.428E-06 | 2.033E-06 |

| | | | | | |
|---|---|---|---|---|---|
| **30** | N/A | 1.559E-05 | 1.023E-05 | 2.380E-06 | 2.063E-06 |
| **40** | N/A | 1.560E-05 | 1.020E-05 | 2.480E-06 | 2.079E-06 |
| **50** | N/A | 1.556E-05 | 1.034E-05 | 2.501E-06 | 1.992E-06 |
| **60** | N/A | 1.577E-05 | 1.030E-05 | 2.556E-06 | 2.085E-06 |
| **70** | N/A | 1.562E-05 | 1.031E-05 | 2.453E-06 | 2.153E-06 |
| **80** | N/A | 1.567E-05 | 1.037E-05 | 2.608E-06 | 2.200E-06 |
| **90** | N/A | 1.564E-05 | 1.042E-05 | 2.507E-06 | 2.253E-06 |

# Appendix E.

# Data of Stretchability of the silver C-NCP

**Table E1. Data sheet of stretchability test shown in Figure 7.**

**Stretchable distance of silver C-NCP printed textile [cm]**

| | 64 wt-% | 67 wt-% | 70 wt-% | 73 wt-% |
|---|---|---|---|---|
| **sample 1** | 1.5 | 1 | 1 | 0.4 |
| **sample 2** | 2.7 | 2 | 1.4 | 0.6 |
| **sample 3** | 2 | 1.6 | 1.2 | 0.3 |
| **sample 4** | 2.3 | 1.8 | 1.4 | 0.6 |
| **sample 5** | 1.7 | 1.2 | 1 | 0.4 |

# Appendix F.

# Data of Plastisol Film Thickness Measurements

**Table F1.** **Data sheet of plastisol film thickness measurements shown in Figure 24.**

| | Desired Thickness of 63 μm | | Desired Thickness of 126 μm | |
|---|---|---|---|---|
| | Average Thickness Before Planarization [μm] | Average Thickness After Planarization [μm] | Average Thickness Before Planarization [μm] | Average Thickness After Planarization [μm] |
| **Sample 1** | 60.333 | 51.333 | 119.333 | 125.333 |
| **Sample 2** | 70.889 | 63.333 | 108.444 | 102.000 |
| **Sample 3** | 60.889 | 51.444 | 133.556 | 130.111 |
| **Sample 4** | 59.222 | 49.556 | 139.000 | 132.889 |
| **Sample 5** | 45.667 | 33.778 | 116.000 | 109.889 |
| **Sample 6** | 42.889 | 33.111 | 107.889 | 103.889 |
| **Sample 7** | 47.556 | 37.889 | 129.000 | 123.778 |
| **Sample 8** | 60.889 | 51.222 | 112.667 | 102.333 |
| **Sample 9** | 50.444 | 40.556 | 104.778 | 103.667 |
| **Sample 10** | 50.333 | 45.667 | 124.333 | 121.667 |

# Appendix G.

# Data of Saline Solution Tests with Conductivity Sensor

**Table G1. Data sheet of saline solution tests from screen-printable silver C-NCP shown in Figure 41 (a).**

| | Measured Current [mA] | | | | | | | | | | |
|---|---|---|---|---|---|---|---|---|---|---|---|
| **Applied Vpp [V]** | **Control Water** | **0.2 wt-% Salt** | **0.4 wt-% Salt** | **0.6 wt-% Salt** | **0.8 wt-% Salt** | **1.0 wt-% Salt** | **1.2 wt-% Salt** | **1.4 wt-% Salt** | **1.6 wt-% Salt** | **1.8 wt-% Salt** | **2.0 wt-% Salt** |
| **0.3** | 0.17 | 1.34 | 1.71 | 2.12 | 2.43 | 2.79 | 3.12 | 3.81 | 4.53 | 5.09 | 5.76 |
| **0.6** | 0.22 | 2.96 | 3.73 | 4.63 | 5.28 | 6.04 | 6.71 | 8.10 | 9.50 | 10.57 | 11.98 |
| **0.9** | 0.38 | 4.63 | 5.83 | 7.21 | 8.26 | 9.41 | 10.42 | 12.55 | 14.69 | 16.28 | 18.40 |
| **1.2** | 0.64 | 6.26 | 7.83 | 9.70 | 11.12 | 12.68 | 14.08 | 16.86 | 19.70 | 21.87 | 24.63 |
| **1.5** | 0.89 | 8.00 | 9.99 | 12.33 | 14.19 | 16.17 | 17.90 | 21.59 | 25.14 | 27.95 | 31.41 |
| **1.8** | 1.08 | 9.65 | 12.06 | 14.86 | 17.11 | 19.54 | 21.63 | 26.19 | 30.53 | 33.82 | 38.04 |
| **2.1** | 1.32 | 11.29 | 14.09 | 17.36 | 20.01 | 22.90 | 25.34 | 30.71 | 35.72 | 39.67 | 44.54 |
| **2.4** | 1.49 | 13.05 | 16.07 | 19.80 | 22.90 | 26.25 | 29.02 | 35.24 | 41.01 | 45.60 | 51.11 |
| **2.7** | 1.65 | 14.63 | 18.12 | 22.36 | 25.94 | 29.83 | 33.01 | 40.52 | 46.90 | 52.09 | 58.69 |
| **3** | 1.81 | 16.20 | 20.12 | 24.86 | 28.92 | 33.29 | 36.87 | 45.43 | 52.46 | 58.27 | 65.24 |

**Table G2. Data sheet of saline solution tests from commercial silver epoxy shown in Figure 41 (b).**

| | Measured Current [mA] | | | | | | | | | | |
|---|---|---|---|---|---|---|---|---|---|---|---|
| **Applied Vpp [V]** | **Control Water** | **0.2 wt-% Salt** | **0.4 wt-% Salt** | **0.6 wt-% Salt** | **0.8 wt-% Salt** | **1.0 wt-% Salt** | **1.2 wt-% Salt** | **1.4 wt-% Salt** | **1.6 wt-% Salt** | **1.8 wt-% Salt** | **2.0 wt-% Salt** |
| **0.3** | 0.17 | 1.85 | 2.76 | 4.01 | 5.07 | 6.41 | 7.10 | 8.29 | 9.44 | 10.40 | 11.02 |
| **0.6** | 0.22 | 3.88 | 5.72 | 8.26 | 10.42 | 13.10 | 14.51 | 16.93 | 19.26 | 21.16 | 22.43 |
| **0.9** | 0.42 | 5.97 | 8.74 | 12.60 | 15.85 | 19.95 | 22.04 | 25.73 | 29.23 | 32.08 | 34.02 |
| **1.2** | 0.68 | 7.97 | 11.65 | 16.78 | 21.13 | 26.54 | 29.34 | 34.16 | 38.88 | 42.60 | 45.14 |
| **1.5** | 0.93 | 10.13 | 14.78 | 21.28 | 26.74 | 33.62 | 37.07 | 43.24 | 49.12 | 53.89 | 57.01 |
| **1.8** | 1.14 | 12.17 | 17.78 | 25.58 | 32.15 | 40.43 | 44.61 | 52.01 | 58.97 | 64.60 | 68.32 |
| **2.1** | 1.36 | 14.21 | 20.73 | 29.80 | 37.48 | 47.19 | 52.01 | 60.78 | 68.74 | 75.34 | 79.64 |
| **2.4** | 1.55 | 16.25 | 23.65 | 34.04 | 42.78 | 53.86 | 59.25 | 69.35 | 78.55 | 85.90 | 90.85 |
| **2.7** | 1.72 | 18.38 | 26.78 | 38.56 | 48.40 | 61.00 | 66.93 | 78.51 | 88.79 | 97.32 | 103.1 |
| **3** | 1.89 | 20.46 | 29.75 | 42.46 | 53.72 | 67.97 | 74.23 | 87.25 | 98.63 | 108.4 | 114.9 |

# Appendix H.

# Wearable Microfluidic Mixer Design

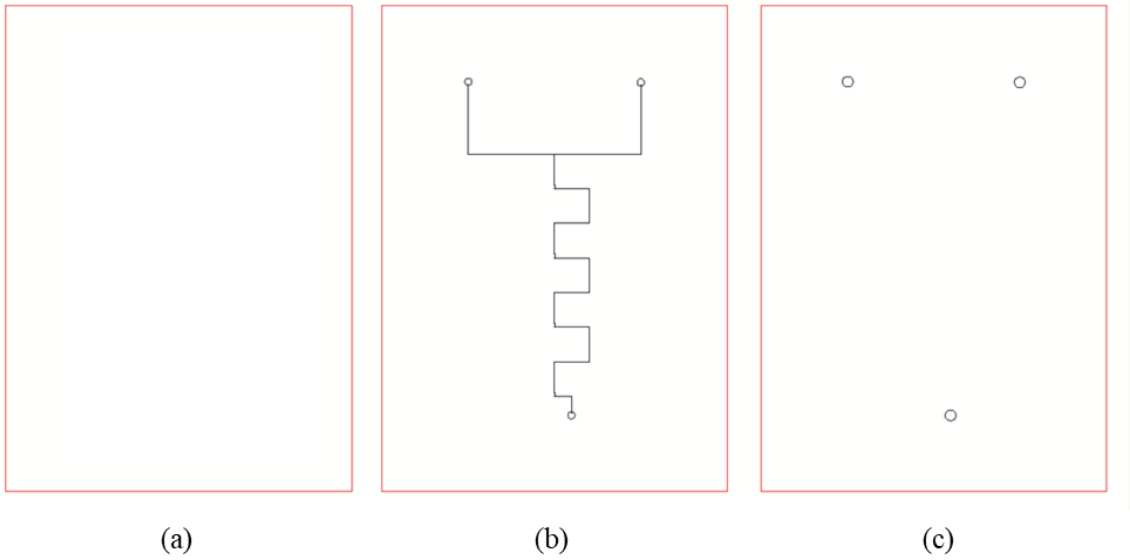


**Figure H1.** **Design of wearable microfluidic mixer: (a) Bottom layer. (b) Channel layer with channel pattern. (c) Top layer with two inlets and one outlet.**

# Appendix I.

# Wearable Microfluidic Conductivity Sensor Design

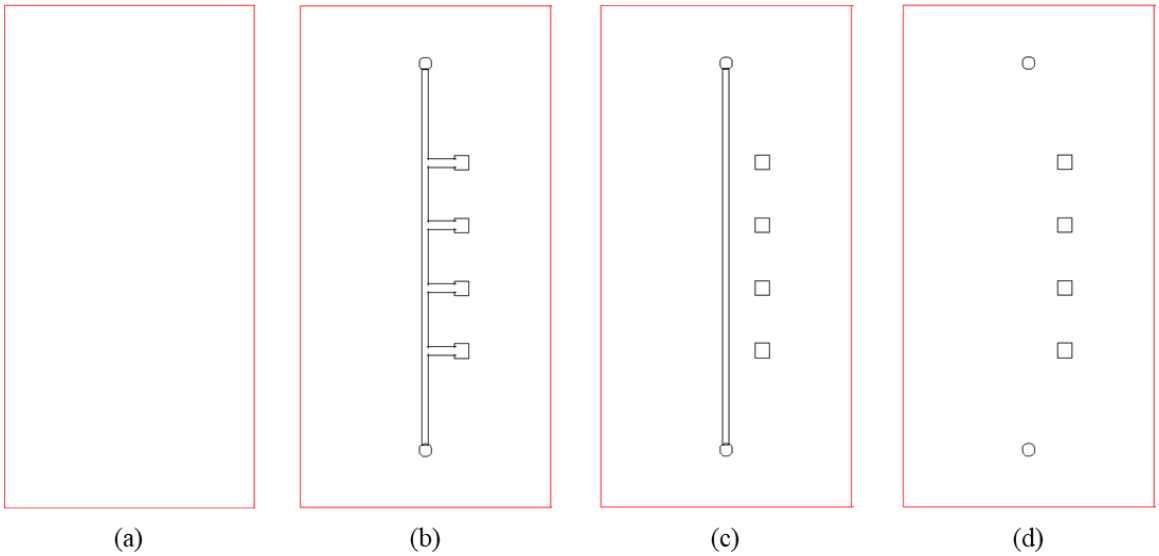


**Figure I1.** **Design of wearable conductivity sensor passive parts: (a) Bottom layer. (b) First channel layer. (c) Second channel layer. (d) Top layer with inlet, outlet, and contact pads.**

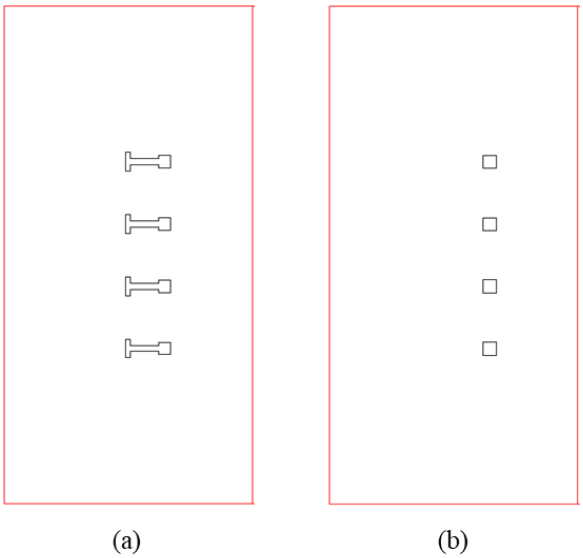


**Figure I2.** **Design of wearable conductivity sensor active parts: (a) Electrodes design (b) Contact pads design.**